Fluorescence measurement of metal uptake by pathogenic bacteria

by

Ashish Kumar

B.Sc., Mahatma Gandhi Institute of Applied Sciences, India, 2011
M.Sc., Madurai Kamaraj University, India, 2013

AN ABSTRACT OF A DISSERTATION

submitted in partial fulfillment of the requirements for the degree

DOCTOR OF PHILOSOPHY

Department of Biochemistry and Molecular Biophysics
College of Arts and Sciences

KANSAS STATE UNIVERSITY
Manhattan, Kansas

2021

Abstract

The increasing antibiotic resistance of Gram-negative bacteria, e.g., *Enterococcus, Staphylococcus, Klebsiella, Acinetobacter, Pseudomonas,* and *Enterobacter* (ESKAPE) pathogens, calls for increased efforts to search for novel chemical agents that target microbial pathways. Bacterial iron acquisition pathways are potentially relevant in the search for new antibiotics. Iron is vital to bacteria because it plays a central role in energy production, DNA synthesis, intermediate metabolism, nitrogen fixation, and oxygen detoxification. At the time of infection or colonization in the host environment, bacteria must acquire iron to proliferate. To do so, they secrete small molecular weight organic compounds, siderophores, that bind iron with high affinity. They also express outer membrane (OM) transporters that recognize and internalize the ferric siderophore complex. Especially, Gram-negative bacteria acquire iron using TonB dependent ferric siderophore transport system. For example, the OM protein FepA actively transports ferric enterobactin (FeEnt) in the periplasm, and the inner membrane (IM) protein TonB provides energy for this ferric siderophore uptake reaction. We originally devised a fluorescence spectroscopic approach that observes real-time ferric-siderophore in *E. coli,* e.g., FeEnt uptake through the OM receptor, FepA. This method monitors the binding of the FeEnt to the outer loops of fluorescently labeled FepA.

Binding quenches fluorescence, but fluorescence recovers as the bacteria transport and deplete the ferric siderophore from the solution. Hence, inhibitors that block the active transport of the siderophore prevent fluorescence recovery. We adapted this approach to functionally characterize multiple *Klebsiella pneumoniae* ferric enterobactin transporters and also applied the methodology to study other ferric siderophore transport reactions. Despite the sensitivity and accuracy of this species-specific approach, experimental manipulations of ESKAPE pathogens are

always concerning points due to potential hazardousness. Hence, we modified the assay in a manner where it allowed the observation of ferric siderophore transport by any of the ESKAPE pathogens, including clinical isolates, without genetically engineering them. A TonB-deficient bacterium, with fluorescently labeled OM receptor, acts as a sensor strain that binds ferric siderophore but cannot transport it. When cohabiting in an environment with other bacterial pathogen, the sensor strain monitored ferric siderophore uptake and thereby TonB action in that bacterial pathogen. We created "Universal" assays of TonB dependent Ferric siderophore transport by any bacterial pathogen with such sensor strains. Using these species-specific and universal assays, it is plausible to look for those compounds that can inhibit TonB action and prevent ferric siderophore transport. These chemicals that block TonB action may inhibit iron acquisition in humans and animals and thereby thwart pathogenesis. Such chemicals may act as novel therapeutics against bacterial infectious diseases.

We used these fluorescent sensors to detect, discriminate, and quantify ferric siderophores in purified form or complex mixtures of metabolites and other biochemicals. We created fluorescent sensors from different bacterial species that recognized different metal complexes: native (FeEnt), glucosylated (FeGEnt), degraded (FeEnt*) ferric enterobactin; the hydroxamates: ferrichrome (Fc), ferric acinetobactin (FeAcn), ferric aerobactin (FeAbn), and ferrioxamine B (FxB); the porphyrins: hemin (Hn) and vitamin B_{12}. In spectroscopic assays, these constructs sensitively detected and quantified the different metal chelates in solution. We showed biochemical specificity, affinity, and membrane transport using these sensors. The sensors are helpful in detecting, discriminating siderophores, and providing diagnostic information about bacterial presence in clinical and food samples.

In the later part, using these fluorescence decoy sensors, we also looked at the mechanistic part of FeEnt transport through FepA. We concluded that rearrangements must occur in the globular N-domain of FepA during FeEnt transport. We suggested that N-domain does not exit the transmembrane channel as a rigid body in the periplasm; instead, it remains within the transmembrane pore as FeEnt enters the periplasm.

Fluorescence measurement of metal uptake by pathogenic bacteria

by

Ashish Kumar

B.Sc., Mahatma Gandhi Institute of Applied Sciences, India, 2011
M.Sc., Madurai Kamaraj University, India, 2013

A DISSERTATION

submitted in partial fulfillment of the requirements for the degree

DOCTOR OF PHILOSOPHY

Department of Biochemistry and Molecular Biophysics
College of Arts and Sciences

KANSAS STATE UNIVERSITY
Manhattan, Kansas

2021

Approved by:

Major Professor
Prof. Phillip E. Klebba

Copyright

Abstract

The increasing antibiotic resistance of Gram-negative bacteria, e.g., *Enterococcus, Staphylococcus, Klebsiella, Acinetobacter, Pseudomonas,* and *Enterobacter* (ESKAPE) pathogens, calls for increased efforts to search for novel chemical agents that target microbial pathways. Bacterial iron acquisition pathways are potentially relevant in the search for new antibiotics. Iron is vital to bacteria because it plays a central role in energy production, DNA synthesis, intermediate metabolism, nitrogen fixation, and oxygen detoxification. At the time of infection or colonization in the host environment, bacteria must acquire iron to proliferate. To do so, they secrete small molecular weight organic compounds, siderophores, that bind iron with high affinity. They also express outer membrane (OM) transporters that recognize and internalize the ferric siderophore complex. Especially, Gram-negative bacteria acquire iron using TonB dependent ferric siderophore transport system. For example, the OM protein FepA actively transports ferric enterobactin (FeEnt) in the periplasm, and the inner membrane (IM) protein TonB provides energy for this ferric siderophore uptake reaction. We originally devised a fluorescence spectroscopic approach that observes real-time ferric-siderophore in *E. coli,* e.g., FeEnt uptake through the OM receptor, FepA. This method monitors the binding of the FeEnt to the outer loops of fluorescently labeled FepA.

Binding quenches fluorescence, but fluorescence recovers as the bacteria transport and deplete the ferric siderophore from the solution. Hence, inhibitors that block the active transport of the siderophore prevent fluorescence recovery. We adapted this approach to functionally characterize multiple *Klebsiella pneumoniae* ferric enterobactin transporters and also applied the methodology to study other ferric siderophore transport reactions. Despite the sensitivity and accuracy of this species-specific approach, experimental manipulations of ESKAPE pathogens are

always concerning points due to potential hazardousness. Hence, we modified the assay in a manner where it allowed the observation of ferric siderophore transport by any of the ESKAPE pathogens, including clinical isolates, without genetically engineering them. A TonB-deficient bacterium, with fluorescently labeled OM receptor, acts as a sensor strain that binds ferric siderophore but cannot transport it. When cohabiting in an environment with other bacterial pathogen, the sensor strain monitored ferric siderophore uptake and thereby TonB action in that bacterial pathogen. We created "Universal" assays of TonB dependent Ferric siderophore transport by any bacterial pathogen with such sensor strains. Using these species-specific and universal assays, it is plausible to look for those compounds that can inhibit TonB action and prevent ferric siderophore transport. These chemicals that block TonB action may inhibit iron acquisition in humans and animals and thereby thwart pathogenesis. Such chemicals may act as novel therapeutics against bacterial infectious diseases.

We used these fluorescent sensors to detect, discriminate, and quantify ferric siderophores in purified form or complex mixtures of metabolites and other biochemicals. We created fluorescent sensors from different bacterial species that recognized different metal complexes: native (FeEnt), glucosylated (FeGEnt), degraded (FeEnt*) ferric enterobactin; the hydroxamates: ferrichrome (Fc), ferric acinetobactin (FeAcn), ferric aerobactin (FeAbn), and ferrioxamine B (FxB); the porphyrins: hemin (Hn) and vitamin B_{12}. In spectroscopic assays, these constructs sensitively detected and quantified the different metal chelates in solution. We showed biochemical specificity, affinity, and membrane transport using these sensors. The sensors are helpful in detecting, discriminating siderophores, and providing diagnostic information about bacterial presence in clinical and food samples.

In the later part, using these fluorescence decoy sensors, we also looked at the mechanistic part of FeEnt transport through FepA. We concluded that rearrangements must occur in the globular N-domain of FepA during FeEnt transport. We suggested that N-domain does not exit the transmembrane channel as a rigid body in the periplasm; instead, it remains within the transmembrane pore as FeEnt enters the periplasm.

Table of Contents

List of Figures

List of Tables

Acknowledgements

First of all, I am eternally grateful to my major professor, Dr. Phillip Klebba, for his continuous support and guidance throughout my Ph.D. studies at Kansas State University. I sincerely thank him for accepting me as a graduate student in his research laboratory and providing continuous guidance and support here at K-State. He ensured that I found a safe, secure, and happy research environment in the laboratory, which helped me extensively do my research work and developed me as an efficient research scientist. It has been my absolute privilege to have you as my major professors. I would also like to thank Dr. Salete Newton (Sally) for extensive guidance and support during good and bad times. Sally continuously encouraged and was always willing and enthusiastic to assist in any way should throughout the research project.

From the bottom of my heart, I would like to thank my committee members Dr. Michael Zolkiewski, Dr. Timothy Durrett, and Dr. Philip Hardwidge, for agreeing to serve on my committee and provide me with invaluable suggestions and scientific interactions from my preliminary examination to the very last committee meeting. Also, I would like to thank Dr. Takashi Ito for serving as the outside chair for my doctoral defense.

My sincere thanks to all current and previous lab members of Dr. Phillip Klebba's lab group. I want to mention and thank Dr. Somnath Chakrovarty, Dr. Aritri Majumdar, Dr. Yan Shipelskiy, Dr. Brittany Nairn, Taihao Yang, and all the undergraduates in the lab. I want to express my sincere gratitude to the whole staff, faculty members and friends of the entire Biochemistry and Molecular Biophysics departments at the K-State for all the help and support.

Finally, I want to express my sincere appreciation to my wonderful family, who stood by me and provided unconditional love and support to pursue my dream of studying abroad. Thanks to all.

Dedication

To my wonderful family and friends

Chapter 1 - Introduction to Gram-negative bacterial iron acquisition

1.1. Importance of iron for bacteria:

Iron is one of the vital metals on earth and is necessary for the survival of all forms of life. Nearly all living organisms require iron since it works as a versatile cofactor for many proteins in biochemical and metabolic reactions because of its redox potential capabilities. Iron plays a central role in energy production, DNA synthesis, intermediate metabolism, oxidative detoxification, and nitrogen metabolism. Moreover, iron helps regulate the biosynthesis of vitamins, porphyrins, toxins, antibiotics, siderophores, pigments, and aromatic compounds (Holden, Breen et al. 2016). At physiological pH, ferrous iron (Fe^{+2}) (Neilands 1953) is soluble in water, but in the presence of oxygen, it gets oxidized (Fe^{+3}) and has very low solubility, and therefore it is not readily bioavailable. To successfully proliferate at the time of colonization and infection, bacteria require iron from the host, but there is minimal free iron available. The majority of the iron in the host is bound and tightly regulated by host proteins with high affinity, which are responsible for storage, transport, and metabolic activities, e.g., transferrin, lactoferrin, ferritin, and an intricate intracellular network of regulatory and delivery proteins such as hepcidin, hemoglobin-haptoglobin, and heme-hemopexin. The tight control in eukaryotes to prevent bacteria from acquiring an essential element for proliferation and growth, is referred to as “nutritional immunity”. Both pathogenic and free-living bacteria have developed several strategies for acquiring iron from this tightly regulated system in the host. Although free iron also presents a potential threat to organisms because it tends to create reactive oxygen species (ROS) via the Fenton reaction, both prokaryotic and eukaryotic organisms have extensive ways to limit ROS

generation (Raymond, Dertz et al. 2003, Skaar, Humayun et al. 2004, Pi, Jones et al. 2012, Holden and Bachman 2015).

1.2. Iron acquisition and pathogenesis:

There are more than 80 enzymes that require iron-containing heme or non-heme cofactors that help the catalysis of biochemical and metabolic reactions in bacteria, fungi, and animals. Some prominent examples include enzymes involved in detoxification of ROS, e.g., catalase and superoxide dismutase, aconitase and succinic dehydrogenase in the citric acid cycle (CAC), proton-pumping oxidoreductases, and class Ia ribotide reductases in *de novo* DNA synthesis. This central role of iron in aerobic reactions makes it a determinant of bacterial pathogenesis and invasiveness. This creates competition at the host-pathogen interface with the eukaryotic immune system trying to sequester iron as much as possible as a defense mechanism so that no free iron is available for pathogens. On the other hand, successful pathogens employ strategies to overcome this defense mechanism and capture iron which ultimately helps in their growth and proliferation (Williams 1979, Payne 1988, Payne 1989, Payne 1993, Dhople, Ibanez et al. 1996, Torres and Payne 1997, Schoolnik 2002, Snyder, Haugen et al. 2004, Buckling, Harrison et al. 2007, Smith 2007).

Biochemical connections between pro-and eukaryotic iron homeostasis are apparent, and many researchers observed the relationship between bacterial iron acquisition and pathogenesis (Bullen 1981, Bullen, Griffiths et al. 2000, Mihara, Tanabe et al. 2004, Bullen, Rogers et al. 2005). Extensive research conducted on these systems confirmed that bacteria need iron for metabolism, and they produce many biosynthetic and transport systems to capture iron from the host or wild environment. Their success in this process largely influences the outcome of bacterial

pathogenesis. Moreover, it is also evident that iron deficiency or disruption of iron uptake process retards bacterial growth, reduce or eliminate virulence (Neilands 1981, Cowart and Foster 1985, Adams, Vartivarian et al. 1990, Conte, Longhi et al. 1994, Coulanges, Andre et al. 1998, Mihara, Tanabe et al. 2004). Overall, extensive evidence support the hypothesis that iron acquisition is a determinant of bacterial pathogenesis. For example, iron deprivation slows bacterial growth, and in response to combat this iron stress, bacteria secrete siderophores. Many Gram-negative bacteria pathogens, e.g., species of *Escherichia, Salmonella, Neisseria, Vibrio, Acinetobacter, Klebsiella*, *Yersinia, Pseudomonas*, *Hemophilus,* and many more acquire iron with the help of TonB dependent iron transporters. Microbial iron scavenging and host iron sequestration are antagonistic processes that influence infection. Iron sequestration by host reduces or eliminates bacterial virulence. Successful pathogens capture iron from their hosts, and vaccination with bacterial iron transportation creates protective humoral and/or cellular immunity (Wolf, Hogan et al. 2004).

1.3. Bacterial siderophores:

As previously stated, bacteria must obtain iron from host proteins for their proliferation and growth. Bacterial pathogens accomplish this task primarily by secreting small molecular weight organic molecules (500-1500 Dalton) called siderophores. These are ferric iron chelators that bind to iron with high affinity: Enterobactin, a catecholate siderophore of the *Enterobacteriaceae* family, binds with Fe^{+3} with the highest known binding affinity (dissociation constant ($K_D = 10^{-52}$ M), and this ferric iron-siderophore complex is transported back in the bacterial cell and utilized (Holden, Breen et al. 2016).

The first siderophore, mycobactin, was discovered in 1950 in acid-fast bacteria and was shown to be essential for *Mycobacterium johnei* growth (Francis, Macturk et al. 1953). Since the discovery of mycobactin and isolation of ferrichrome from the smut fungus *Ustilago sphaerogena* (Neilands 1953), over 500 siderophores have been identified, highlighting their importance and the evolutionary pressure on bacteria to acquire iron in order to survive in the host environment. Many siderophores are considered important virulence factors, especially in those pathogens that encode multiple siderophores (Francis, Macturk et al. 1953, Holden and Bachman 2015).

Based on their complexation of Fe^{+3}, bacterial siderophores are generally divided into three major family groups: catecholate, hydroxamate, and carboxylate group (Figure 1.1). Though all the families have their distinct characteristic properties that affect their affinities to iron, in general, all three families utilize negatively charged oxygen atoms to coordinate ferric iron. Many mixed-typed siderophores also have been characterized apart from the major "bacterial siderophore" family group (Francis, Macturk et al. 1953, Holden and Bachman 2015).

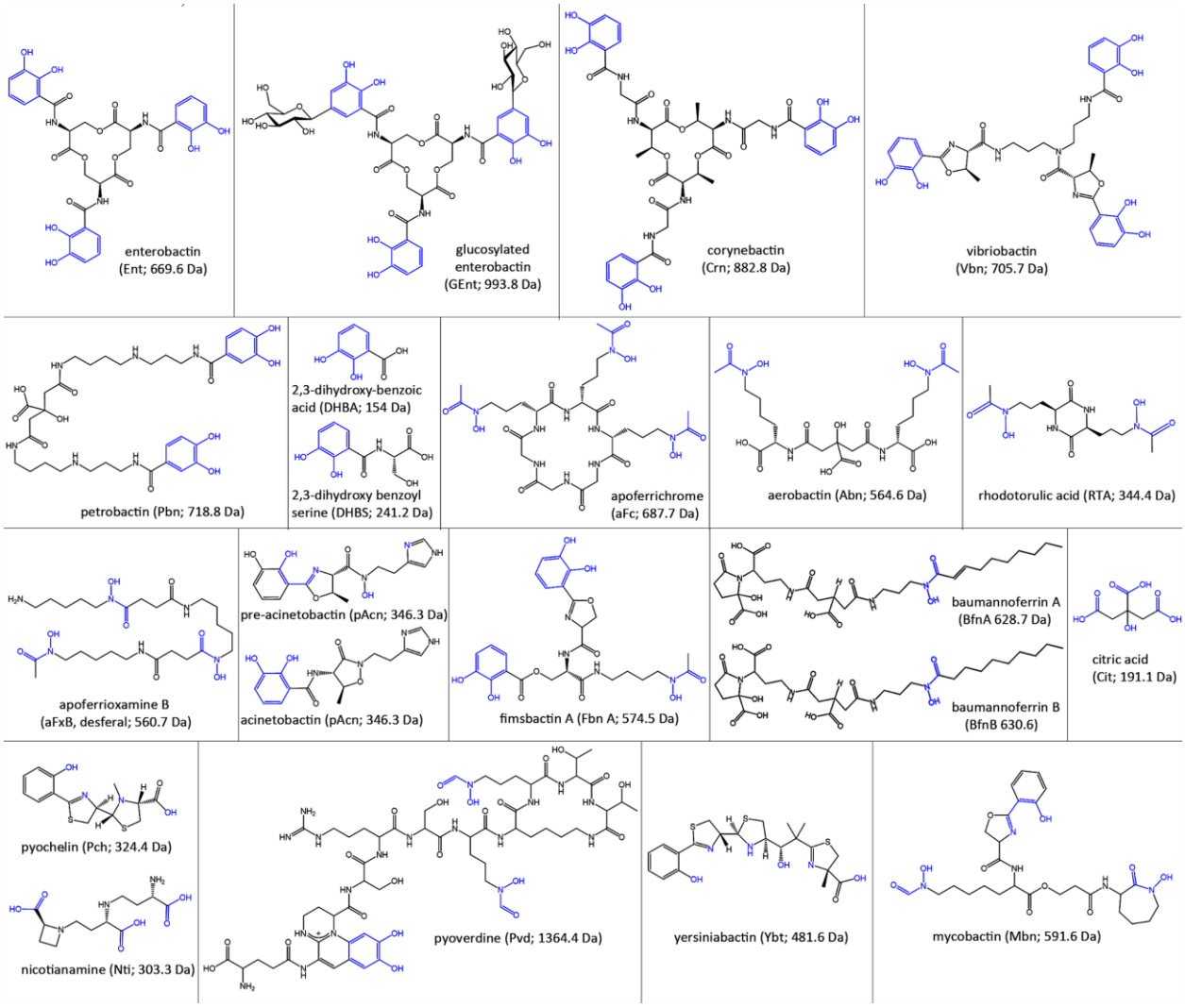

Figure 1.1. Structure of bacterial siderophores:

Bacteria synthesize and/or utilize variety of siderophores. This Figure shows the structures, abbreviations and masses of the apo-siderophores, with their iron chelation moieties (in blue). Figure adapted (Klebba, Newton et al. 2021). Copyright {2021} American Chemical Society.

1.4. Iron uptake in *Escherichia coli* and other Gram-negative bacteria and their clinical relevance:

Based on the presence of an outer membrane, bacterial iron uptake systems vary in Gram-negative bacteria and Gram-positive bacteria. For example, Gram-negative bacteria *Escherichia coli* and other pathogenic genera like *Enterococcus, Klebsiella, Acinetobacter, Pseudomonas,* and *Enterobacter* contain inner membrane (IM) and outer membrane (OM) separated by periplasmic space. A thin peptidoglycan layer is also present in this periplasmic space. The outer membrane of Gram-negative bacterial cell contains open channel porins (Nikaido and Vaara 1985, Rich, Papalia et al.), making the membrane porous up to 600 Da, allowing passive diffusion of small molecules at high concentration (Newton, Igo et al. 1999, Smallwood, Jordan et al. 2014). Large molecules (>600 Da) and/or nutrients present at very low concentrations in the host or wild environment need to be transported actively across the outer membrane. Active transport of nutrients is difficult through OM because of the presence of porins. This issue is overcome presumably by transferring energy from the inner membrane (IM) to the outer membrane (OM). Gram-negative bacteria, including species such as *Klebsiella, Yersinia, Pseudomonas*, and *Acinetobacter* use the TonB system located in the inner membrane for this active transport of nutrients. This system comprises three transmembrane proteins composed of TonB/ExbB/ExbD (Higgs, Larsen et al. 2002). TonB and ExbD possess a single transmembrane domain with a periplasmic domain, whereas ExbB contains three transmembrane domains with a cytoplasmic loop (Baker and Postle 2013). Ultimately this complex of three proteins uses an electrochemical gradient present in IM and helps transport molecules across the OM by interacting with outer membrane protein receptors when the ligand binds to it.

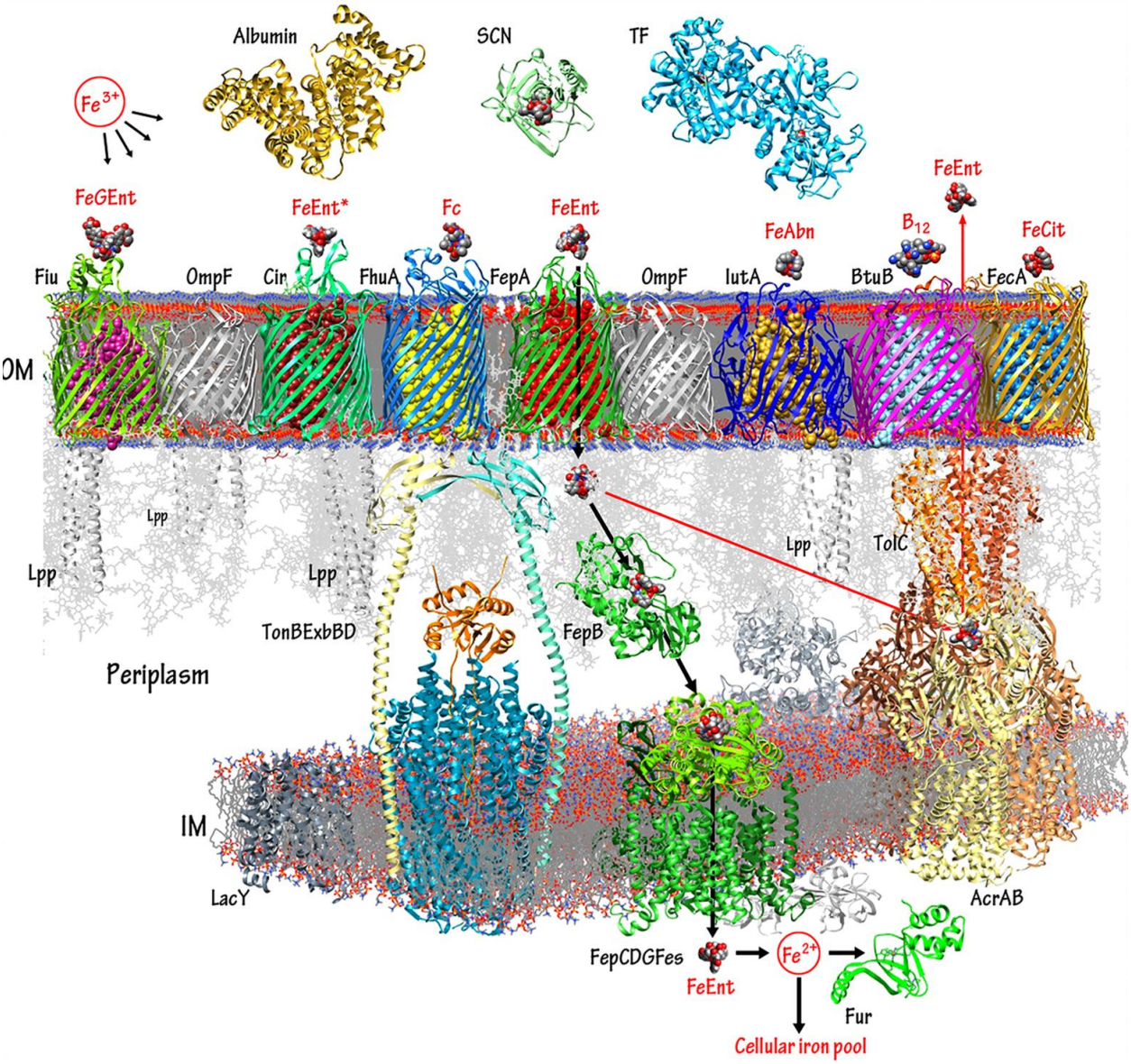

Figure 1.2. Model for TonB dependent FeEnt transport in Gram-negative bacterium *E. coli*:

The Figure depicts a variety of OM receptors (crystalized and modeled). Black (import) and red (export) arrows show the FeEnt transport across the membrane using different protein components. FeEnt enters in periplasm through FepA then guided to IM after binding to FepB, and through ATP hydrolysis, it gets transported inside cytosol with the help of FepCDG. If excess FeEnt enters the cell, it is expelled out with the help of the export complex TolC. Figure adapted from (Klebba, Newton et al. 2021). Copyright {2021} American Chemical Society.

For example, the outer membrane protein FepA actively transports the iron complex ferric enterobactin (FeEnt), and the inner membrane protein TonB provides the energy for this uptake

reaction (Figure 1.2). The superfamily of energy- and TonB dependent ~80 kDa OMPs which transport ferric siderophore complex or other nutrients are called TonB dependent transporters (TBDTs) (Schauer, Rodionov et al. 2008). Since their discovery (McIntosh and Earhart 1976, Pugsley and Reeves 1977), many scientific groups have tried to understand their properties, and based on this, many other acronyms exist for this category of outer membrane proteins (Rich, Papalia et al.), such as iron-regulated membrane proteins (IRMP) (Klebba, McIntosh et al. 1982), iron-regulated OM proteins (IROMP) (Morton and Williams 1989), ligand-gated porins (LGP) (Rutz, Liu et al. 1992). None of these acronyms is entirely correct as the proteins in this class are not diffusive porins, and they are not even true transporters, a term that is usually reserved for ATP-driven IM permeases. However, LGP can be considered the best option because perhaps it correctly describes their mechanistic attributes (Klebba, Newton et al. 2021). These LGPs, e.g., FepA, are characterized by 150 residues long globular N-domain, which regulates ligand transport. This N-domain is surrounded by a C-terminal 22-stranded beta-barrel structure topped with large loops that form a cell surface vestibule for ligand binding (Buchanan, Smith et al. 1999). During the transport of siderophore or nutrient across the outer membrane, TonB interacts with a conserved peptide sequence in the N-terminal region called “TonB box” (Guterman and Dann 1973), and this interaction causes conformational changes that open TBDT channels for ligand transport to periplasm. Though structural changes that facilitate ligand uptake through TBDTs are not fully understood yet, it is known that binding and transport of ligand takes place in two separate stages: the first stage involves binding of the ligand, which is an energy-independent process (Ferguson, Chakraborty et al. 2002) and the second stage involves the transport of ligand into the periplasm, and this process is energy-dependent (Rutz, Liu et al. 1992). At the time of ligand binding, loops of the receptors close around the ligand, localizing the ligand in the vestibule. This

receptor-ligand binding exposes the TonB box that can directly interact with TonB (Pawelek, Croteau et al. 2006). During the transport process, TonB- ExbBD IM complex harvests electrochemical force from the electrochemical proton gradient created by the proton gradient across the IM and transduce energy to OM, which drives conformational changes in TBDTs that allow the transport of ligand to the periplasm (Klebba 2003). Inside the periplasm, periplasmic carrier protein, e.g., FepB (Li, Li et al. 2016), recognizes and interacts with FeEnt and then shuttle the ligand to FepCDG (Shea and McIntosh 1991), ATP-binding cassette (ABC) transporters which helps in the transport of ligand to the cytoplasm by ATP hydrolysis. Inside the cytoplasm, esterase release iron, and then this metal is used for cell metabolism (Leong and Neilands 1976, Ecker, Lancaster et al. 1982).

Gram-negative bacterial outer membrane usually possesses multiple TBDTs e.g., *Enterobacteriaceae* family encodes 7 to12 receptors and most of them are mainly involved in iron and other metal uptake. Other bacterial families may encode more TBDTs (*Pseudomonadaceae*: 35-38; *Caulobacteriacae*: 63; *Xanthamonadaceae*: 42-70) (Schauer, Rodionov et al. 2008) and their substrate specificities may vary. Most of the function of TBDTs in these families are predicted purely based on bioinformatics analysis e.g., 5 outer membrane proteins were identified in *Caulobacter cresentus* which are regulated by iron but only one was experimentally demonstrated to transport hemin (Balhesteros, Shipelskiy et al. 2017).

TonB dependent systems are ubiquitous in Gram-negative bacteria and blocking the function of this system either by chemical or immunological inhibitors may reduce bacterial growth in humans and animals. It is desirable to look for antibiotics that can target these pathways because it is possible that bacteria may suffer less from the development of resistance because

bacteria with altered or mutant TonB proteins fail to proliferate in the iron-deprived environment and show impaired host-colonization. Many existing antibiotics target bacterial cell envelop biochemistry (Kuhn 2019, Brown, Gordon et al. 2020, Baquero and Levin 2021). Compounds which will target the iron transport process will be specific to prokaryotic pathways as eukaryotes utilize different pathways for iron transport (Agarwal and Yee 2019, Gao, Li et al. 2019, Testi, Boffi et al. 2019). Until now, there are no natural antibiotics available that specifically target these iron transport pathways. Though it has been shown that iron enhances quinone antibiotic streptonigrin's activity against *Escherichia coli* (Yeowell and White 1982), *Neisseria gonorrhoeae* (Cohen, Chai et al. 1987, Dyer, McKenna et al. 1987) and *Haemophilus influenzae* (Holland, Towner et al. 1991), yet there is no known antibiotic which can inhibit TonB dependent acquisition.

Moreover, it is possible to target individual iron uptake systems, but that may not impair pathogenesis or host colonization as bacteria usually produce multiple, redundant transporters for ferric/ferrous iron transport. For example, *E. coli* K-12 produces 8 TonB dependent iron transport system, wild isolates produce more, and pathogenic bacteria encode even more receptors for iron transport. The eight transporters of *E. coli* are responsible for the transport of different iron complexes: ferric catecholate (FepA, Fiu and Cir), ferric hydroxamates (FhuA, FhuE, and IutA), ferric citrate (FecA), and vitamin B_{12} (BtuB) (Klebba, Newton et al. 2021).

On the other hand, the host innate immune system produces various components, e.g., transferrin and lactoferrin, that reduce the iron availability to the invading bacteria, which ultimately emphasize the importance of chemical and immunological interventions that target bacterial iron uptake.

1.5. Genetic regulation of iron uptake:

To successfully cope up with the limited/excess amount of metal, bacterial have evolved many strategies to respond. These strategies help in metal regulation with minimum energy expenditure and preventing overload of metal in cells e.g., excess iron would be highly toxic for cells because iron plays important role in enhancing oxygen toxicity as it efficiently catalyzes Fenton reaction which convert hydrogen peroxide into highly toxic reactive hydroxyl radicals. Both Gram-negative and Gram-positive bacteria regulate the expression of OM proteins and siderophore production genes, involved in iron metabolism (uptake) with the help of metalloregulators (Newton, Klebba et al. 2005, da Silva Neto, Braz et al. 2009), Ferric Uptake Regulator (Fur). Fur belongs to the FUR family of metalloregulators that are ubiquitously present in prokaryotes and that also includes Zur (Zn uptake), Mur (manganese uptake), Nur (nickel uptake), PerR (peroxide stress response) and Irr (heme dependent iron responsive regulator) (Lee and Helmann 2007, Faulkner, Ma et al. 2012). Proteins of FUR family alter the expression of genes at transcriptional level by regulating in both positive and negative manner. Fur was first identified in *E. coli* but is present in both Gram-negative and Gram-positive bacteria. It functions as transcriptional repressor, bind to upstream of target gene with high affinity and inhibit its function in iron rich condition. Apart from iron binding site, studies have shown the presence of one structural Zn^{+2} atom per Fur monomer which helps in stabilizing dimer upon iron binding (Caux-Thang, Parent et al. 2015).

In iron-rich conditions, Fe^{+2} binds to Fur protein which causes dimerization of Fur, and this complex binds upstream of genes to a specific sequence called “Fur box” or “iron box” and blocks the expression of that gene (Baichoo and Helmann 2002). Fur box was initially found in *E. coli*, and with the help of foot-printing assays, it was shown that it is composed of the consensus

sequence 5’ GATAATGATAATCATTATC 3’. Initially, it was considered 9-bp inverted repeats separated by single base pair (9-1-9). However, consequence studies showed that Fur box consists of a head-head-tail orientation of three repeats of GATAAT motif rather than 9-1-9 palindrome (Escolar, Perez-Martin et al. 1998). Apart from Fe+2, another divalent cation, Mn^{+2}, can also bind to Fur and help in inhibiting gene expression. However, because of the relative richness of Fe^{+2}, it is considered a natural activator of Fur (Neilands 1995).

Fur function is not limited to iron regulation. Fur also modulates many other cellular processes, including signal transduction, synthesis of nucleic acid, zinc and manganese homeostasis, expression of virulence factors and toxicity, redox reactions, defense against oxidative stress, and redox regulation (Lee and Helmann 2007).

1.6. Ferric siderophore transport by TBDTs of ESKAPE pathogens:

Bacteria have evolved various molecular strategies to start the iron uptake process when in need of iron. This process involves a variety of outer membrane siderophores and/or Hn receptors on the cell surface. These specific systems of these diverse Gram-negative bacteria share an underlying mechanistic component: the TonB/ExbBD complex that provides energy to OM for active transport of ligand. In the case of ESKAPE bacteria, including *K. pneumoniae*, *A. baumannii*, *P. aeruginosa*, *E. coli,* and other Gram-negative bacterial pathogens, evidence shows a close relationship between iron acquisition and bacterial virulence. The activities of the different LGPs emphasize the significance of the generic and specialized iron transport mechanism of bacterial pathogenesis (Table 1.1). For example, uptake of FeAbn, FeGEnt, and Hn are consistently associated with invasiveness, tissue tropism, or infectivity in pathogenic variants of *E. coli* (UPEC and EHEC) and the pathogens of other genera. *P. aeruginosa* and *Y. pestis* both utilize

Hn from the host, and they produce both hemophore-dependent and -independent transport systems to obtain it. Most of the time, utilization of other ferric siderophores is highly specialized. Apart from *Y. pestis*, the CRE pathogens *E. coli* and *K. pneumoniae* both acquire FeYbt via FyuA, whereas *P. aeruginosa* does not encode such a receptor in its genome. *A. baumannii* is the exception of these commonalities as most of its strains do not transport FeAbn and Hn, but its genome encodes for several specific iron transport systems (Klebba, Newton et al. 2021) .

1.6.1. *E. coli*:

Most of the *E. coli* strains live in the gut of humans and animals as harmless commensal microbes. Moreover, some *E. coli* strains such as Nissle 1917 reduce symptoms of colitis and inflammatory bowel diseases in humans (Kokesova, Frolova et al. 2006). However, this harmless nature is not true for all *E. coli* strains. Some pathogenic determinants, e.g., siderophore biosynthetic genes, toxins, or other molecules which promote tissue invasion or tropism, are acquired by *E. coli* strains, making them pathogenic. There are numerous categories of pathogenic *E. coli*: ETEC (entero-toxigenic), EIEC (entero-invasive), EHEC (entero- hemorrhagic (including the widespread O157:H7)), EPEC (entero-pathogenic), EAEC (entero-aggregative), and AIEC (adherent-invasive). These pathogenic isolates usually possess additional iron acquisition systems which are not found in laboratory *E. coli* strains. For example, EHEC pathogenic strain O157:H7 obtains iron from Hn or hemoglobin through OM receptor ChuA (Torres and Payne 1997). Few of the LGPs are exclusively found in pathogenic strains compared to laboratory strains. However, some of the pathogenic strains also contain multiple receptors for a single ferric siderophore. For example, MG1655 possesses six OM receptors for iron uptake,

whereas UPEC strain produces 10-15, illustrating the connection between iron uptake versatility and virulence (Tang and Saier 2014).

1.6.2. *K. pneumoniae*:

K. pneumoniae strains produce four types of siderophore: Enterobactin (Ent), glycosylated form of Ent which is called salmochelin (GEnt/Sal), yersiniabactin (Ybt) and Aerobactin (Abn). The expression and role of each of the siderophores in virulence vary according to strain type. It is believed that *K. pneumoniae* secretes multiple siderophores in order to increase virulence and/or to avoid neutralization of one of the siderophores by the host and for successful colonization in the different tissues in the host (Miethke and Marahiel 2007, Holden and Bachman 2015). Out of these four siderophores secreted, enterobactin possesses the highest affinity ($K_D = 10^{-52}$ M), whereas aerobactin has the lowest affinity ($K_D = 10^{-27}$ M) for iron (Brock, Williams et al. 1991). Based on the phenotype of strains, *K. pneumoniae* can be categorized mainly into classical (cKP) and hypervirulent (hvKP) strains and enterobactin expression is ubiquitous among all known *K. pneumoniae* strains. It is widely accepted that *K. pneumoniae* utilizes this iron uptake system primarily. Genes that code for the proteins products required for the biosynthesis of the enterobactin in *K. pneumoniae* are carried on the chromosome in the entABCDEF gene cluster, whereas for the transport of the FeEnt, genes are carried on fepABCDEG gene cluster, fepA codes explicitly for the outer membrane receptor protein FepA which binds to FeEnt with high affinity (K_D = 0.4 AM) (Hsieh, Lin et al. 2008, Muller, Valdebenito et al. 2009, Chakravorty, Shipelskiy et al. 2019). Ent functionality is upregulated when fepA expression is enhanced at the time of *K. pneumoniae* infection. This increased expression of Ent is responsible for the colonization of and dissemination from lungs but a host innate immune protein lipocalin-2 (Lcn2, or neutrophil

gelatinase-associated lipocalin [NGAL], siderocalin, 24p3, or uterocalin) produced by neutrophils and mucosal surface at the time of infection, bind Ent, competing with the *K. pneumoniae* Ent receptor (Bachman, Oyler et al. 2011, Paczosa and Mecsas 2016). Lipocalin-2 shows a bacteriostatic effect as it does not allow some of the bacterial siderophore to scavenge iron by binding to them itself and inhibiting bacterial growth by not allowing bacteria to gain iron and proliferate. Apart from binding to Ent, lipocalin-2 shows some acute inflammatory effects: most probably through the production of IL-8, neutrophils are recruited at the site of infection when lipocalin-2 is overexpressed. So ultimately, *K. pneumoniae* strains which produce only Ent as a means for getting iron from the host, will be cleared from the host with the help of lipocalin-2 (Wasserman, Soter et al. 1977, Bachman, Miller et al. 2009, Bachman, Oyler et al. 2011).

Salmochelin (Sal), the glucosylated form of enterobactin (Runci, Gentile et al.) (Runci, Gentile et al.), is present in some of the isolates of *K. pneumoniae* that can evade Lcn-2. GEnt does not bind to lipocalin, and genes which confer expression of this modified version of enterobactin are present on either chromosome or plasmid within the iroA gene cluster, iroBCDE. This FeGEnt is transported by OM transporter IroN across OM bilayer (Bachman, Miller et al. 2009, Paczosa and Mecsas 2016). Because salmochelin is not recognized by lipocalin due to steric hindrance, there is no lipocalin dependent induction of inflammation at the site of infection and siderophore neutralization, and undoubtedly, in an Lcn-2-sufficient host, Sal expression is enough for the enhanced *K. pneumoniae* colonization of the nasopharynx (Bachman, Miller et al. 2009). Because of this property of evading Lcn-2, it is easy to predict that *K. pneumonia* strains that produce salmochelin are more virulent than strains producing only enterobactin. According to a study, more than 90% of hvKP strains associated with pyogenic liver abscess produce salmochelin, whereas

only 2 to 4% of the hospital-acquired infectious *K. pneumoniae* carry salmochelin (Bachman, Miller et al. 2009).

Another mixed type siderophore, yersiniabactin (Ybt) that can also evade lipocalin-2. This siderophore has a moderate affinity for iron ($K_D = 10^{-36.6}$ M). Originally it was discovered in Yersinia, but few other genera like Klebsiella also produce this siderophore (Wasserman, Soter et al. 1977, Bachman, Miller et al. 2009, Paczosa and Mecsas 2016). ybtQ encodes for the OM receptor protein, which helps in the transport of Ybt and irp gene encodes for the proteins required for the biosynthesis of this Ybt (Paczosa and Mecsas 2016). *K. pneumoniae* strains that express Ybt are not recognized by lipocalin-2 because of which there is increased bacterial load present during lung infection. However, in the presence of transferrin, Ybt cannot acquire iron for bacterial growth. Thus, bacteria fail to disseminate from the lung. It has been shown in mouse infection models that Ybt is a critical virulence factor for cKP strains but not for hvKP (Bachman, Miller et al. 2009, Paczosa and Mecsas 2016).

Aerobactin (Abn), a citrate-hydroxamate siderophore that has moderate affinity for the iron ($K_D = 10^{-27}$ M), is found mainly in hvKP strains (>90%) compared to the cKP strains (6%). Gibson and Magrath, in 1969, first isolated the aerobactin from the iron-deficient media of *Aerobacter aerogenes* (Gibson and Magrath 1969). It was reported that many *E. coli* virulent strains possessed aerobactin mediated iron transport system, which was either plasmid- or chromosomally encoded (Williams 1979, Warner, Williams et al. 1981). Aerobactin gene cluster iucABCD encodes for the biosynthesis of aerobactin, and iutA, which encodes for the transport of Aerobactin (Abn), are present on the same virulence plasmid. Independent groups have investigated and confirmed each of the components of the biosynthetic pathway. Firstly, sequential activities of the hydroxylase IucD and acetyltransferase IucB produce N6-acetyl-N6-hydroxylysine (ahLys) from L-lysine.

Then one molecule of ahLys is added to the primary carboxylate of citrate by the aerobactin synthetase IucA stereo-specifically. Subsequently, the second ahLys molecule is added to the same group by the second aerobactin synthetase IucC (Russo and Gulick 2019). Recently, a group confirmed this biosynthetic pathway by heterologous expression of all four genes in *E. coli* responsible for biosynthesis for aerobactin (Bailey, Alexander et al. 2018). Apart from carrying genes responsible for the biosynthesis and transport of the aerobactin, this plasmid also carries rmpA, which enhances the production of capsule production (Holden and Bachman 2015, Paczosa and Mecsas 2016). That is why most of the time presence of the aerobactin in the hvKP is associated with the hyper-capsule. One of the most important characteristics of the hvKP is that it has increased (6 to 10- fold) siderophore activity than cKP strains. Out of four siderophores produced by hvKP, only aerobactin accounted for more than 90% of siderophore activity (Russo, Olson et al. 2014). This siderophore is critical for optimum bacterial growth and survival in human ascites, serum ex vivo, and virulence in an outbred mouse systemic and pulmonary infection model (Russo, Olson et al. 2014). Being the primary virulence factor for hvKP, it is still unclear whether for the increased virulence of hvKP, enhanced total amount of siderophores or specific characteristics of aerobactin are the critical feature or not. However, it has been widely accepted and proven that genes that produce salmochelin and aerobactin are hvKP specific. However, salmochelin role in systemic infection and in the hvKP pathogenesis is yet to be defined (Russo, Olson et al. 2015, Russo and Marr 2019). Andrew M. Gulick's group exploited the existing knowledge about aerobactin production to use this pathway as an anti-virulence target as aerobactin seems to be one of the most important virulence factors for hvKP (Russo and Gulick 2019). They developed a high-throughput screening assay to identify compounds that inhibit aerobactin production and further probed hit compounds by orthogonal assays. High-throughput

screen used sensitive Malachite green (MG) based assay where byproduct pyrophosphate (PPi) was cleaved by inorganic pyrophosphatase (IPP) to produce inorganic phosphate (Pi). Both Initial screening employed over 110,000 commercially available compounds, and secondary screening identified several IucA inhibitors with activity at micromolar concentrations. Some of the properties like incubation time, target enzyme dependence, and potential to antagonize unrelated enzymes were shown by the compounds identified by this new screening method. However, the development of this validated HTS format would be helpful to move forward in the right direction. One of the most significant advantages of finding out inhibitors for this pathway's proteins, which are new targets, is that inhibitors will not be affected by pre-existing antimicrobial resistance determinants, as these are new targets (Bailey, Alexander et al. 2018).

1.6.3. *A. baumannii*:

A. baumannii belong to Gram-negative *coccobacillus* in the Family *Moraxcellaceae* which is short, nonmotile, rod-shaped, oxidase- negative. *A. baumannii* is one important organism responsible for hospital acquired infections. According to reports in 2019, nosocomial infections which were caused by this bacterium, half of the strains were carbapenem-resistant *Acinetobacter* (Ayobami, Willrich et al. 2019). The increasing propensity of this bacterium to acquire antibiotic resistance is a serious threat to human health, and urgent treatments are required to combat deadly infections e.g., pneumonia, wound, bloodstream, and urinary tract infections caused by this bacterium. Additionally, this bacterium promotes abnormally high mortality rate compared to other Gram-negative bacteria. Further *A. baumannii* illustrate the impact of iron acquisition on pathogenesis as it produces atypical siderophores to capture iron in host environment and alter its

OM protein composition in order to optimize the uptake of its own and other ferric siderophores (Actis, Tolmasky et al. 1993, Daniel, Haentjens et al. 1999, Dorsey, Beglin et al. 2003).

Table 1.1. TonB dependent receptors:

TBDTs	Strain	Ligand	Amino acid residues	Mass (Da)
Commensal *E. coli*				
FecA	MG1655	FeCit	741	81,707
FepA	MG1655	FeEnt	724	79,771
FhuA	MG1655	Fc	714	78,742
Fiu	MG1655	FeDHBS	727	78,432
FhuE	MG1655	FeRta	693	77,411
Cir	MG1655	FeDHBS	638	71,149
BtuB	MG1655	B_{12}	594	66,325
Pathogenic *E. coli*				
IutA	083:H1	FeAbn	708	78,061
IroN	083:H1	FeGEnt	701	76,525
ChuA	0157:H7	heme	632	69,436
YncD	UPEC C15	heme	677	74,900
YddB	UPEC 042	heme	771	87,206
LGP1	0157:H7	heme	634	71,005
LGP2	0157:H7	heme	687	76,150
K. pneumoniae				
FepA1	Kp52145	FeEnt	717	79,665
FepA2	Kp52145	ND	701	77,382
FepA4	Kp52145	FeEnt	728	80,070
IroN	Kp52145	FeGEnt	700	76,760

FhuA	Kp52145	Fc	715	79,054
Fiu	Kp52145	FeDHBS	727	78,023
FhuE	Kp52145	FeRTA	695	76,897
Cir	Kp52145	“	632	70,367
BtuB	Kp52145	B_{12}	592	66,035
IutA	Kp52145	FeAbn	708	78,043
ChuA	Kp52145	heme	613	67,571
FyuA	Kp52145	FeYbt	652	71,400
YncD	hvKP1	Not Defined (ND)	677	74,569
FcuA	hvKP	“	703	76,166
LGP1	hvKP	“	680	74,658
LGP2	hvKP	“	737	81,135
A. baumannii				
Fiu	17978	FeDHBS	771	84,285
FepA	17978	FeEnt	730	80,248
FhuA	17978	Fc	679	75,739
BtuB	17978	B_{12}	598	65,781
BfnH	17978	FeBfn	728	80,491
PiuA	17978	FeDHBS	736	80,054
PirA	17978	FeDHBS	714	78,022
BauA	17978	FeAcn	712	77,497
FbsN	17978	FeFbn	629	68,763
LGP1	17978	ND	862	93,996
LGP2	17978	“	781	88,811
LGP3	17978	“	697	78,847
LGP4	19606	“	674	77,325

LGP5	19606	“	681	75,757
LGP6	19606	“	669	74,690
LGP7	19606	“	613	65,455

This table illustrate the TonB dependent receptors from variety of pathogens, their ligand, information originated from bacterial strains, number of the amino acids in mature protein and molecular weight. For the extensive details, please see (Klebba, Newton et al. 2021).

Virulence of A. *baumannii* is affected by iron deficiency and in that response this bacterium upregulates the expression of genes which are involved in iron acquisition, biofilm production, respiration and motility (Eijkelkamp, Hassan et al. 2011, Nwugo, Gaddy et al. 2011, Runci, Gentile et al. 2019). Ferric uptake regulator (Fur) negatively regulates the expression of iron-related biosynthetic and transport genes by binding to “Fur box” region which is present upstream of these related genes. This Fur box is found in a wide range of strains of *A. baumannii*. In particular, the primary structure of *A. baumannii* strain BM2580 shows 63% identity to Fur box of *E. coli* K-12. Apart from this, temperature also affects the upregulation of iron uptake system; upregulated more at 28°C compared to 37°C (Daniel, Haentjens et al. 1999, Mihara, Tanabe et al. 2004, Eijkelkamp, Hassan et al. 2011).

Acinetobactin (Goldenzweig, Schwartz et al.), Baumannoferrin (BfnA, BfnB) and fimsbactin (Fbn) are three native, chromosomally encoded siderophores of *A. baumannii* but apart from that other putative siderophore encoding genes clusters also exist (bioinformatically annotated) in the genome but they are not yet functionally characterized.

Acn (Yamamoto, Okujo et al. 1994) is the most studied siderophore in *A. baumannii* and this gene cluster is found in the majority of the clinical isolates and sequenced genome except *A. baumannii* SDF (Vallenet, Nordmann et al. 2008, Antunes, Imperi et al. 2011, Eijkelkamp, Hassan

et al. 2011). Acn exist in two forms: preacinetobactin (pAcn) and Acn, and under acidic condition they undergo conformational changes. This pH-dependent conformational change exists at the site of acute infection which makes this duo form virulence factor. Also, both form pAcn/Acn bind to iron as 2:1 complex and in iron deprived condition, both forms enable *A. baumannii* growth (Shapiro and Wencewicz 2016, Harding, Hennon et al. 2018). Although OM protein BauA is the pertinent receptor for FeAcn based on the crystalized structure of BauA in complex with FeAcn, yet exact selectivity of BauA for FepAcn and FeAcn is uncertain because both compounds promote growth. Furthermore, periplasmic protein BauB binds both FepAcn and FeAcn with nanomolar affinity (Bailey, Bohac et al. 2018, Bohac, Fang et al. 2019).

In *A. baumannii*, presence or absence of siderophore biosynthetic or transport gene can affect the extent of its virulence. For example, Acn synthesis is required for *A. baumannii* pathogenesis: Acn synthesis and transport protein BasD and BauA, respectively, are virulence determinants of *A. baumannii* ATCC 19606T in the Galleria mellonella larvae infection model and in a murine model of systemic infection (Gaddy, Arivett et al. 2012, Russo and MacDonald 2020).

A. baumannii AYE has another siderophore biosynthetic cluster in their genome which encodes hydroxamates siderophore BfnA and B, which are less genetically and biochemically defined (Penwell, DeGrace et al. 2015). *A. baumannii* AYE does not contain entA locus so it does not produce Acn. Biosynthetic and transport gene cluster for this siderophore consist of bfnA-L and exists in majority of sequenced strains and BfnH is the OM protein that recognize and bind to Bfn. The role of BfnA and B in the pathogenesis is yet not clear (Penwell, Arivett et al. 2012, Penwell, DeGrace et al. 2015).

Acinetobacter strains *A. baylyi* ADP1 produce third type of iron acquisition system gene cluster fbnA-F which contains mixed chelation (catechol-hydroxamate) group. FbnA is

predominant siderophore in this group which is recognized by OM receptor FbnS and then periplasmic protein BauB, their role of Fbn in pathogenesis is not yet clear (Proschak, Lubuta et al. 2013, Bohac, Fang et al. 2019).

Apart from these ferric siderophore system, *A. baumannii* also rely on the hemin (Hn) as iron source from host. Like many other bacterial pathogens, *A. baumannii* shows hemolytic activity in iron deprived condition (Fiester, Arivett et al. 2016) and as a consequences release Hn from erythrocyte hemoglobin. Many strains of this bacteria contain *plc1* and *plc2* that encode phospholipase C enzyme that has the capability to lyse host red blood cells (Vallenet, Nordmann et al. 2008, Antunes, Imperi et al. 2011, Fiester, Arivett et al. 2016). Especially *plc1* plays vital role for the virulence of *A. baumannii* ATCC 19606 in the Galleria mellonella infection model (Fiester, Arivett et al. 2016). According to reports three different phospholipase D enzymes also affect *A. baumannii* virulence but their role in iron acquisition is not known yet (Jacobs, Hood et al. 2010, Antunes, Imperi et al. 2011).

1.6.4. *P. aeruginosa*:

P. aeruginosa is catalase and oxidase-positive Gram-negative bacillus which belongs to *Pseudomonadaceae* family that forms biofilm and is responsible for a variety of diseases in plant, animals and humans. This is an opportunistic pathogen which causes serious diseases in patients who are suffering from cystic fibrosis. Mucus formation in relevant tissues associated with this disease favors *P. aeruginosa* to readily colonize with biofilms that directly corelates with its virulence (Lamont, Konings et al. 2009). Like other bacteria, it also employs strategies like siderophore secretion to obtain iron from host tissues and depend on the type of infection (acute

or chronic), it adjusts its preferred iron source to minimize the energy need to obtain it from host (Peek, Bhatnagar et al. 2012).

P. aeruginosa usually synthesize mainly two atypical siderophores; pyochelin; Pch (Liu and Shokrani 1978) and pyoverdine; Pvd (Cox and Adams 1985)to overcome the need of iron. Pch (324Da) has lower molecular weight than Pvd (482Da). Surprisingly, Pch has the lower affinity for Fe^{3+} (K_D= 10^{-5} M) (Brandel, Humbert et al. 2012) compared to other known siderophores exist in nature. For the biosynthesis of Pch, fewer genes are expressed compared to biosynthesis of Pvd that's why when the environmental iron level drops down below micromolar level, Pch is produced first by *P. aeruginosa* (Dumas, Ross-Gillespie et al. 2013). On the other hand, Pvd has higher affinity for Fe^{3+} (K_D= 10^{-32} M) (Wolz, Hohloch et al. 1994) which makes it easier for this siderophore to remove iron from LF/TF (Jeong, Hawes et al. 1997). One of the advantages of is that this siderophore is not recognized and removed from the circulation by SCN. The role of Pvd in *P. aeruginosa* pathogenesis is not limited to only capture iron as apart from regulating its own synthesis. It also regulates the expression of two other extracellular virulence factor, the protease Prp and exotoxin A. It is also reported that strains that do not produce Pvd are less virulent compared to reduction in the virulence in TonB deficient strains in murine and rabbit infection model (Klebba, Newton et al. 2021).

1.7. Significance of the work:

Iron is a fundamental metal for bacteria, and it works as cofactor in a variety of metabolic process. The unique TonB dependent iron acquisition system presents it as a vulnerable target for Gram-negative bacteria using immunochemical inhibition or chemically targeting TonB action. Attempts have been made to block the iron transport process by using anti-TBDT antibodies that

prevent the recognition and binding of ferric siderophores by binding to loops involved in the binding process. To generate these kind of vaccines, rough *E. coli* K-12 has been used, which raises the questions about the efficacy of these antibodies against ESKAPE pathogens because these pathogens are encapsulated and produce lipopolysaccharide (LPS) O-antigens that shield TBDT surface epitopes from antibody binding. So, the concept of these kinds of immunochemical intervention faces practical problems which would be difficult to circumvent. For the chemical interventions, the best target would be blocking the ligand uptake process by blocking the action of TonB, which is ubiquitous for iron acquisition in all Gram-negative bacteria. However, it is not entirely feasible that the compound which inhibits EcoTonB action could inhibit TonB action in other pathogens, e.g., *K. pneumoniae, A. baumannii,* and *P. aeruginosa*. Because these pathogens differ in nucleotide sequence identity of *tonB*, which raises the point that generic chemical compounds could not inhibit TonB action in all pathogens. Apart from that, targeting individual ligand-TBDT binding reactions by generic chemical compounds would also face similar problems as diversity in the TBDT in different bacteria. A search for therapeutics requires an assay that can identify them. This study created a species-specific fluorescent spectroscopic assay that observes real-time TonB dependent ferric siderophore/ metal complex uptake reaction in ESKAPE pathogens. Subsequent fluorescence quenching and recovery gives an edge to adapt this method in microtiter format and screen for chemicals that can inhibit this uptake reaction, followed by secondary assays to validate specific inhibition. Such chemicals may constitute novel therapeutics that can thwart pathogenesis by blocking TonB action. To eliminate the need to deal with experimental manipulations of hazardous ESKAPE pathogens, we converted these species-specific assays into universal fluorescence assays in a manner where we could screen for inhibitors of TonB actions of multiple organisms simultaneously. High throughput screening assays using

fluorescence spectroscopic methods may provide novel therapeutics that may prevent iron acquisition in humans and animals and may constitute novel therapeutics that can thwart bacterial infectious diseases. These universal fluorescence assays will also help understand uncharacterized iron acquisition pathways of known/unknown bacteria by providing information about iron uptake capabilities of different kinds of ferric siderophores across the outer membrane.

In the latter part of the study, we created multiple fluorescent decoy sensors that work as analytical tools for diagnosing bacterial pathogen siderophores and studying microbial iron acquisition. These FD sensors provide information about the presence, concentrations (nanomolar), the specific profile of siderophores and discriminate against structurally similar ferric complexes as well in a mixture. This technique is faster, simple, reproducible, and less hazardous than radioactive methods. These assays can detect the presence of siderophores in infected human and animal organs, tissues, and fluids, pathogenic microorganisms contaminate meats, foods, and other agricultural products. In some cases, characteristic siderophores are diagnostic of organisms. Also, these sensors have capabilities to detect the pathways or LGP that binds to siderophore conjugated antibiotics and ultimately provide complete information about the biochemical attributes, e.g., binding affinities and transport kinetics.

Chapter 2 - Materials and methods

This section describes the methods used for the complete study. Any specifications in the plans or additional procedures are described separately in respective chapters.

2.1. Bacterial strains and plasmids:

Overnight cultures of *E. coli, K. pneumoniae* Kp52.145 (Lery, Frangeul et al. 2014), *P. aeruginosa, A. Baumannii ATCC19798/ATCC 19606, E. cloacae (Rutz, Abdullah et al. 1991)* or any other bacteria used in the study were grown in Luria-Bertani (LB) broth (BD Difco, USA) in the presence of appropriate antibiotics at 37°C with shaking at 200 rpm. For different purposes e.g., nutrition assay, fluorescence assay, cells were sub-cultured in Nutrient Broth (NB) or iron-free MOPS (Neidhardt, Bloch et al. 1974) minimal medium reconstituted with micronutrients and amino acids, as required according to the need of the experiment. Antibiotics were used as follows: Streptomycin – 100 µg/ml, Chloramphenicol – 20 µg/ml, Ampicillin -100 µg/ml.

Table 2.1. List of strains used for study:

Strains	Relevant genotype	References
MG1665	F^-, λ-, *rph-1*	(Blattner, Plunkett et al. 1997)
BN1071	F^- *thi entA pro trp rpsL*	(Klebba, McIntosh et al. 1982)
BL21	F^- dcm ompT hsdS (rB^-mB^-) gal	Stratagene
OKN1	BN1071 *ΔtonB*	(Ma, Kaserer et al. 2007)
OKN3	BN1071 *ΔfepA*	(Ma, Kaserer et al. 2007)
OKN13	BN1071 *ΔtonB ΔfepA*	(Ma, Kaserer et al. 2007)

OKN359	BN1071 *ΔfepA ΔfiuA Δcir*	(Ma, Kaserer et al. 2007)
NEB5α	K-12 *fhuA2 recA1 relA endA1 thi-1 hsdR17 Δ (lacZ)M15*	New England Biolabs
KKN5	Kp52.145 *ΔentA ΔfepA_1658 ΔfepA_4984 ΔfepA_2380 ΔfepAp_0027*	This study

Table 2.2. List of plasmids used:

Plasmid	Relevant genotype	References
pHSG575	Cm^R	(Hashimoto-Gotoh, Franklin et 1981)
pITS23	*E. coli fepA*$^+$ on pHSG575	(Smallwood, Marco et al. 2009)
pITS25	*K. pneumoniae fepA*$^+$*_1658* on pHSG575	This study
pITS26	*K. pneumoniae fepA*$^+$*_4984* on pHSG575	This study
pITS27	*K. pneumoniae fepA*$^+$*_2380* on pHSG575	This study
pITS28	*E. coli iutA*$^+$ on pHSG575	This study
pITS29	*E. coli btuB*$^+$ on pHSG575	This study
pITS30	*A. baumannii piuA*$^+$ on pHSG575	This study

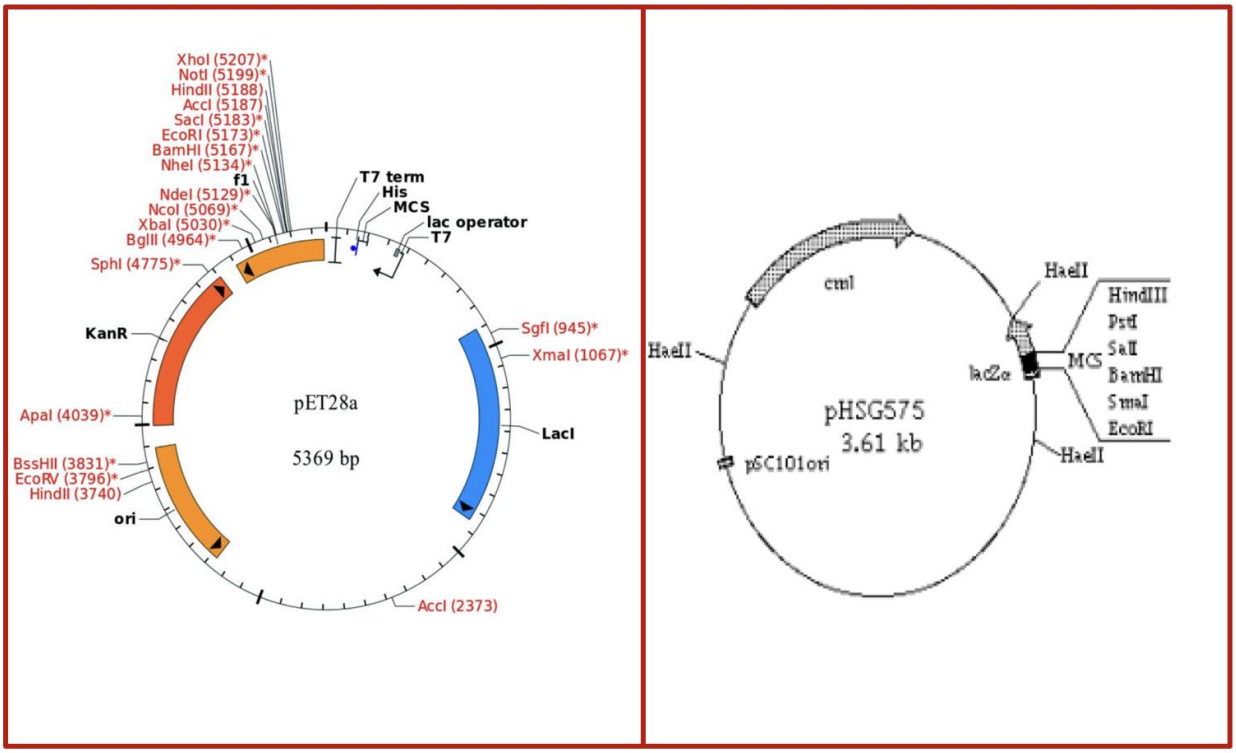

Figure 2.1. Plasmid Maps of His-tag expression vector pET28a and *E. coli* expression vector pHSG575:

2.2. Plasmid isolation:

We used the QIAquick Miniprep kit from QIAGEN and followed the protocol recommended in their guidebook for performing isolation of plasmid (minipreps). For the isolation of a low-copy number of plasmid and their derivatives, we used 5 ml cell culture grown in LB and used double volumes of buffer recommended. The entire volume was passed through a single QIAquick miniprep spin column, washed thoroughly with wash buffers, and eluted in 20-25 ul nuclease-free de-ionized water or elution buffer. Alternatively, we used Monarch Plasmid Miniprep kit from New England Biolabs for the same purpose, following the protocol recommended by the company.

We used the QIAquick PCR purification kit and QIAquick Gel extraction kit, both from QIAGEN, to purify PCR products and extract DNA from agarose gels, using the recommended protocol.

2.3. One step gene replacement using PCR product:

We performed one-step in-frame gene deletion to delete chromosomal genes in *K. pneumoniae* Kp52.145 strain (Datsenko and Wanner 2000). We used PCR amplified product with an antibiotic cassette flanked with 36 nucleotides (nt) on both sides, homologous to the target gene. Briefly, we transformed pKD46 encoding λ-Red recombinase into host strain and selected transformants on LB agar containing ampicillin at 30°C. We grew transformants in 20 mL of SOB cultures with ampicillin and 2% L- (+) arabinose until O.D. at A_{600} nm reached 0.5 to 0.6 and made them electrocompetent (competent cell preparation). For deletion, we amplified PCR product (~1.1 kb with 36 nt flanking homologous) by amplifying a chloramphenicol-resistance gene cassette from pKD3 template plasmid, incubated with DpnI, and purified the product from the agarose gel. We transformed these products using electroporation and selected transformants on an LB agar plate containing chloramphenicol after overnight incubation. Transformants were grown in LB with antibiotics, isolated the plasmids, and checked for proper deletion by PCR using different primers.

To make the clean deletion, we deleted the chloramphenicol cassette by introducing by transformation into the strain a helper plasmid called pCP20, that expresses a FLP-recombinase. The action of the enzyme takes place at 42°C, a temperature that at the same time causes the plasmid to be lost from the bacterial cell (its replication is thermo-sensitive). Then we selected colonies at 30°C on ampicillin plates. The few colonies we chose were non-selective at 43°C for

thermal activation of FLP and loss of antibiotic resistance. We finally verified the loss of antibiotic resistance cassette by PCR and sequencing with appropriate primers.

2.4. Preparation of competent cells using $CaCl_2$ and heat-shock transformation:

We grew 5 ml LB culture of host strain overnight in the presence of appropriate antibiotics. Then we sub-cultured cells (1:50) in 50ml LB containing antibiotics and incubated at 37°C in shaking condition until O.D. 600 nm reached 0.5 (mid-log phase; takes 2-3 hours) and kept the cells on ice for 30 minutes. The culture was transferred to Corex tubes and centrifuged at 5000 rpm for 10 minutes at 4°C. We discarded the supernatant, resuspended the pellet very gently in 25 mL of ice-cold 0.1 M $CaCl_2$, and kept cells on ice for another 20 minutes. In the final step, we again centrifuged cells, discarded the pellet and, resuspended the pellet in 0.5 mL ice-cold 0.1M $CaCl_2$, 15% glycerol mix. We prepared 100 ul aliquots of cells, immediately stored at -80°C freezer, and used these aliquots whenever the needed it for heat-shock transformation.

For heat-shock transformation of competent cells, we took an aliquot of competent cells and thawed it on ice (usually takes less than 5 minutes), and 100 ng of plasmid was added to the cells, mixed gently, and kept on ice for another half an hour. Cells were then heat shocked (42°C) for exactly 90 seconds, and then kept on ice for 2 minutes, and then 900 ul of LB was added to cells and allowed for incubation at 37°C for another one hour. We plated 100 ul cells on an LB-agar plate containing proper antibiotics and allowed incubation at 37°C overnight. The next day, we observed the plate and selected a single colony for future experiments.

2.5. Preparation of electrocompetent cells and electroporation:

For *E. coli* competent cell preparation, we grew a 5 ml LB culture of host strain overnight in the presence of appropriate antibiotics. Then we sub-cultured cells (1:50) in 50 ml LB containing antibiotics and incubated at 37°C in shaking condition until O.D. 600 nm reached 0.5 (mid-log phase; takes 2-3 hours) and kept the cells on ice for 30 minutes. The culture was transferred to Corex tubes and centrifuged at 7500 rpm for 10 minutes at 4°C. We discarded the supernatant and resuspended the pellet very gently in 20 mL of ice-cold distilled water and centrifuged again. We repeated the washing step twice, first with 10 ml and then 5 ml distilled water. This time, we resuspended the pellet in 2 mL ice-cold sterile 10% glycerol water. Again, centrifuged cells for another 5 minutes, discarded the pellet, and resuspended pellet in 200 ul ice-cold sterile 10% glycerol water. We prepared 40 ul aliquots of cells, immediately stored at -80°C freezer, and used these aliquots whenever needed for electroporation.

For *K. pneumoniae* electrocompetent cell preparation, we grew a 5 ml LB culture of host strain overnight in the presence of appropriate antibiotics. Then we sub-cultured cells (1:50) in 10ml LB containing antibiotics and incubated at 37°C in shaking condition until O.D. 600 nm reached 0.5-0.6 (mid-log phase; 2-4 hours) and kept the cells on ice for 30 minutes. We transferred 9 ml cell culture to Corex tubes and centrifuged at 14000 rpm for 20 minutes at 4°C. We discarded the supernatant, resuspended the pellet in 4 ml of ice-cold distilled water, and centrifuged again, and repeated this process twice. Finally, we resuspended the pellet in 400 ul of ice-cold water, centrifuged again, discarded supernatant, and immediately used the resulting pellet for electroporation. We usually prepared fresh electrocompetent cells using *K. pneumoniae* strain and used them immediately.

We used an *E. coli* gene Pulser instrument (Bio-Rad) for electroporation; we used the same for *K. pneumoniae* competent cells. We thawed electrocompetent cells on ice and gently mixed 50 ng of salt-free plasmid with the cells. We transferred this mixture to pre-chilled electroporation cuvette and made sure the cells were at the bottom of the cuvette. Cells were pulsed at a preset voltage of 2.5 kV for around 2 seconds. Immediately after the pulse was complete, we added 750 ul of super optimal broth with catabolic repression (SOC) media and transferred this mixture to a fresh centrifuge tube and incubated it shaking for one hour at 37°C. After incubation, we plated 100 ul cells on an LB-agar plate containing proper antibiotics and allowed incubation at 37°C overnight. The next day, we observed the plate and picked a single colony for future experiments.

2.6. Site-directed mutagenesis:

Throughout the study, for the site-specific Cysteine (Cys) residue substitutions, we used two-stage PCR based using QuikChange Site-directed Mutagenesis (Stratagene Cloning Systems, San Diego, CA) method. We started two separate PCR reactions with single primers (forward and reverse) for five reaction cycles and mixed these two reactions and ran another 18-20 reaction cycle for amplification. For mutagenesis PCR, we used PfuTurbo Cx Hot-Start DNA Polymerase (Agilent Technologies). We set two separate 50 ul reactions using 10X PfuTurbo Cx buffer, 0.1-0.2 ug DNA template, 0.2 mM dNTP mix, 100 ng/µL of Primer (forward or reverse), and 0.5 µL DNA Polymerase. We set thermal cycling at 95°C for 2 minutes, 94°C for 30 seconds, 60°C for 1 minute, and extension at 68°C for 2 minutes/kb of template for five cycles. In the next step, we mixed 25 ul mixture of two reactions in a separate PCR tube and added 1 ul of DNA polymerase to it and set this reaction in thermal cycler for another 18-20 cycle using the same set up of denaturing, annealing, and extension conditions as before. We used 25 ul of this final product for

further processing and added 1 ul of DpnI (New England Biolabs) in 25ul PCR product and incubated it for two hours at 37°C. We directly used this final product for transformation by any of the two methods discussed above section.

2.7. Prediction of the tertiary structure of Outer Membrane (OM) proteins and Cys substitution sites:

For site-directed mutagenesis, we first predicted the tertiary structure of the proteins, e.g., KpnFepA_1658, with the help of the Modeler function of the CHIMERA program. We looked for the identity between the primary structure sequence in a related outer membrane transporter to use those proteins as a reference for predicting the overall fold of these non-crystallized receptors. It was important to predict the structures of the OM receptors used in these studies to facilitate the choice of locations to introduce Cys substitutions in the protein structure to label it with a suitable fluorophore. For example, we engineered the mutations in pKpnFepA_1658 using a QuikChange II XL mutagenesis kit (Agilent, Santa Clara, CA). Using pKpnFepA_1658 as a template, we introduced Cys substitution at position I218C, D273C, A324C, A382C, T545C, and T693C. We verified changes performed in these constructs by DNA sequencing analysis. We transformed these constructs in *E. coli* and *K. pneumoniae fepA*- host and evaluated FeEnt transport by both siderophore nutrition assay and fluorescence spectroscopic assay. We used the same strategy while working with other receptors, which we explained in respective chapters.

2.8. Siderophore nutrition test:

This test is a modified qualitative assay to observe cells' ability to transport siderophore, e.g., FeEnt transport by FepA, in the presence of a chelator in media. After growing the cells

overnight in LB, we sub-cultured cells in nutrient broth (NB) for 5-6 hours at 37°C with appropriate antibiotics. *E. coli* does not transport apo-ferrichrome A (apoFcA), so we used apoFcA as a specific chelator of Fe^{+3} in the media to the final concentration of 100 uM. We added chelator, antibiotics, and 100 ul bacterial cells in a glass tube. Then added 3 ml of molten NB Top agar in another glass tube, mixed them properly, placed them in a 6-well cell culture plate, and let it solidify. After the agar solidified, we put a sterile disc in the middle of each well, added 5ul of respective siderophores at 50 uM on the disk, and put the plates overnight (9-10 hours) for incubation at 37°C. Results were visualized next day. For some experiments, we added BME along with cells for the reduction of disulfide bonds.

2.9. Protein purification using Ni-NTA affinity column:

We used this method to purify his-tagged proteins, e.g., EcoFepB. We used an overnight grown culture of *E. coli BL21* containing pET28a_FepB and Cys mutants in LB with kanamycin (50ug/mL) at 37°C, shaking at 200 rpm. Then we sub-cultured cells 1:100 in 200 ml LB containing antibiotics and incubated it the same shaking incubator at 37°C. We waited until O.D. 600 nm reached 0.5 (mid-log phase; usually takes 2-3 hours), and added 0.1mM IPTG to the culture, and allowed for incubation for another 4-5 hours. Then we centrifuged the cells at high speed; 10000 x g for 10 minutes and resuspended the pellet in 20 ml of lysis buffer (PBS pH 7.4 with DNase, RNase, 2mM DTT, and 5 mM Imidazole). To lyse the cells, we used a French Press with a pressure of 14,000 psi and centrifuged the resulting lysate at 5000 x g for 10 minutes to remove unbroken cells and cell debris. To remove the cell membranes in the supernatant, we spun down the sample in ultracentrifuge; 30000 x g for 30 minutes and saved cytoplasmic fraction; supernatant for purification. We passed the cytoplasmic fraction three times over a Talon Superflow cobalt resin

column to bind the His-tag-containing proteins. Then we washed the protein-bound column with two column volumes of PBS pH 7.4 with 5 mM imidazole, then five column volumes of PBS pH 7.4 with 20 mM imidazole, and a final wash step of five column volumes of PBS pH 7.4 with 40 mM imidazole. We used 20 ml PBS pH 7.4 with 250 mM imidazole for the elution of His-tagged protein. Ten fractions (2 ml each) were collected and applied on SDS-PAGE followed by Coomassie dye staining to evaluate the presence of desired protein. We observed a significant amount of protein in the 40 mM imidazole wash fraction and 250 mM eluted fraction. We pooled relevant eluted fractions with most of the protein and dialyzed them against labeling buffer (4-5 times) to remove imidazole. To concentrate protein, precipitated it with 7 volumes of cold acetone, mixed and kept in -20°C overnight. The next day, we spun down the sample at 10000 x g for 30 minutes and immediately removed acetone and kept the sample for drying for 5 minutes, and then added 500 ul of labeling buffer and used for fluorophore labeling and binding experiment.

2.10. Analysis of expression of OM proteins:

We studied the expression and fluorescent labeling (described in detail in other methods) of TonB dependent transporters by SDS PAGE analysis and immunoblot of outer membrane fractions and whole-cell lysates. We used overnight grown cells in LB and sub-cultured cells in minimal media MOPS for 5-6 hours at 37°C with appropriate antibiotics until cells reached O.D. 600 nm ~1.0. We loaded the cells on 10% SDS-PAGE gel for gel- electrophoresis after lysing cells by boiling for 5 minutes with SDS-PAGE boiling buffer. After completing gel electrophoresis, we transferred protein gel to nitrocellulose membrane using a semi-dry western transfer apparatus (Bio-Rad). We blocked the membrane for 30 minutes with blocking buffer; TBSG (1X TBS plus 1% gelatin). We discarded the blocking buffer and placed the membrane in a box containing mouse

anti-FepA monoclonal mAb41 (Murphy, Kalve et al. 1990) solution and incubated it overnight at 4°C. The next day, after taking out antibody solution, we washed the membrane five times, 5 minutes each, with TBS plus a 0.05% Tween 20 solution. After washing, we placed the membrane in a dish that contained 300 ul [^{125}I]-protein A conjugate in 15 ml TBS buffer for about 3 hours and then exposed it to an autoradiography imaging screen overnight. We visualized the adsorbed [^{125}I]-protein on a Typhoon 8600 Biomolecular Scanner (GE/Amersham Biosciences).

2.11. Fluorescent labeling of Cys mutants and SDS-PAGE:

For the fluoresceination of outer membrane (OM) receptors in live *E. coli* cells or any ESKAPE bacterial cells, we used overnight grown bacterial cells in Luria broth (LB) and sub-cultured (1:100 dilution) in MOPS media with appropriate antibiotics until the optical density at 600 nm reached 1.0 to 1.5 (5-6 hours). After getting to the desired O.D., we pelleted down bacterial cells at 7000 x g for 10 mins and resuspended them in labeling buffer (50 mM NaHPO4, pH 6.7) and centrifuged the cells at the same condition again for one more time. After adding labeling buffer again to the resulting pellet from the previous step, we labeled cells by adding freshly made 5 uM fluorescein maleimide (FM) (E_{493} nm = 81,500 M^{-1} at pH 8.0) to the cells and incubated cells for 15 min at 37°C (shaking condition), quenched the reaction with 130 mM 2-mercaptoethanol (BME), pelleted, washed the pellet with phosphate-buffered saline (PBS) and resuspended the pellet again in phosphate-buffered saline (PBS) and used these cells for SDS-PAGE, outer membrane separation and, for spectroscopic binding. For spectroscopic transport assay of siderophore, we used PBS + 0.4% glucose.

2.12. Preparation of Outer membrane (OM) fractions:

For separation of OM fraction, we used overnight grown bacterial cells in Luria broth (LB) at 37°C and sub-cultured (1:100 dilution) in MOPS media with appropriate antibiotics until the optical density at 600 nm reached 1.0 to 1.5 for *E. coli* cells (5-6 hours). We pelleted cells at 5000 x g for 10 minutes, resuspended the pellet in 2 ml lysis buffer (50 mM tris Cl, pH 7.5), and added an appropriate amount of DNAse and RNAse. We used French press to break the cells at 14000 psi, passing the bacterial suspension two or three times. Then we centrifuged cell lysate at 3000 x g for 10 mins to remove cell debris, transferred the resulting supernatant in a microfuge tube, and centrifuged at 14000 x g in Beckman centrifuge for an hour to separate cell envelop (pellet) and cytosol/periplasm (supernatant). After this, we discarded the supernatant and resuspended the pellet again in 200 ul of lysis buffer with 200 ul of 1% Sodium lauroyl sarcosinate (sarkosyl) and incubated this mixture for 30 mins at room temperature and then again centrifuged for another hour for separation of IM (supernatant) and OM (pellet). We resuspended the resulting pellet in distilled water which contained OM fraction and used it for SDS-PAGE.

2.13. Fluorescence spectroscopic assay:

We performed spectroscopic assays using an SLM/OLIS spectrofluorometer with an SLM 8000 chassis (Aminco, Lake Forest, CA), upgraded to automatic control by an OLIS central processing unit, operating system, and analysis software (OLIS, Inc., Bogart, GA). The excitation and emission wavelengths we used for all assays were 488 and 520 nm, respectively. For fluorescence assays of siderophore transport, we used 2 x 107 cells per ml diluted in buffer (PBS + 0.4% glucose) in a 3 ml quartz cuvette, and the temperature of the cuvette chamber was 37°C. We allowed the initial fluorescence reading to stabilize. At 100 seconds, we added a siderophore

in the cuvette at a proper concentration and monitored the change in fluorescence reading during binding and transport. For the universal assay, we added a sensor (fluorescent-labeled cells; binding competent but transport deficient) with desired test strain, e.g., ESKAPE bacteria, and after adding siderophore at desired final concentration, we tracked change in fluorescence emission. For binding assay, we used only sensor strains and added siderophore at different concentrations at the interval of 100 seconds gradually until the fluorescence quenching was stabled and then collected the data.

2.14. Statistical analysis:

For spectroscopic analysis of ferric siderophore transport assays, we performed all experiments in triplicates and plotted the mean of the normalized fluorescence on the y-axis and time (second) on the x-axis.

For the binding assays, for each data points, we performed experiments in triplicates and made 3 determinations of the fluorescence quenching in response to gradually increasing concentration of ferric siderophores complex. The graphs represent non-linear fits of the mean values to a single-binding site model using Grafit 6.2 (Erithacus Ltd. West Sussex, UK). Resulted Std. errors are shown for each data point as vertical bars. The mean std. errors of the K_D values from the fitted curves were in the range of 15% to 30% for each binding affinity curve we created, for example: EcoFepA_A698C-FM = 17.3%, KpnIroN_T210C-FM = 26.3%, AbaFepA_S278C-FM = 21.1% and PaeFepA_S271C-FM = 22.4%.

Chapter 3 - Functional characterization of ferric siderophore receptors of *Klebsiella pneumoniae*

3.1 Introduction:

Antibiotic drug-resistance among bacteria is a significant challenge for healthcare providers across the globe. Threats posed by these pathogens are further aggravated by the incidences of Multi-Drug Resistant (MDR) and Extremely Drug-Resistant strains (XDR) (Navon-Venezia, Kondratyeva et al. 2017). Unless the incidences of antibiotic resistance are slowed down, by 2050, at least 10 million lives per year and economic output worth 100 trillion USD will be lost to drug-resistant infections (Navon-Venezia, Kondratyeva et al. 2017). Among the vast array of infectious bacteria, the ESKAPE pathogens (***E****nterococcus*, ***S****taphylococcus*, ***K****lebsiella*, ***A****cinetobacter*, ***P****seudomonas*, and ***E****nterobacter*) have earned considerable notoriety due to their propensity towards acquiring MDR and XDR properties (Boucher, Talbot et al. 2009).

"*Klebsiella pneumoniae*" (Kpn) is an encapsulated, non-motile, Gram-negative bacillus that belongs to the *Enterobacteriaceae* family. Apart from being ubiquitously present in surface water and soil, it is primarily present as a commensal resident of the mammalian gastrointestinal tract and one of the most epidemiologically essential species. Kpn is the third-most-common cause of opportunistic nosocomial infections, and this pathotype of Kpn is also known as classical *Klebsiella pneumoniae* (cKP). This pathotype can infiltrate the urinary tract, bloodstream, lungs, and surgical wounds, thus causing various human infections such as urinary tract infections, pneumonia, sepsis, wound infection, and bacteremia. Apart from these infections, Kpn can cause pyogenic liver abscesses, meningitis, and endophthalmitis, which are commonly known as

community-acquired infections and represent a significant health care threat. However, the increasing propensity of this deadly pathogen to acquire resistance to antibiotics has increased the existing threat as it is becoming quite challenging to treat patients. That list includes especially carbapenem-resistant strains of Kpn, which are resistant to nearly all known antibiotics and exhibit high mortality rates of 41% to 50% for bloodstream infections, and extended-spectrum lactamases expressing strains that show resistance to cephalosporins and monobactams (ESBLs) (Holden and Bachman 2015, Palacios, Broberg et al. 2017). Apart from this drug acquiring Kpn pathotype (cKP), the emergence of a novel hypervirulent pathotype (hvKP) is widely recognized by the medical community across the globe, which is well known now for its globally associated infections such as hepatic abscesses, endophthalmitis, meningitis, osteomyelitis, and necrotizing fasciitis, in an otherwise healthy individual. Acquiring drug resistance by cKP strains makes it challenging to treat, but it is not directly related to enhanced virulence.

On the other hand, hvKP strains acquire additional virulence genes containing large plasmids and some chromosomal elements. It has been shown that biomarkers present on this virulence plasmid accurately differentiate hvKP from cKP. The ability of these hvKP strains to infect both healthy and immunocompromised individuals and increase the tendency of these infections to be invasive, make them more dangerous compared to cKP strains. Recent reports suggested that "superbug' might be evolving with the confluence of both drug resistance and hypervirulence determinants in clinical isolates of Kpn strain. These drug-resistant hypervirulent strains would be tough to treat and, in short, result in a medical crisis (Paczosa and Mecsas 2016, Bailey, Bohac et al. 2018). Multiple virulence factors have been identified and studied which play essential roles in Kpn infection, and a list of these factors mainly contain capsule production, lipopolysaccharide (LPS), siderophores, and fimbriae. Many other factors also play an essential

role in *K. pneumoniae* virulence, and can be added to this virulence factor list, such as outer membrane proteins (porins, efflux pumps, and genes involved in allantoin metabolism). However, a complete understanding of the mechanism of action and significance of those factors requires additional studies.

All available antibiotics have one of the following five modes of action:

Inhibition of cell wall synthesis

Inhibition of cell membrane function

Inhibition of protein synthesis

Inhibition of nucleic acid synthesis

Inhibition of metabolic processes

Microorganisms have adapted resistance against these widely used antibiotics, prompting researchers to look for antimicrobials with a novel mode of action. Developing metal acquisition as a target for antibiotic activity would be an exciting step forward to combat antibiotic resistance (Wencewicz 2016). One such specific target could be by iron acquisition pathways in pathogens, e.g., ESKAPE bacteria. Iron is an essential nutrient required for bacterial growth and proliferation and plays the role as a cofactor in many biochemical and metabolic processes. Extensive evidences are available linking iron acquisition to pathogenesis, as covered in the recently published review by Klebba group (Klebba, Newton et al. 2021). Bacteria secrete siderophores in iron-deficient conditions, bind iron with high affinity, and transport this iron-siderophore complex inside the cell actively across the outer membrane with the help of TonB protein (Holden and Bachman 2015). In contrast, hosts have developed nutritional immunity against invading pathogens by sequestering iron by eukaryotic proteins, e.g., transferrin and lactoferrin, to minimize free available iron for pathogen (Weinberg 1975). Antibiotics that will target TonB dependent iron acquisition system

may suffer less from resistance as bacteria with altered TonB or lacking TonB fail to thrive in the iron-deficient host environment and show impaired host colonization (Tsolis, Baumler et al. 1996, Pi, Jones et al. 2012). Most of the Gram-negative bacteria, including *Klebsiella pneumoniae*, utilize TonB dependent transport system to acquire iron for their growth and proliferation. *K. pneumoniae* is known to produce four siderophores: enterobactin (Ent), aerobactin (Abn), yersiniabactin (Ybt), and glucosylated enterobactin (GEnt) (Russo, Olson et al. 2018). The production of multiple siderophores counteracts the host's ability to neutralize individual siderophores. Plus, different siderophores may promote colonization of varying tissues in the host (Miethke and Marahiel 2007, Holden and Bachman 2015). Ent production is ubiquitous in both classical and hypervirulent *K. pneumonia,* utilizing ferric catecholates in both the wild and host environments. Both Ent production and FepA expression are upregulated during infection by *K. pneumoniae*, enhancing colonization of the lungs (Brock, Williams et al. 1991, Lai, Peng et al. 2001). Of these four, there is scientific evidence that suggests that aerobactin plays a vital role in the bacteria's survival. Deleting the aerobactin biosynthesis (IucA) proved to be lethal (Russo, Olson et al. 2015). One of the most crucial characteristics of the hvKP is that it has increased (6 to 10-fold) siderophore activity compared to cKP strain. Out of four siderophores produced by hvKP, only aerobactin accounted for more than 90% of siderophore activity (Russo, Olson et al. 2014). Plus, aerobactin is a critical factor necessary for bacterial optimum growth and survival in human ascites, serum *ex vivo*, and virulence in an outbred mouse systemic and pulmonary infection model (Russo, Olson et al. 2015).

Fluorescence modification of site directed Cys sulfhydryl in the outer loops of *E. coli* FepA allows spectroscopic observation of FeEnt transport by living bacterial cells in real-time (Cao, Warfel et al. 2003, Smallwood, Jordan et al. 2014). This method monitors the binding of the FeEnt

to the outer loops of fluorescently labeled FepA. Binding quenches the fluorescence, but fluorescence recovers as the bacteria internalize and deplete the ferric siderophore in the solution. This ligand binding induced fluorescence quenching and recovery, allows us to monitor FeEnt binding and transport in the living cell even at nanomolar concentrations. This methodology will enable us to find novel therapeutics against TonB dependent transport as inhibitors of TonB interfere in fluorescence recovery. Previously, our lab group utilized this approach to develop a fluorescence high throughput screening (FLHTS) approach to observe real-time FeEnt uptake through FepA, and its inhibition, in living *E. coli*. This FLHTS allowed us to screen thousands of chemical compounds. We identified many compounds that specifically inhibited TonB dependent activity, verified by their abilities to interfere in FeEnt and ferrichrome (Fc) transport and colicin B (ColB) and Ia (ColIa) killing, without affecting PMF-dependent lactose uptake (Nairn, Eliasson et al. 2017).

In this study, we performed a genome-wide search of *K. pneumoniae* strain Kp52.145 for FepA homologs and found four active FepA homologs; KpnFepA_1658 KpnFepA_4984, KpnFepA_2380, and KpnFepA_0027 (IroN; encoded on native plasmid pII) and, genetically modified them to attach fluorescent probes. Apart from functionally characterizing these multiple FeEnt/FeGEnt transporters of *K. pneumoniae*, we engineered Cys residues in all four *K. pneumoniae* FepAs (KpnFepAs) and adapted FLHTS to observe FeEnt uptake by KpnFepAs in both *E. coli* and *K. pneumoniae*. These four putative FeEnt transporters efficiently function in the FLHTS assay, validating the assay against Gram-negative bacterial pathogen *K. pneumoniae*. These FLHTS assays are not limited to TonB dependent FeEnt transporters only; we adapted this methodology to other TonB dependent receptors and showed ferric aerobactin (FeAbn) transport through Iron Uptake Transporter (IutA) and vitamin B_{12} through BtuB. Compounds already

identified by FLHTS survey against *E. coli* and *A. baumannii* or future studies to find out compounds to block TonB dependent transport may constitute novel antimicrobial therapeutic agents that can thwart bacterial pathogenesis.

3.2. Methodology:

3.2.1. Generation of recombinant construct in *E. coli* background:

We performed a genome-wide search of *the K. pneumoniae* Kp52.145 strain. We looked for the putative TonB dependent transporters of catecholate siderophores, and we found four locus tags that have been annotated as FeEnt/FeGEnt transporter based on computational analysis. Out of four of these, three locus tags are on the chromosome; BN49_1658, BN49_4984, BN49_2380, and one on the native plasmid pII; BN49_pII0027. We amplified all these genes separately from the *K. pneumoniae* genome and subsequently amplified the pITS23 vector and stitched amplified gene fragments separately with pITS23 using Gibson method (Gibson, Young et al. 2009) using NEBuilder HiFi cloning kit (New England BioLabs) and verified these constructs by sequencing. We transformed these recombinant plasmids separately in OKN3 and OKN359 for checking the expression in *E. coli* background and selected transformants on LB agar plate containing Chloramphenicol and Streptomycin. For cloning of *iutA* and *btuB*, we amplified these genes from the pABN6 plasmid and genomic DNA of *E. coli* MG1655 strain and followed the same steps for expressing these genes in OKN359 background as we did for *K. pneumoniae fepAs.*

3.2.2. Outer membrane separation:

We separated outer membranes to check the expression of KpnFepAs, EcoIutA and EcoBtuB constructs, and compared the TBDTs expressions with respective controls. We

inoculated cells overnight in LB and sub-cultured (1:100) it in iron-deficient MOPS media with appropriate antibiotics and incubated at shaking condition for 5-6 hours at 37°C until the O.D. 600 nm reached 1-1.2. We spun down cells and discarded the supernatant, resuspended pellet in 2 ml lysis buffer (50 mM Tris Cl, pH 7.5), and processed as described in the material and method section. In the final steps, we dissolved the pellet in 200 ul PBS, read the absorbance at 280 (A_{280}), and calculated the protein concentration in each sample. We mixed 120 ug of OM protein in 100 ul of water with 100 ul with SDS boiling buffer and boiled for 5 minutes. We loaded a total of 30 ug (50 ul of the sample) protein on SDS-PAGE for gel-electrophoresis. We then performed Coomassie blue staining/distaining process to visualize protein bands on the UVP imager.

3.2.3. Site-directed mutagenesis to introduce Cys substitution in TonB dependent receptors:

To generate Cys substitution in the tertiary structure of putative TonB dependent receptors (KpnFepAs) and EcoIutA used in this study, we compared the identity between primary structure sequences with already crystallized TonB dependent receptors available, e.g., *E. coli* FepA (PDB sequence 1FEP). We used the latter to predict the tertiary structure (overall folded protein) structure of all KpnFepAs using the Modeler function of CHIMERA (Pettersen, Goddard et al. 2004). We relied on the guideline that >25% sequence identity strongly predicts overall identical protein fold (Ginalski 2006, Stokes-Rees and Sliz 2010). We used the respective modeled protein structure for each receptor to select 4-6 residues in different predicted surface loops. For KpnFepAs, most of the time, we chose residues analogous to the loop residues in EcoFepA (using CLUSTALW) that we successfully fluoresceinated (Smallwood, Marco et al. 2009, Smallwood,

Jordan et al. 2014). We used a QuikChange II XL mutagenesis kit (Agilent, Santa Clara, CA) to create mutations and verified all the different constructs by sequencing.

3.2.4. Siderophore nutrition assay:

To check the functionality and evaluation of FeEnt and FeAbn transport by all KpnFepAs and EcoIutA constructs, respectively, we performed the siderophore nutrition test. Overnight grown culture in LB was sub-cultured (1:100) in NB with appropriate antibiotics and incubated shaking for another 5-6 hours at 37°C. We used OKN3, OKN359, OKN3/pITS23, OKN359/pITS23 as controls whenever appropriate. We added 100 ul of aliquots of these cells to NB TOP agar containing apo-ferrichrome A (apoFcA) and appropriate antibiotics. Then, we mixed it, poured this mixture into a 6-well plate, and kept it at room temperature to solidify. We applied 5 ul of 50 µM siderophores (FeEnt and FeAbn) on the paper disk in the respective wells and incubated plates overnight at 37°C and observed the bacterial growth around the disk.

3.2.5. Fluorescent labeling of the cell lysate and spectroscopic transport assay:

For fluoresceination of Cys mutants of KpnFepAs, EcoIutAs, and EcoBtuB in living bacterial cells, we used overnight growth cells in LB and sub-cultured these cells in iron-deficient MOPS minimal media with appropriate antibiotics and allowed incubation shaking at 37°C until an O.D. 600 nm reached 1.0-1.5. We labeled live cells with 5 µM fluorescein maleimide (FM) in 50 mM NaHPO4, pH 6.7, for 15 minutes shaking at 37°C and then quenched the reaction with 130 mM BME. We pelleted cells, washed twice with phosphate-buffered saline (PBS), and resuspended the bacterial cells in (PBS) plus 0.4% glucose. We used these labeled cells for spectroscopic analysis of siderophore transport.

In the case of EcoIutA, after labeling live cells grown under iron-deficient condition, we isolated outer membrane fractions and boiled with 1% SDS for 5 minutes and cooled it down. Then we incubated these fractions with 5 µM FM for 15 minutes at 37°C, quenched the reaction by adding 130 mM BME, added 7 volumes of ice-cold acetone, and kept it at -20°C for 2-4 hours. We centrifuged the samples at high speed for 20 minutes and decanted supernatant, resuspended pellet in PBS, and loaded the samples on SDS-PAGE for fluorescent image analysis.

We observed fluorophore-labeled cells in an SLM AMINCO 8100 fluorescence spectrometer, upgraded with an OLIS operating system and software (OLIS SpectralWorks, OLIS Inc., Bogart, GA), to control its shutters, polarizers, and data collection. For FeEnt and FeAbn transport by individual Gram-negative bacterial cells, we added iron-siderophore complex to 2 $x10^7$ labeled cells in a quartz cuvette (final volume, 2 mL) with stirring at 37°C, and monitored siderophore binding and transport.

3.3. Results:

3.3.1. Identification of potential ferric catecholate Transporters in *Klebsiella pneumoniae*:

We used CLUSTALW2 alignments to analyze TonB dependent FeEnt transport in the genome of *K. pneumoniae* (Figure 3.1). We performed a genome-wide search in the *K. pneumoniae* Kp52.145 strain genome and looked for putative outer membrane TonB dependent receptors for catecholate siderophore transport; FeEnt, based on its genetic similarity to *E. coli fepA*. We found four loci that had been bioinformatically annotated as putative TonB dependent outer membrane FeEnt/FeGEnt transporters. Out of four of these TBDT transporters, three loci are on the chromosome; BN49_1658, BN49_4984, BN49_2380, and one on the native plasmid pII;

BN49_pII0027. Gene names for these putative TBDTs in the genome are as follows; BN49_1658: *fepA,* BN49_4984: *fepA1,* and BN49_pII0027: *iroN*. According to annotations, Locus tag BN49_2380 encodes for unnamed protein product similar to TBDT transporter from *E. coli* O6:K15:H31 strain 536 – UPEC. We also included this gene for further study. For consistency throughout this document, I will use these four gene names based on their locus tag information: *KpnfepA_1658*, *KpnfepA_4984*, *KpnfepA_iroN*, and *KpnfepA_2380*. After aligning mature protein sequences of these genes' protein products with EcoFepA (PDB sequence 1FEP), we found out KpnFepA_1658, KpnFepA_4984, KpnFepA_2380 and KpnFepA_IroN protein sequence showed 81%, 72%, 51% and 51% identity with EcoFepA, respectively. We also looked for conserved Fur box (GATAAT motif) in the promoter region in all putative transporter as this box is ubiquitously present in the promoter region of iron-regulated operon; all putative TBDTs contains Fur- sequences which are relatable to *E. coli* consensus Fur-sequence.

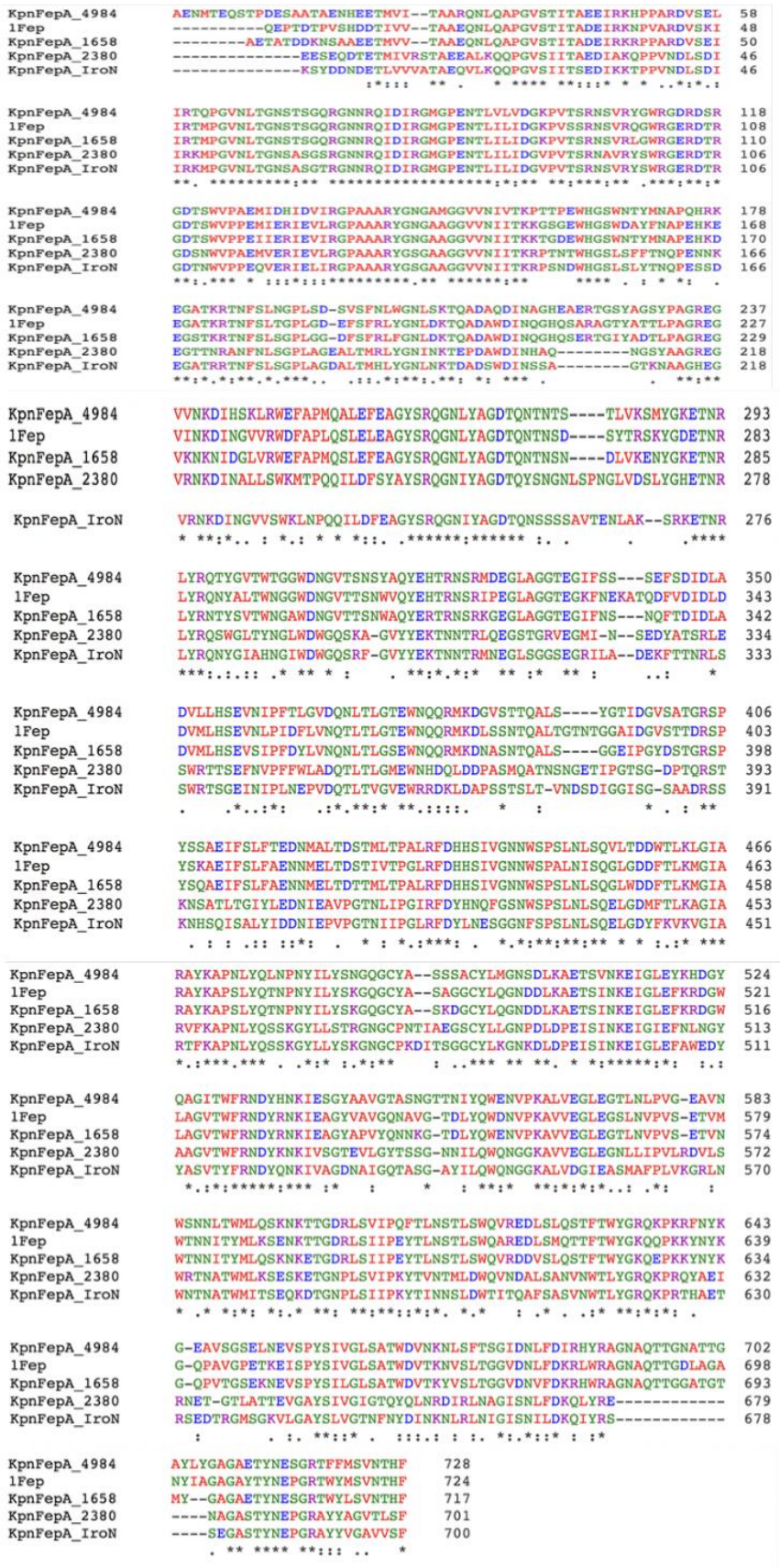
KpnFepA_4984 AENMTEQSTPDESAATAENHEETMVI--TAARQNLQAPGVSTITAEEIRKHPPARDVSEL 58
1Fep ----------QEPTDTPVSHDDTIVV--TAAEQNLQAPGVSTITADEIRKNPVARDVSKI 48
KpnFepA_1658 ---------AETATDDKNSAAEETMVV--TAAEQNLQAPGVSTITADEIRKRPPARDVSEI 50
KpnFepA_2380 --------------EESEQDTETMIVRSTAEEALKQQPGVSIITAEDIAKQPPVNDLSDI 46
KpnFepA_IroN --------------KSYDDNDETLVVVATAEQVLKQQPGVSIITSEDIKKTPPVNDLSDI 46
KpnFepA_4984 IRTQPGVNLTGNSTSGQRGNNRQIDIRGMGPENTLVLVDGKPVTSRNSVRYGWRGDRDSR 118
1Fep IRTMPGVNLTGNSTSGQRGNNRQIDIRGMGPENTLILIDGKPVSSRNSVRQGWRGERDTR 108
KpnFepA_1658 IRTMPGVNLTGNSTSGQRGNNRQIDIRGMGPENTLILIDGKPVTSRNSVRLGWRGERDTR 110
KpnFepA_2380 IRKMPGVNLTGNSASGSRGNNRQIDIRGMGPENTLILIDGVPVTSRNAVRYSWRGERDTR 106
KpnFepA_IroN IRKMPGVNLTGNSASGTRGNNRQIDIRGMGPENTLILIDGVPVTSRNSVRYSWRGERDTR 106
KpnFepA_4984 GDTSWVPAEMIDHIDVIRGPAAARYGNGAMGGVVNIVTKPTTPEWHGSWNTYMNAPQHRK 178
1Fep GDTSWVPPEMIERIEVLRGPAAARYGNGAAGGVVNIITKKGSGEWHGSWDAYFNAPEHKE 168
KpnFepA_1658 GDTSWVPPEIIERIEVIRGPAAARYGNGAAGGVVNIITKKTGDEWHGSWNTYMNAPEHKD 170
KpnFepA_2380 GDSNWVPAEMVERIEVLRGPAAARYGSGAAGGVVNIITKRPTNTWHGSLSFFTNQPENNK 166
KpnFepA_IroN GDTNWVPPEQVERIELIRGPAAARYGSGAAGGVVNIITKRPSNDWHGSLSLYTNQPESSD 166
KpnFepA_4984 EGATKRTNFSLNGPLSD-SVSFNLWGNLSKTQADAQDINAGHEAERTGSYAGSYPAGREG 237
1Fep EGATKRTNFSLTGPLGD-EFSFRLYGNLDKTQADAWDINQGHQSARAGTYATTLPAGREG 227
KpnFepA_1658 EGSTKRTNFSLSGPLGG-DFSFRLFGNLDKTQADAWDINQGHQSERTGIYADTLPAGREG 229
KpnFepA_2380 EGTTNRANFNLSGPLAGEALTMRLYGNINKTEPDAWDINHAQ--------NGSYAAGREG 218
KpnFepA_IroN EGATRRTNFSLSGPLAGDALTMHLYGNLNKTDADSWDINSSA--------GTKNAAGHEG 218
KpnFepA_4984 VVNKDIHSKLRWEFAPMQALEFEAGYSRQGNLYAGDTQNTNTS----TLVKSMYGKETNR 293
1Fep VINKDINGVVRWDFAPLQSLELEAGYSRQGNLYAGDTQNTNSD----SYTRSKYGDETNR 283
KpnFepA_1658 VKNKNIDGLVRWEFAPMQSLEFEAGYSRQGNLYAGDTQNTNSN----DLVKENYGKETNR 285
KpnFepA_2380 VRNKDINALLSWKMTPQQILDFSYAYSRQGNIYAGDTQYSNGNLSPNGLVDSLYGHETNR 278
KpnFepA_IroN VRNKDINGVVSWKLNPQQILDFEAGYSRQGNIYAGDTQNSSSSAVTENLAK--SRKETNR 276
KpnFepA_4984 LYRQTYGVTWTGGWDNGVTSNSYAQYEHTRNSRMDEGLAGGTEGIFSS---SEFSDIDLA 350
1Fep LYRQNYALTWNGGWDNGVTTSNWVQYEHTRNSRIPEGLAGGTEGKFNEKATQDFVDIDLD 343
KpnFepA_1658 LYRNTYSVTWNGAWDNGVTTSNWAQYERTRNSRKGEGLAGGTEGIFNS---NQFTDIDLA 342
KpnFepA_2380 LYRQSWGLTYNGLWDWGQSKA-GVYYEKTNNTRLQEGSTGRVEGMI-N--SEDYATSRLE 334
KpnFepA_IroN LYRQNYGIAHNGIWDWGQSRF-GVYYEKTNNTRMNEGLSGGSEGRILA--DEKFTTNRLS 333
KpnFepA_4984 DVLLHSEVNIPFTLGVDQNLTLGTEWNQQRMKDGVSTTQALS----YGTIDGVSATGRSP 406
1Fep DVMLHSEVNLPIDFLVNQTLTLGTEWNQQRMKDLSSNTQALTGTNTGGAIDGVSTTDRSP 403
KpnFepA_1658 DVMLHSEVSIPFDYLVNQNLTLGSEWNQQRMKDNASNTQALS----GGEIPGYDSTGRSP 398
KpnFepA_2380 SWRTTSEFNVPFFWLADQTLTLGMEWNHDQLDDPASMQATNSNGETIPGTSG-DPTQRST 393
KpnFepA_IroN SWRTSGEINIPLNEPVDQTLTVGVEWRRDKLDAPSSTSLT-VNDSDIGGISG-SAADRSS 391
KpnFepA_4984 YSSAEIFSLFTEDNMALTDSTMLTPALRFDHHSIVGNNWSPSLNLSQVLTDDWTLKLGIA 466
1Fep YSKAEIFSLFAENNMELTDSTIVTPGLRFDHHSIVGNNWSPALNISQGLGDDFTLKMGIA 463
KpnFepA_1658 YSQAEIFSLFAENNMELTDTTMLTPALRFDHHSIVGNNWSPSLNLSQGLWDDFTLKMGIA 458
KpnFepA_2380 KNSATLTGIYLEDNIEAVPGTNLIPGIRFDYHNQFGSNWSPSLNLSQELGDMFTLKAGIA 453
KpnFepA_IroN KNHSQISALYIDDNIEPVPGTNIIPGLRFDYLNESGGNFSPSLNLSQELGDYFKVKVGIA 451
KpnFepA_4984 RAYKAPNLYQLNPNYILYSNGQGCYA--SSSACYLMGNSDLKAETSVNKEIGLEYKHDGY 524
1Fep RAYKAPSLYQTNPNYILYSKGQGCYA--SAGGCYLQGNDDLKAETSINKEIGLEFKRDGW 521
KpnFepA_1658 RAYKAPSLYQTNPNYILYSKGQGCYA--SKDGCYLQGNDDLKAETSINKEIGLEFKRDGW 516
KpnFepA_2380 RVFKAPNLYQSSKGYLLSTRGNGCPNTIAEGSCYLLGNPDLDPEISINKEIGIEFNLNGY 513
KpnFepA_IroN RTFKAPNLYQSSKGYLLYSKGNGCPKDITSGGCYLKGNKDLDPEISINKEIGLEFAWEDY 511
KpnFepA_4984 QAGITWFRNDYHNKIESGYAAVGTASNGTTNIYQWENVPKALVEGLEGTLNLPVG-EAVN 583
1Fep LAGVTWFRNDYRNKIEAGYVAVGQNAVG-TDLYQWDNVPKAVVEGLEGSLNVPVS-ETVM 579
KpnFepA_1658 LAGVTWFRNDYRNKIEAGYAPVYQNNKG-TDLYQWENVPKAVVEGLEGTLNVPVS-ETVN 574
KpnFepA_2380 AAGVTWFRNDYKNKIVSGTEVLGYTSSG-NNILQWQNGGKAVVEGLEGNLLIPVLRDVLS 572
KpnFepA_IroN YASVTYFRNDYQNKIVAGDNAIGQTASG-AYILQWQNGGKALVDGIEASMAFPLVKGRLN 570
KpnFepA_4984 WSNNLTWMLQSKNKTTGDRLSVIPQFTLNSTLSWQVREDLSLQSTFTWYGRQKPKRFNYK 643
1Fep WTNNITYMLKSENKTTGDRLSIIPEYTLNSTLSWQAREDLSMQTTFTWYGKQQPKKYNYK 639
KpnFepA_1658 WTNNITYMLQSKNKETGDRLSIIPEYTLNSTLSWQVRDDVSLQSTFTWYGKQEPKKYNYK 634
KpnFepA_2380 WRTNATWMLKSESKETGNPLSVIPKYTVNTMLDWQVNDALSANVNWTLYGRQKPRQYAEI 632
KpnFepA_IroN WNTNATWMITSEQKDTGNPLSIIPKYTINNSLDWTITQAFSASVNWTLYGRQKPRTHAET 630
KpnFepA_4984 G-EAVSGSELNEVSPYSIVGLSATWDVNKNLSFTSGIDNLFDIRHYRAGNAQTTGNATTG 702
1Fep G-QPAVGPETKEISPYSIVGLSATWDVTKNVSLTGGVDNLFDKRLWRAGNAQTTGDLAGA 698
KpnFepA_1658 G-QPVTGSEKNEVSPYSILGLSATWDVTKYVSLTGGVDNVFDKRHWRAGNAQTTGGATGT 693
KpnFepA_2380 RNET-GTLATTEVGAYSIVGIGTQYQLNRDIRLNAGISNLFDKQLYRE---------- 679
KpnFepA_IroN RSEDTRGMSGKVLGAYSLVGTNFNYDINKNLRLNIGISNILDKQIYRS---------- 678
KpnFepA_4984 AYLYGAGAETYNESGRTFFMSVNTHF 728
1Fep NYIAGAGAYTYNEPGRTWYMSVNTHF 724
KpnFepA_1658 MY--GAGAETYNESGRTWYLSVNTHF 717
KpnFepA_2380 ----NAGASTYNEPGRAYYAGVTLSF 701
KpnFepA_IroN ----SEGASTYNEPGRAYYVGAVVSF 700

Figure 3.1. CLUSTALW2 analysis of mature protein of *K. pneumoniae* putative TonB dependent transporters of FeEnt with *E. coli* FepA (PDB sequence 1FEP):

We used multiple sequence alignment tools to align all four Putative FepA transporters in Kpn52.145 strain and *E. coli* FepA. An asterisk (*) indicates positions with a single fully conserved residue in all proteins in the above representation. A colon (:) indicates conservation between groups of strongly similar properties, and A period (.) indicates conservation between groups of weakly similar properties.

3.3.2. Cloning and expression of OM TBDTs:

For the generation of recombinant *KpnfepA* constructs in *E. coli* cells, we amplified the open reading frame (ORF) of each *KpnfepA* separately using genomic DNA of *K. pneumoniae* Kp52.145 strain as a template; *KpnfepA_1658*: 2154 base pairs (bp), *KpnfepA_4984*: 2187 bp, *KpnfepA_2380*: 2106 bp respectively. For cloning of *E. coli iutA* (2124 bp) and *btuB* (1785 bp) gene amplification (Figure 3.2, 3.3, 3.4, 3.5, and 3.6), we used plasmid pABN6, a derivative of plasmid pColV-K30, and genomic DNA of *E. coli* K-12 MG1655 strain as a template respectively. Simultaneously, we amplified the pITS23 vector as well. (Figure 3.2, 3.3, 3.4, 3.5, and 3.6). We used standard molecular weight markers as a control. We stitched each fragment of different genes separately with the pITS23 vector as the backbone.

We cloned all these five genes under the control of *E. coli* fepA promoter and Fur box in the promoter region. Except for KpnfepA_1658 and EcoIutA, which have a nucleotide sequence that encodes for their respective protein's signal sequence before the open reading frame. All other three genes are cloned in a way that they possess nucleotide sequence which encodes EcoFepA signal sequence before individual gene's ORFs. For the amplification of each gene and vector and ligation reaction, we relied on the method described by Gibson using the NEBuilder HiFi cloning kit (New England Biolabs).

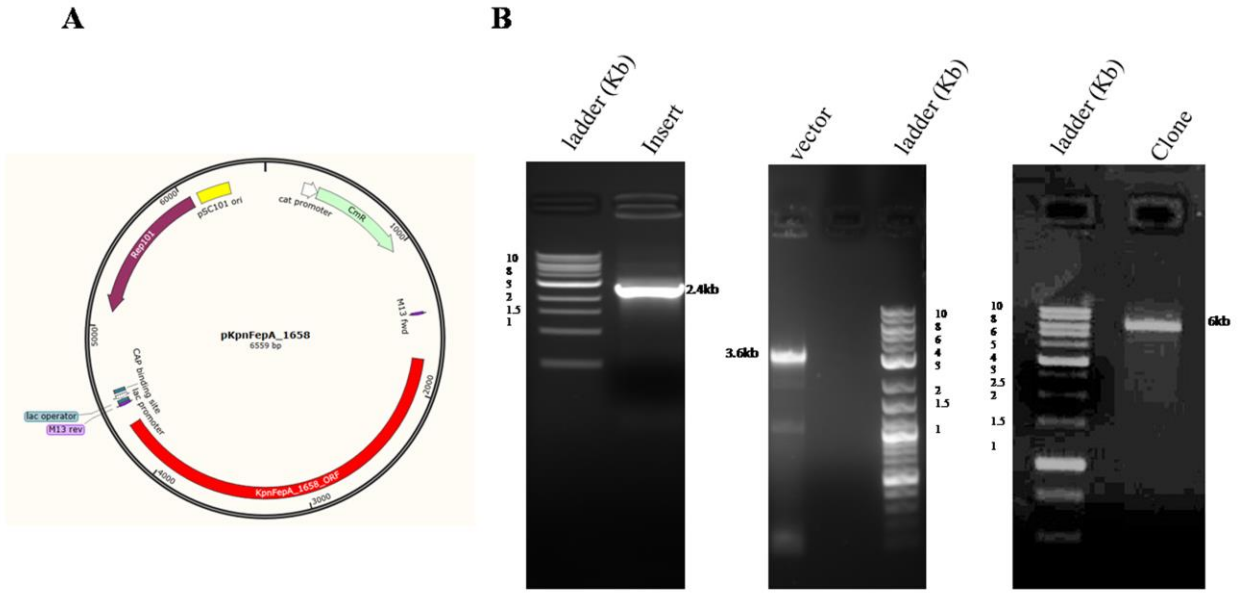

Figure 3.2. Recombinant plasmid and cloning strategy of *EpnfepA_1658*:

Panel A shows recombinant plasmid *pKpnfepA_1658*, and panel B shows the amplification of *KpnFepA_1658*, pITS23, and confirmation of recombinant plasmid using M13 universal primers using agarose gel electrophoresis.

This method utilizes a one-step isothermal reaction. Two adjacent amplified DNA fragments (insert and vector) sharing terminal sequence overlaps at both ends are joined into a covalently sealed product in one step at a constant temperature. All these reactions (removing 5' ends, annealing, and filling gaps) take place in a tube at 50ºC, containing a mixture of different enzymes; T5 exonuclease removes nucleotide at 5' ends of a double-stranded DNA molecule. In contrast, complementary single-stranded DNA overhangs are joined, and Phusion DNA polymerase fills gaps, and Taq DNA ligase seals the nicks. After the completion of the reaction, each recombinant product was transformed in OKN3 and OKN359 both and plated on LB agar that contained streptomycin and chloramphenicol. Transformants were isolated and grown again. We primarily confirmed the presence of respective DNA (gene) fragments in vector background

by running PCR reaction using M13 universal forward and reverse primer. We confirmed the proper clone using agarose gel electrophoresis and visualizing amplified DNA bands of appropriate size using standard molecular weight markers (Figure 3.2, 3.3, 3.4, 3.5, and 3.6). All the gene products appeared on agarose gel at around 3000 base pairs (bp), confirming a recombinant insert gene. Finally, Sanger sequencing results for each recombinant construct confirmed the presence of proper cloning of each gene.

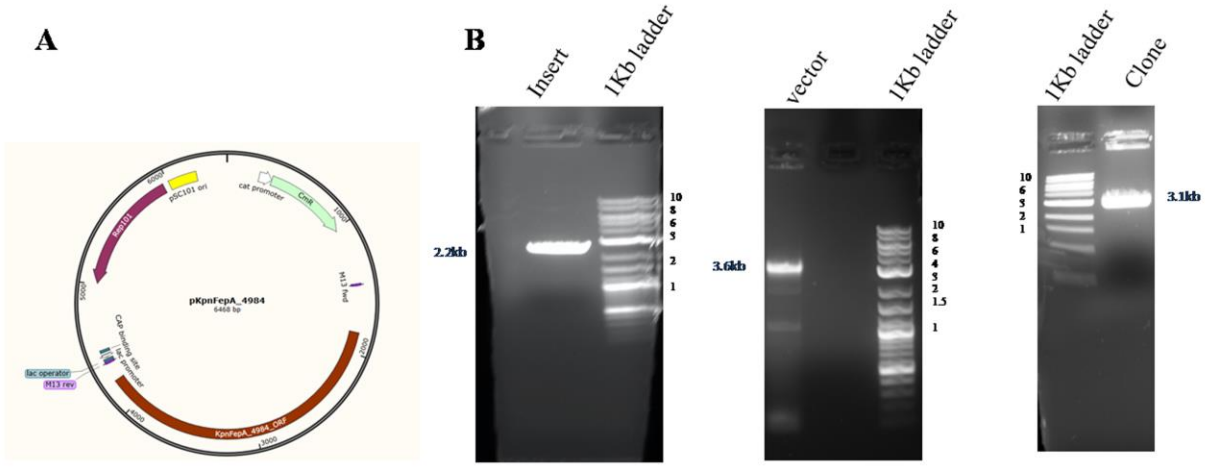

Figure 3.3. Recombinant plasmid and cloning strategy of *KpnfepA_4984*:
Figure A shows recombinant plasmid *pKpnfepA_4984,* and panel B shows the amplification of *KpnFepA_4984*, pITS23, and confirmation of recombinant plasmid using M13 universal primers using agarose gel electrophoresis.

We looked for the expression of relevant proteins encoded by different recombinant constructs (Figure 3.7). We expressed these receptors under iron-deficient conditions and isolated outer membrane fraction containing cell envelop protein and applied 40 ug of protein fractions on SDS-PAGE followed by Coomassie blue staining and then destaining. Secondly, we developed an

immunoblot of KpnFepAs fractions against *E. coli* anti-FepA monoclonal antibody (mAb 41) (Figure 3.7). We used a secondary antibody conjugated to alkaline phosphatase as a reporter to detect different KpnFepAs in the outer membrane fraction. However, immunoblotting was not enough to quantify protein levels accurately because these monoclonal antibodies are generated against *E. coli* FepA. There were differences between primary protein structure *E. coli* and *K. pneumoniae* FepAs. But Coomassie blue staining of OM fractions was enough to quantify the expressions of OM proteins accurately. As a control, we used OM fractions of OKN359, BN1071, and OKN359/pITS23 grown in iron-deficient conditions, the same as other constructs. Results indicated proper expression of all the relevant proteins in the outer membrane when grown in iron-deficient condition to promote Fur activity (Figure 3.7).

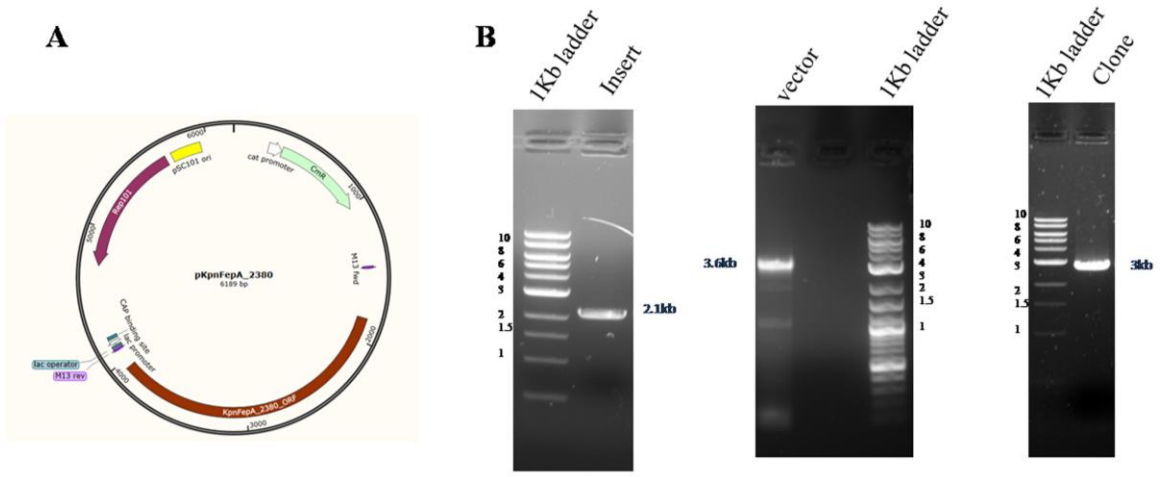

Figure 3.4. Recombinant plasmid and cloning strategy of *KpnfepA_2380*:

Figure A depicts recombinant plasmid *pKpnfepA_2380*, and panel B represents the amplification of *KpnFepA_2380*, pITS23, and confirmation of recombinant plasmid using M13 universal primers using agarose gel electrophoresis.

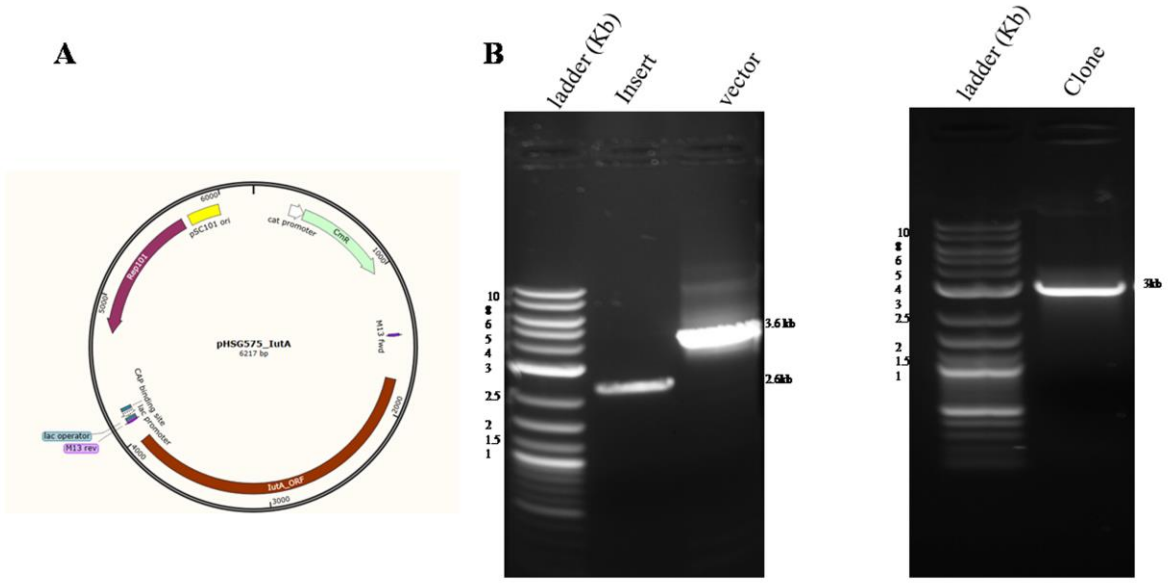

Figure 3.5. Recombinant plasmid and cloning strategy of *pEcoiutA*:

Figure A shows recombinant plasmid p*EcoiutA*, and panel B represents the amplification of *EcoiutA*, pITS23, and confirmation of recombinant plasmid using M13 universal primers using agarose gel electrophoresis.

3.3.3. Generation of Cys mutants in KpnFepAs, EcoIutA and EcoBtuB:

For the genetic engineering of Cys substitutions in the outer loops of OM transporters, it was necessary to know their tertiary structure. In the case of the cobalamin ($VitB_{12}$) receptor, we used the available crystal structure of *E. coli* BtuB (PDB ID: 1NQE) and selected few residues for Cys substitution in the loop region; preferably Serine, Threonine, and Alanine. After finding potential sites for replacement, we performed site-directed mutagenesis to convert native residues in BtuB to Cys: T185C, S286C, T450C, and T491C (Figure 3.16 A).

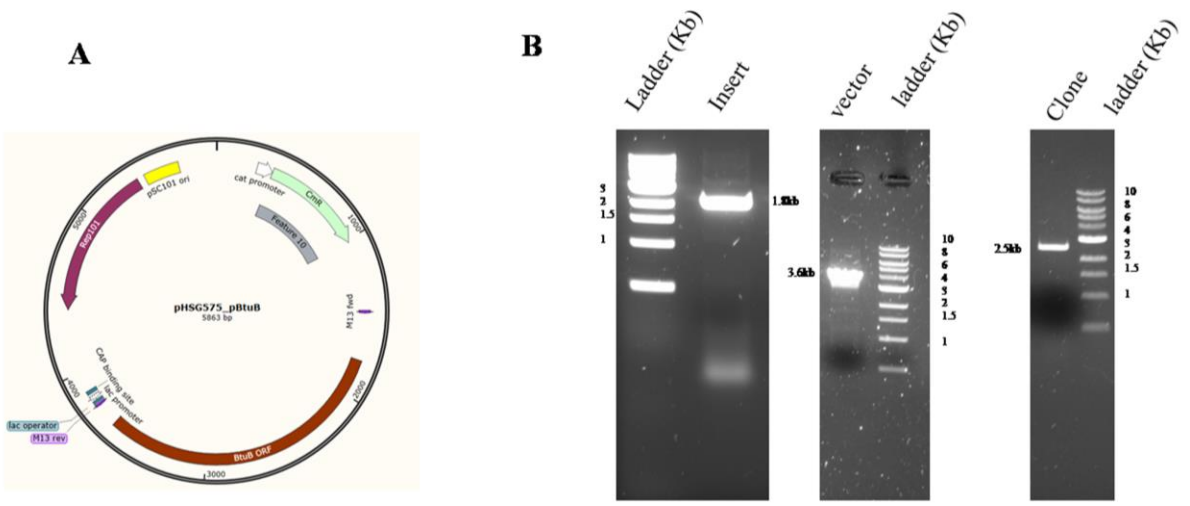

Figure 3.6. Recombinant plasmid and cloning strategy of *pEcobtuB*:

Panel A shows recombinant plasmid p*EcobtuB,* and panel B represents the amplification of *EcobtuB,* pITS23 and, confirmation of recombinant plasmid using M13 universal primers using agarose gel electrophoresis.

Because no crystal structure exists for KpnFepAs, we relied on ortholog EcoFepA to predict their tertiary structure as all KpnFepAs show more than 50% structural identity with EcoFepA. More than 50% similarity with EcoFepA makes it a better template structure to use for the purpose. After aligning KpnFepAs primary protein structure sequence with its EcoFepA ortholog, we used the Modeler function of the CHIMERA program to predict the tertiary structure of all KpnFepAs. Based on the amino acid residue positions used to create Cys residues in EcoFepA (Smallwood, Marco et al. 2009, Smallwood, Jordan et al. 2014), we identified potential sites in KpnFepAs for fluoresceination in outer loops. We converted their native residues to Cys using site-directed mutagenesis. For KpnFepA_1658 we created I218C, D273C, A324C, A382C, T545C and T693C (Figure 3.8A). In KpnFepA_4984 we generated S226C, T281C, A332C, A390C, T534C and A703C (Figure 3.9A). and finally, for the KpnFepA_2380, we chose S211C, T255C, T316C, A630C and T681C (Figure 3.14A).

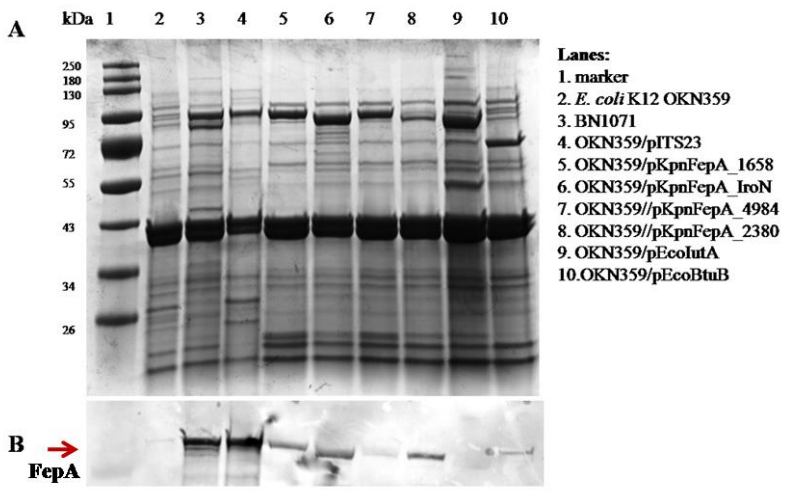

Figure 3.7. Expression of OM receptors and immunoblot against anti-EcoFepA monoclonal antibody (mAb41):

Panel A shows the Coomassie blue staining of SDS PAGE of outer membrane fractions of multiple receptors after grown under iron-deficient media. Panel B shows the Immunoblot of the exact fractions as panel A, developed against anti-EcoFepA monoclonal antibodies (mAb41).

In the case of EcoIutA, we used a slightly different approach to predict its tertiary structure. We used all TonB dependent transporters from *E. coli* MG1655 whose crystal structures are available; FecA, FepA, BtuB, FhuA, Fiu, FhuE, and Cir. We compared identity between the primary structure sequence of each TBDTs with EcoIutA. We found out EcoBtuB shared around 22% identity with EcoIutA, which was best among all, so we used EcoBtuB as a template to predict the overall folded structure of EcoIutA and selected few potential residues in different loops to be mutagenized to Cys: S172C, A174C, A245C, T251C, A389C and T548C (Figure 3.10A). We validated the authenticity of all these constructs by sequencing each mutagenized construct with appropriate primers.

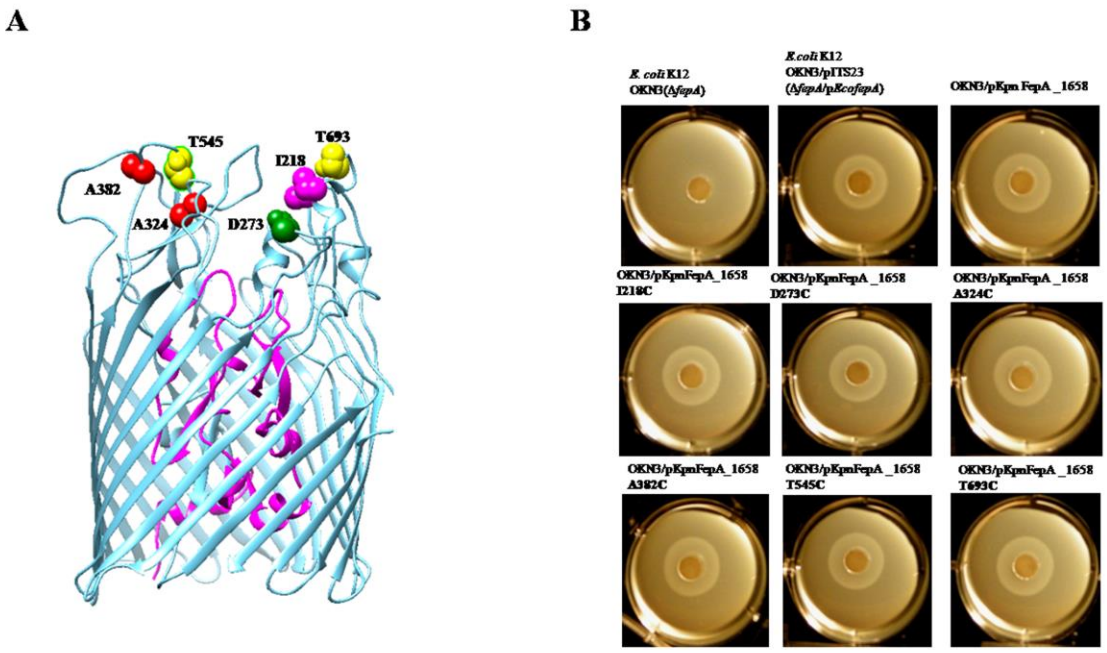

Figure 3.8. Tertiary structure prediction of KpnFepA_1658 and siderophore nutrition test of KpnFepA_1658 and its Cys derivatives:

A, we predicted the protein structure using the CHIMERA program and selected the residues in the loop regions to be a substitute to Cys using site-directed mutagenesis. B, all the constructs were grown under iron-deficient condition (including OKN3 and OKN3/pITS23) and used them to perform siderophore nutrition test to check the functionality of constructs. Halos around the disk represents bacterial growth, which is the indication that Cys mutation did not adversely affect the ligand transport ability of recombinant protein.

3.3.4. Siderophore nutrition test:

We performed siderophore nutrition test to check the functionality of each putative KpnFepA construct and their mutants for efficient FeEnt transport (Figure 3.8B and 3.9B) and recombinant EcoIutA constructs and its mutants for FeAbn transport (Figure 3.10B). Replacing residues to Cys in OM receptor proteins did not affect the ability to transport its ligand, in this case for both FeEnt and FeAbn. KpnFepA_1658 and its mutant transported FeEnt typically as EcoFepA (Figure 3.8B) whereas KpnFepA_4984 and its mutant strains transported FeEnt, but the halo

around the disk was diffusive compared to KpnFepA_1658 or EcoFepA (Figure 3.9B), which suggest a slower transport rate of FeEnt through this receptor. Among these putative FeEnt transporters in *K. pneumoniae*, KpnFepA_2380 did not show bacterial growth around the disk, which suggested this transporter is functionally inactive in transporting FeEnt (data not shown). We used OKN3 as the negative control in this assay which does not contain any native FepA protein, so this strain did not transport FeEnt, whereas OKN3 harboring plasmid pEcoFepA transported FeEnt.

Similarly, we observed FeAbn transport through OKN359/pEcoIutA and all mutants (Figure 3.10B). These data suggested that EcoIutA constructs were active for FeAbn transport and that KpnFepA_1658 and KpnFepA_4984 were functionally functional for FeEnt transport, whereas KpnFepA_2380 was not active for FeEnt transport, despite that fact it was expressed in the outer membrane fraction although quantitatively lesser than other KpnFepAs. EcoIutA and all its Cys derivatives transported FeAbn in the siderophore nutrition test, indicating regular ligand transport by Cys derivatives of EcoIutAs.

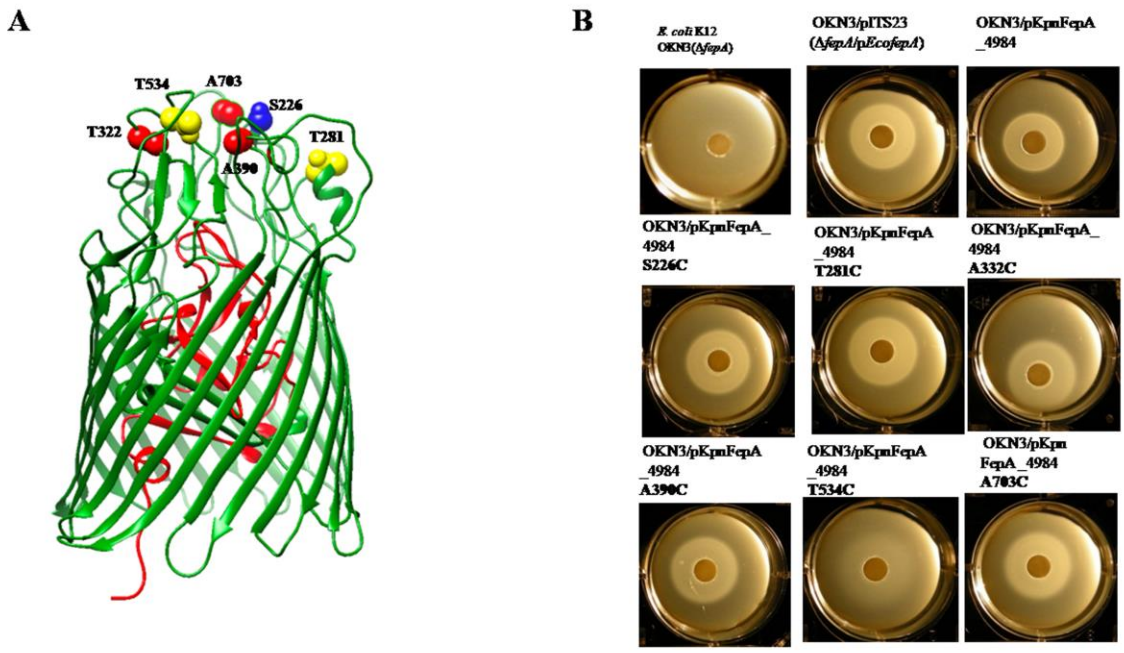

Figure 3.9. Tertiary structure prediction of KpnFepA_4984 and siderophore nutrition test of KpnFepA_4984 and its Cys derivatives:

A, we predicted the protein structure using the CHIMERA program and selected the residues in the loop regions to be substituted to Cys using site-directed mutagenesis. B, all the constructs were grown under iron-deficient condition (including OKN3 and OKN3/pITS23) and used them to perform siderophore nutrition test to check the functionality of constructs. Halo shows the growth of bacteria around the disk, which indicates that Cys mutation did not adversely affect the ligand transport ability of recombinant protein.

3.3.5. Fluorescent labeling of Cys substitution in the surface loops of OM receptors *in vitro*:

Native *E. coli* FepA contains two free Cys residue (C487, C494) in loop 7, involved in the formation of the disulfide bond, which is necessary for effective FeEnt transport. Reducing this disulfide bond abrupted FeEnt transport through *E. coli* FepA (Smallwood, Marco et al. 2009, Smallwood, Jordan et al. 2014, Majumdar, Trinh et al. 2020). These native Cys residues in EcoFepA do not react with extrinsic fluorophore e.g., fluorescein maleimide (FM), until reduced

by a reducing agent (Li, Li et al. 2016), therefore we are able to specifically label FepA or any other OM transporter at a precise, single engineered Cys residues.

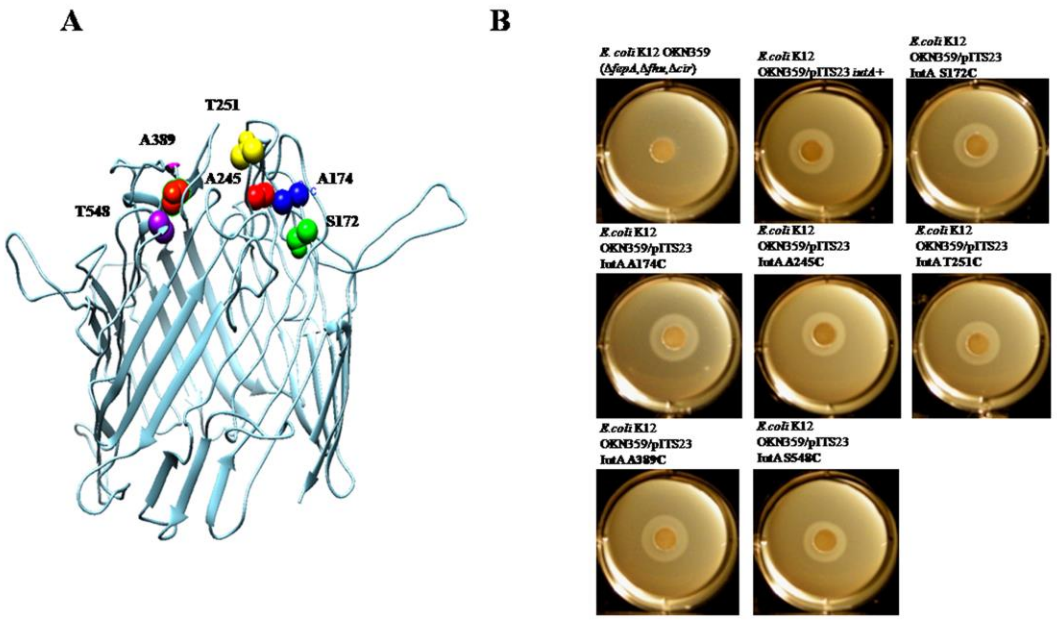

Figure 3.10. Tertiary structure prediction of EcoIutA and siderophore nutrition test of EcoIutA and its Cys derivatives:

A, we predicted the protein structure using the CHIMERA program and selected the residues in the loop regions to be substituted to Cys using site-directed mutagenesis. B, all the constructs were grown under iron-deficient condition (including OKN359 and OKN359/pITS23) and used them to perform siderophore nutrition test to check the functionality of constructs. A halo around the disk shows bacterial growth, which indicates that Cys mutation did not adversely affect the ligand transport ability of recombinant protein.

KpnFepA_1658 mature protein also contains two Cys residues (C482, C489) which are six residues apart and presumably involved in disulfide bond formation and do not react with an extrinsic fluorophore. We transformed recombinant plasmid *KpnfepA_1658* and its Cys mutants in OKN3. We labeled live cells grown under iron-deficient medium specifically with 5 μM FM at pH 6.7 to avoid nonspecific labeling of amino acids containing amine group as their side chains,

e.g., Lysine (Figure 3.11B upper). A fluorescent image of SDS-PAGE indicated that WT KpnFepA_1658 did not react with FM and showed no sign of labeling. So, the presence of disulfide bond formation in native form did not get labeled by the extrinsic fluorophore and might be necessary for efficient FeEnt transport as EcoFepA. All Cys derivatives of KpnFepA_1658 were well labeled except T545C, which was less labeled than all other Cys derivatives of KpnFepA_1658. We used OKN3, BN1071, WT EcoFepA, and EcoFepA_A698C as controls in this labeling experiment. Except for EcoFepA_A698C, no additional control got FM labeled as expected (Figure 3.11B upper). After isolating outer membrane fractions of these constructs and then labeling these fractions followed by fluorescent imaging of SDS-PAGE also reiterate efficient and specific labeling of these Cys residues without any nonspecific labeling background noise (Figure 3.11B lower). We also looked at FM labeling of these constructs in the *K. pneumoniae* background. For that, we transformed all these KpnFepA_1658 WT and its Cys derivatives in KKN5 and FM labeled them after growing them in iron-deficient condition. In *the K. pneumoniae* background, Cys derivatives D273C, A382C, and T693C were well labeled, whereas I218C, A324C, and T545C were poorly labeled compared to *E. coli* background (Figure 3.12A).

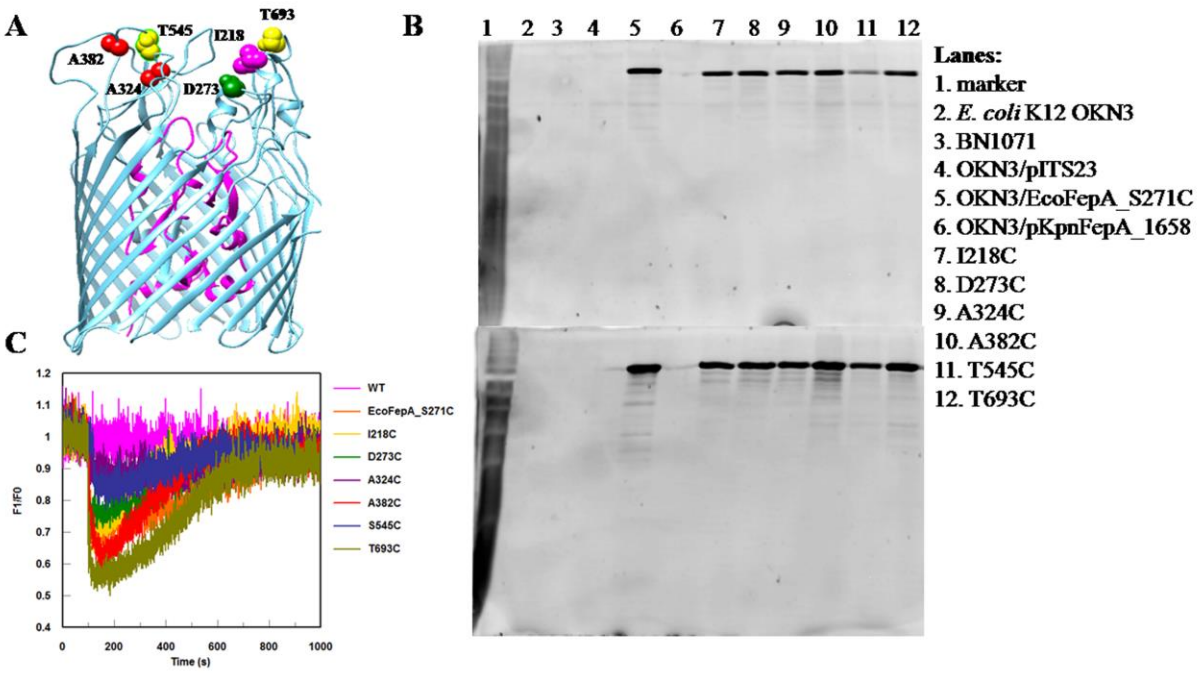

Figure 3.11. Fluoresceination of Cys derivatives of KpnFepA_1658 and fluorescence spectroscopic assay of FeEnt transport in *E. coli* background:

Panel B shows the fluorescent image of the SDS PAGE of the whole cell lysate (upper) and outer membrane fractions (lower) of KpnFepA_1658 and Cys derivatives with proper controls. Cells were grown under the iron-deficient condition and labeled with FM and subjected to SDS-PAGE. Panel C shows the fluorescence spectroscopic assay that monitors FeEnt binding (quenching of fluorescence) and subsequent transport (fluorescence recovery) of FeEnt inside the cell.

All putative KpnFepAs share more than 50% sequence identity with EcoFepA. KpnFepA_1658 shows 81% similarity, which raised the possibility that monoclonal antibodies raised against EcoFepA could also detect KpnFepA_1658. We developed an immunoblot of KpnFepA_1658 using a pool of anti-EcoFepA monoclonal antibodies. From our collection, monoclonal antibody 41 (mAb41) detected KpnFepA_1658 efficiently. Although this antibody mixture also detected other putative catecholate receptors, in some cases, detection was poor (Figure 3.7). Quantification of the expression of different KpnFepAs using mAb41 was not feasible. So, we relied on SDS-PAGE followed by Coomassie blue staining of the outer membrane protein fractions (approximately 40 ug) of these different KpnFepAs. We isolated OM fractions

after grown cells under the iron-deficient condition to quantify the expression level of all OM TBDTs used in this study (Figure 3.7).

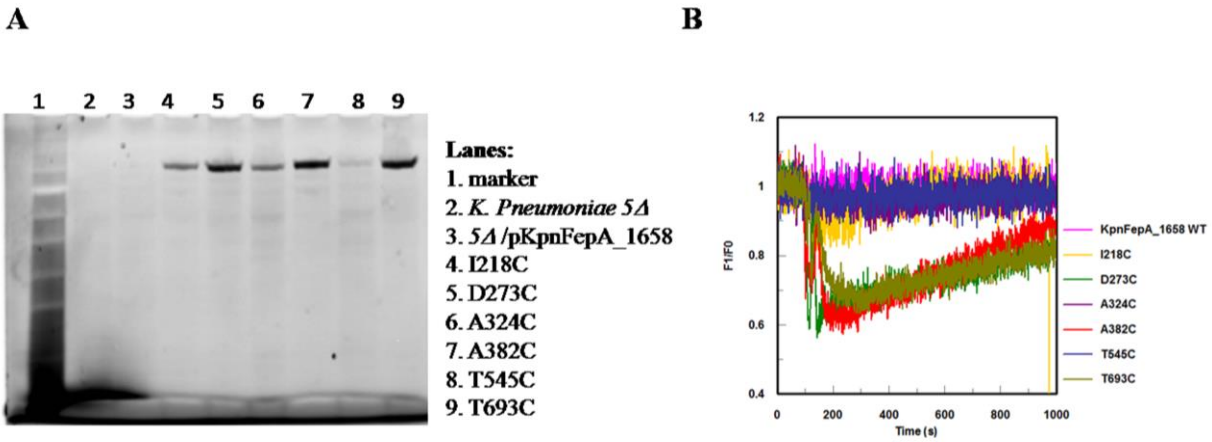

Figure 3.12. Fluoresceination of Cys derivatives of KpnFepA_1658 and fluorescence spectroscopic assay of FeEnt transport in *K. pneumoniae* background:

Panel A shows the fluorescent image of the SDS PAGE of the whole cell lysate of KpnFepA_1658 and Cys derivatives with proper controls. Cells were grown under the iron-deficient condition and labeled with FM and subjected to SDS-PAGE. Panel C shows fluorescence spectroscopic assay, which monitors FeEnt binding (quenching of fluorescence) and subsequent transport (fluorescence rebound) of FeEnt inside *K. pneumoniae* cell.

As discussed before, EcoFepA, AbaFepA (Nairn, Eliasson et al. 2017), and KpnFepA_1658 contain two free Cys residues in its native protein structure, which are involved in disulfide bond formation and necessary for effective FeEnt transport. Likewise, KpnFepA_4984 (C490, C497), KpnFepA_2380 (C451, C460), and KpnFepA_IroN (C475, C484) also contain two free Cys in its protein structure mostly 6 to 9 residues apart from each other and presumably involved in disulfide formation. The native form of these proteins did not participate in alkylation upon treated with FM. The Siderophore nutrition test also revealed that reducing these native Cys pairs disrupted FeEnt transport through *K. pneumoniae* FepAs (Data not shown). The fluorescent image of SDS-PAGE of Cys derivatives of KpnFepA_4984 in OKN3 background showed proper

labeling of these constructs when grown under iron-deficient condition followed by attachment of FM *in vivo (*Figure 3.13A). However, the extent of labeling of these constructs was not too intense compared to KpnFepA_1658 Cys derivative in both *E. coli* and *K. pneumoniae* backgrounds. Also, KpnFepA_4984 expression in the outer membrane fraction revealed less expression compared to KpnFepA_1658 or EcoFepA. Among all these putative FeEnt transporters, KpnFepA_2380 appeared to be least expressed in the outer membrane. Its Cys derivatives did not show intense FM labeling compared to other KpnFepAs Cys derivatives (3.14B). Siderophore nutrition tests and fluorescence imaging of Cys mutants of KpnFepA_1658 and KpnFepA_4984 indicate FeEnt transport through these transporters. In contrast, so far, KpnFepA_2380 status is not clear as siderophore nutrition test did not show FeEnt transport through this receptor. The outer membrane fraction and labeling experiment shows that this receptor is not well expressed in both *E. coli* and *K. pneumoniae* under iron-deficient conditions.

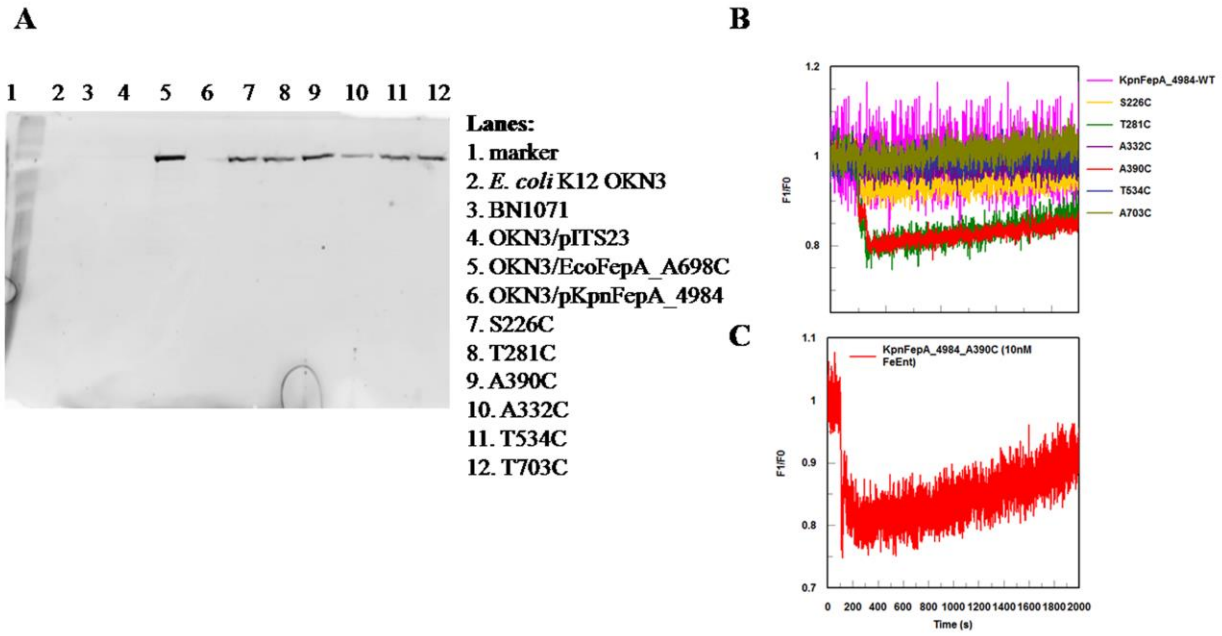

Figure 3.13. Fluoresceination of Cys derivatives of KpnFepA_4984 and fluorescence spectroscopic assays of FeEnt transport in *E. coli* and *K. pneumoniae* background:

Panel A shows the fluorescent image of the SDS PAGE of the whole cell lysate of KpnFepA_4984 and Cys derivatives with proper controls. Cells were grown under the iron-deficient condition and labeled with FM and subjected to SDS-PAGE. Panel B and panel C show fluorescence spectroscopic assay that monitors FeEnt binding (quenching of fluorescence) and subsequent transport (fluorescence rebound) of FeEnt inside *E. coli* and *K. pneumoniae* cells.

In vivo FM labeling of EcoIutA and its derivatives showed mixed responses; whole cell lysates of Cys derivatives A245C, T251C and T548C were labeled *in vivo* but S172C, A174C and A389C did not show any sign of labeling (3.15C). EcoIutA shared 22% identity with EcoBtuB protein sequence and may be predicting EcoIutA protein folded structure using EcoBtuB as template did not turn out accurate. Also, it could be possible that the residues S172, A174 and A389 were not located at loop region but somewhere else; in transmembrane internal region of beta barrel where they could not be accessible to FM. We separated outer membrane fractions from these Cys derivatives of EcoIutA and denatured them using 1% SDS followed by boiling these samples for 5 minutes and then again labeled with 5µM FM at standard condition we used before.

Fluorescent image of SDS-PAGE of outer membrane fractions revealed that denaturing proteins exposed engineered Cys residues to be labeled by FM which were not accessible to FM previously in non-denatured folded condition (Figure 3.15B lower left). We also used EcoBtuB crystal structure to predict residues in the loop region for Cys substitutions and fluorescent images showed all Cys derivatives of EcoBtuB we created in this study were labeled well with FM (Figure 3.16B).

3.3.6. Fluorescent spectroscopic assay for FeEnt, FeAbn and Vitamin B_{12} transport:

Using fluorescence spectroscopy assay, we evaluated every Cys derivative of different KpnFepAs, EcoIutA, and EcoBtuB to monitor FeEnt, FeAbn, and VitB_{12} binding and transport, respectively, in *E. coli* background and *K. pneumoniae* background.

Each fluorescently labeled Cys derivative of KpnFepA_1658 behaved differently in terms of binding and transporting FeEnt inside cells in *E. coli* background (Figure 3.11C). Fluorescently labeled substitutions D273C, A382C, and T693C were quenched more than I218C, A324C, and T545C; consistent with fluorescent SDS-PAGE results. Wild-type KpnFepA_1658 and other controls (OKN3, BN1071, OKN3/pKpnFepA_1658) used in the study were not fluorescently labeled because of the absence of free sulfhydryl. They did not show detectable quenching and recovery upon addition of FeEnt, which shows the specificity of the fluorophore to targeted Cys-modified FepA. We also performed fluorescent transport assay for FeEnt transport in *the K. pneumoniae* background (Figure 3.12B).

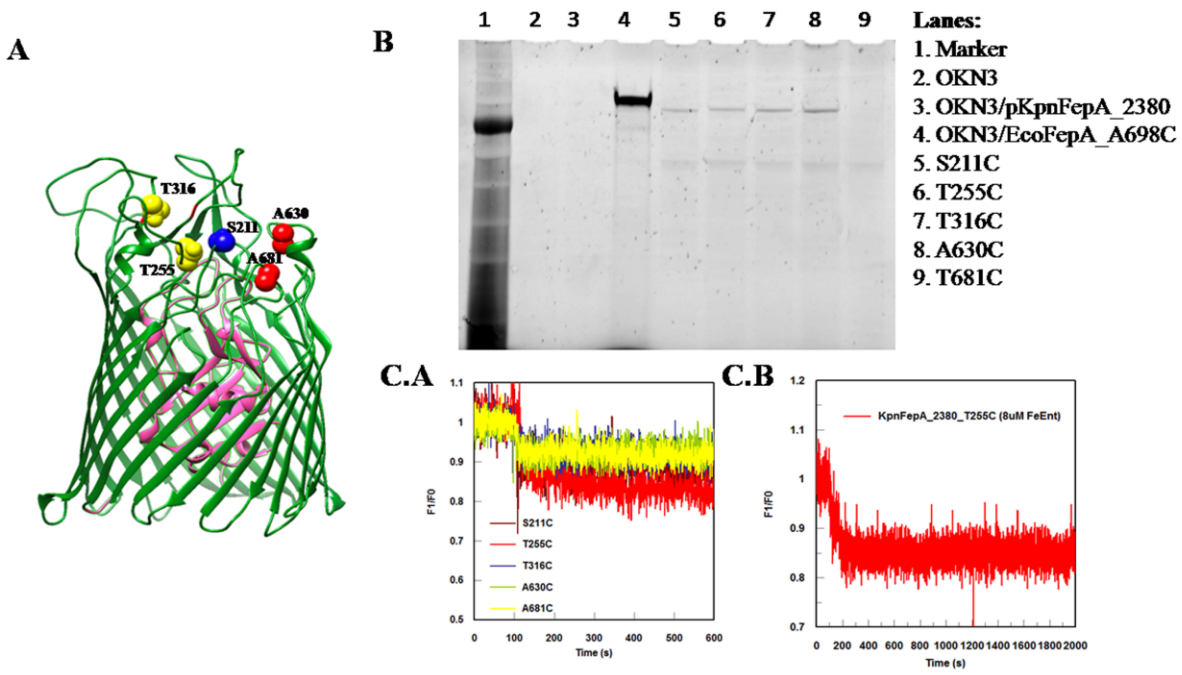

Figure 3.14. Tertiary structure prediction of KpnFepA_2380 and fluoresceination of Cys derivatives of KpnFepA_2380 and fluorescence spectroscopic assay of FeEnt transport in *E. coli* and *K. pneumoniae* background:

Panel A depicts the predicted protein structure of KpnFepA_2380 using the CHIMERA program and selected residues in the loop regions to be substituted to Cys using site-directed mutagenesis. Panel B shows the fluorescent image of the SDS PAGE of the whole cell lysate of KpnFepA_2380 and its Cys derivatives with proper controls. Cells were grown under the iron-deficient condition and labeled with F.M. and subjected to SDS-PAGE. Panel C.A and panel C.B. show fluorescence spectroscopic assay that monitors FeEnt binding (quenching of fluorescence) and subsequent transport (fluorescence rebound) of FeEnt inside *E. coli* and *K. pneumoniae* cells.

FM well-labeled all the Cys mutants of KpnFepA_1658 in *K. pneumoniae* background, and labeling was comparable with *E. coli* background as well. Although D273C, A382C, and T693C were well labeled and showed better quenching and fluorescence recovery pattern than other mutants in *the K. pneumoniae* background. Alternatively, lesser fluorescence quenching in *K. pneumoniae* background than *E. coli* may derive from full-length LPS O-antigen and polysaccharide capsule in its cell envelope, which create a more hydrophilic surface than that of rough *E. coli* K-12. We still observe dose-dependent quenching and recovery during FeEnt uptake

in *K. pneumoniae* with acceptable reproducibility. In the case of KpnFepA_4984 Cys derivatives, except A332C, all the other mutants (S226C, T281C, A390C, T534C, and T703C) were well labeled (Figure 3.13B). Still, the overall labeling of each KpnFepA_4984 Cys derivative was less intense than EcoFepA_A698C and KpnFepA_1658 Cys derivatives. In *the E. coli* background, Cys derivatives of KpnFepA_4984 showed quenching ranging from 0 to 20%. T281C and A390C showed maximum quenching around 20%, which is lesser than other maximum quenched Cys derivatives of KpnFepA_1658 upon binding to FeEnt. It took approximately 30-40 minutes for the fluorescence to recover to the original level for Cys derivatives T281C and A390C, reflecting a slower FeEnt transport rate through this receptor compared to KpnFepA_1658 and KpnIroN, which transported FeEnt quickly compared to the former one. We also looked FeEnt binding, and the transport pattern of FeEnt through FM labeled Cys derivative A390C of KpnFepA_4984 in *K. pneumoniae* background (Figure 3.13C). It showed around 20% quenching and took about 30-40 minutes for fluorescence recovery, which is almost similar as we observed in *the E. coli* background. For Cys derivatives of KpnFepA_2380, all the mutants were poorly FM labeled. Also, this protein did not express well in *the E. coli* background even after expressing this gene under EcoFepA promoter and signal sequence. Upon binding FeEnt to Fluorescently labeled mutants of this receptor showed 5% (T316C) to 20% (T255C) quenching. Still, fluorescence did not recover even after 30 minutes (Figure 3.14 C. A), showing that this receptor transport at the slowest rate compared to all the other FeEnt receptors we discussed before.

So far, we showed fluorescence spectroscopic methods which monitor FeEnt binding and transport by using EcoFepA (Smallwood, Jordan et al. 2014), AbaFepA (Nairn, Eliasson et al. 2017), and KpnFepAs (in this study). But there are other TonB dependent receptors in the bacterial system that transport various other siderophores other than FeEnt and play a vital role in bacterial

pathogenesis. One such receptor is the iron uptake transporter (IutA) which recognizes ferric aerobactin (FeAbn) and transports it across the outer membrane (OM). Hypervirulent *K. pneumoniae* strains secrete siderophores, out of which more than 90% account for aerobactin. In contrast, in classical *K. pneumoniae*, it accounts for only about 6%, directly linking Abn's role in bacterial pathogenesis.

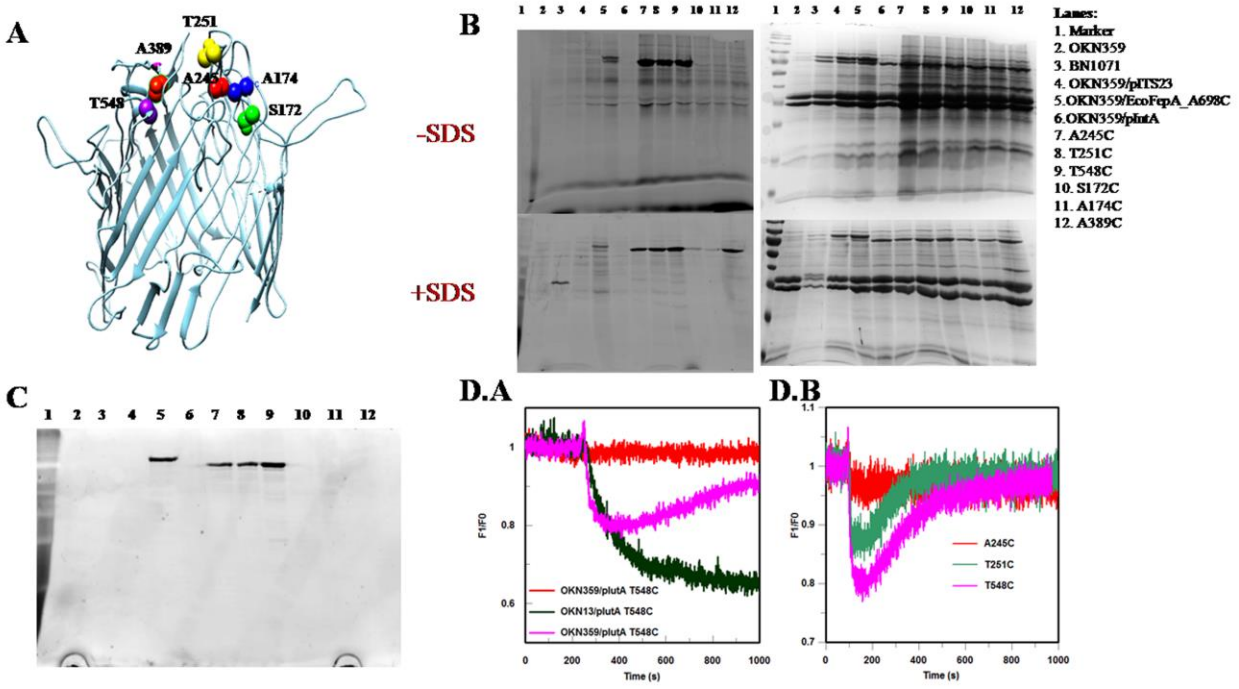

Figure 3.15. Tertiary structure model of EcoIutA, fluoresceination of Cys derivatives, OM separation, and FeAbn transport:

Panel A depicts the predicted protein structure of EcoIutA using the CHIMERA program and selected residues in the loop regions to be substituted to Cys using site-directed mutagenesis. Panel B shows the fluorescent image of the SDS PAGE of the whole cell lysate of EcoIutA and its Cys derivatives with proper controls. Cells were grown under the iron-deficient condition and labeled with FM and subjected to SDS-PAGE. Panel C (upper left and lower left) shows the fluorescent image of the OM fractions without and with SDS treatment, respectively, and panel C (upper right

and lower right) shows the Coomassie blue staining of the fractions from panel C (upper left and lower left) respectively. Panel D.A. offers the fluorescent spectroscopic assay controls for FeAbn transport, and panel D.B. shows the FeAbn binding and transport of Cys derivatives of EcoIutA using fluorescence spectroscopic assay.

We adapted the spectroscopic fluorescence method to monitor the binding of FeAbn to *E. coli* IutA and transport across the outer membrane. We selected a few residues in the outer loop region of the predicted EcoIutA tertiary structure for substitution to Cys; out of 6 Cys derivatives we created, only 3 (A245C, T251C, and T5478) were accessible to FM (Figure (3.15C). Each of these mutants showed different binding to FeAbn in terms of fluorescence quenching. EcoIutA Cys derivative T548C was the only construct that showed 20% quenching upon adding 10 nM FeAbt, and others (A245C, T255C) showed 5 to 10% quenching (Figure 3.15D.B), and others (S172C, A174C, and A389C) were not even FM labeled. Additionally, upon quenching, fluorescence recovered within 10-15 minutes entirely in *E. coli* background. Adaptation of this another siderophore transport across IutA showed the breadth of this fluorescence spectroscopic method for monitoring different TonB dependent siderophore binding and transport. In addition to these siderophore transport, we also adapted this methodology for TonB dependent receptor BtuB, which recognizes and actively transports vitamin B12 across the outer membrane. We created four Cys derivatives of this receptor and looked for binding and transport through these derivatives. Only FM labeled Cys derivative S286C was quenched up to 30% upon addition of 2.5 nM vitamin B_{12}, and fluorescence recovered within 10 minutes.

By contrast, all the other labeled Cys derivatives (T185C, T450C, T491C) did not show any quenching (Figure 3.16D lower). Overall, we functionally characterized three of *K. pneumoniae* FepA and showed transport of FeEnt using the spectroscopic method. We also

adapted this method to show the transport of FeAbn and vitamin B_{12} using their respective transporters, which shows the breadth of this methodology for any high-affinity ligand transport.

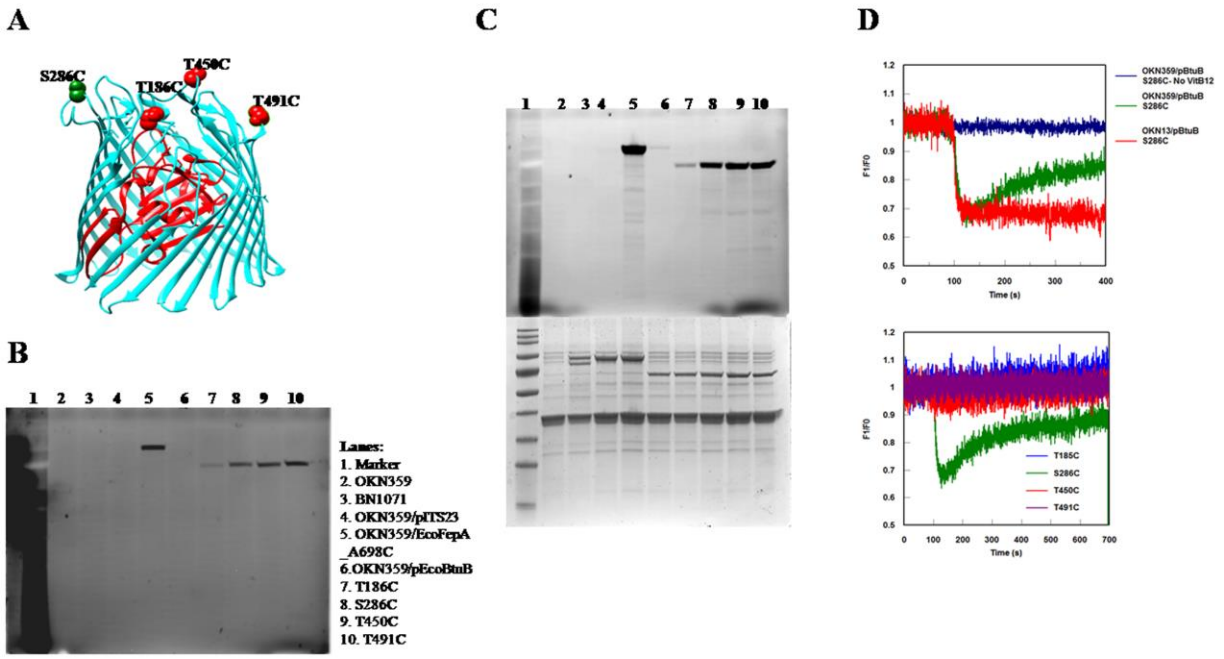

Figure 3.16. The tertiary structure of EcoBtuB, fluoresceination of Cys derivatives, OM separation, and Vitamin B_{12} transport:

Panel A depicts the protein structure of EcoBtuB with selected residues in the loop regions to be substituted to Cys using site-directed mutagenesis. Panel B shows the fluorescent image of the SDS PAGE of the whole cell lysate of EcoBtuB and its Cys derivatives with proper controls. Cells were grown under the iron-deficient condition and labeled with FM and subjected to SDS-PAGE. Panel C (upper) shows the fluorescent image of the OM fractions, and panel C (lower) shows the Coomassie blue staining of the fractions from panel C (upper). Panel D (upper) shows the fluorescent spectroscopic assay controls for Vitamin B_{12} transport. Panel D (lower) shows the Vitamin B_{12} binding and transport of Cys derivatives of EcoBtuB using fluorescence spectroscopic assay.

3.4. Discussion:

Bacterial infections are the long-standing threats that intensified over the past decade. In 2009, for example, there were around 100,000 deaths in US hospitals and 2/3 mortality caused by Gram-negative bacteria. Among these, 20% of bacteria strains were resistant to all known antibiotics (Elemam, Rahimian et al. 2009). Despite the fact, at that time, WHO notified urgent need for antibiotics against Gram-negative CRE/ESKAPE pathogens, but pharmaceutical companies lessened the effort to combat microbial pathogens. Moreover, in 2019, there were around 2.8 million infections with ESKAPE and other antibiotic-resistant bacteria and out of which more than 35,000 US deaths were reported (Klebba, Newton et al. 2021). Classically, two popular antimicrobial treatments exist; either inhibiting essential biochemical pathways in microbes (antibiotics) or molecular constructs (vaccines) that have clinical application and have saved millions of lives. But the evolution of resistance in these pathogens, which has arisen due to natural selection of variations, has undermined both approaches. Usually, antibiotic resistance occurs due to the change in the permeability of cell envelopes because of mutations and antibiotic exporting capabilities of prokaryotic cell envelop proteins (Nikaido 2003, Yu, McDermott et al. 2003). At the same time, vaccine inefficacy results from the change in the antigenic determinant of the pathogen. So ultimately, we are in urgent need to find out new biochemical pathways or proteins or other possible molecules which can be a vulnerable target for drugs or vaccines.

At the time of colonization in human and animal hosts, microbes must acquire iron for growth and proliferation (Pi, Jones et al. 2012). Gram-negative bacterial TBDTs at the outer surface recognize and bind with iron complexes with high affinity and specificity, are transported across OM bilayer upon activation of the action by inner membrane TonB protein. Virtually all Gram-negative bacteria acquire iron using TonB dependent process; virulence determinates

(Bullen 1981, Bullen, Rogers et al. 2005), which explain the interest of blocking TonB action retarding bacterial growth. We initially developed the fluorescence spectroscopy method to monitor the high-affinity ligand binding and TonB dependent uptake process of FeEnt in *E. coli* FepA (Smallwood, Jordan et al. 2014). We have also adapted this methodology for *A. baumannii* FepA and customized these for FLHTS, which allows us to screen for the chemical compounds that can inhibit TonB action (Nairn, Eliasson et al. 2017). One of these real-time-based cell assays advantages is that we do not require reconstitution of TonB dependent transport *in vitro*. Apart from that, convenience, predictability, miniaturization, automation, and multiplexing are some of the advantages this live-cell assay offers. In this study, we broadened the scope of these fluorescence spectroscopic assays in multiple ways; First, we characterized multiple catecholate receptors in *K. pneumoniae* which preferably recognize, bind, and transport FeEnt. Second, we showed the breadth of this assay for hydroxamate siderophore FeAbn transport through EcoIutA. Third, we showed that these assays are not restricted for observation of TonB dependent siderophore transport only, instead of all kinds of TonB dependent ligand transport in Gram-negative bacteria, i.e., Vit B_{12} transport through EcoBtuB.

K. pneumoniae strains encode siderophore biosynthetic operon systems for enterobactin (Ent), glucosylated enterobactin (GEnt), aerobactin (Abn), and yersiniabactin production (Ybt) (Holden and Bachman 2015). All these systems are Fur- regulated which are activated upon iron deprivation in the host. Using identities in primary structures between different putative KpnFepAs and EcoFepA by CLUSTALW, we predicted the tertiary protein structure using the Modeler function of CHIMERA. Then targeted residues in the loop regions of these predicted KpnFepAs and introduced single Cys residues at those specific positions. Overall, in most cases, these residues in the loop regions in KpnFepAs at equivalent sites to those in EcoFepA did not

compromise FeEnt transport even after KpnFepAs were fluoresceinated. EcoFepA contains a disulfide-bonded Cys pair in L7 (Buchanan, Smith et al. 1999). All the KpnFepAs also have Cys pairs in the same loop probably which are essential for FeEnt transport and do not transport FeEnt if reduced by any reducing agent, as in EcoFepA by BME (Majumdar, Trinh et al. 2020). Like wild-type EcoFepA, none of the WT KpnFepA got FM labeled by our procedure. FM specifically labeled only engineered individual FepA Cys substitutions, with minimal background labeling. We used OKN3, OKN359, BN1071, and respective recombinant strains as negative controls in our FM labeling experiments. None of the proteins in the whole cell lysate showed signs of labeling by FM, which reiterates the specificity of FM to only engineered Cys substituted FepA in our experiments.

All the putative FepAs from *K. pneumoniae* shared more than 50% sequence similarity with EcoFepA, so we used a pool of collection of monoclonal antibodies raised against EcoFepA to check any cross-reactivity with KpnFepAs, and we found out monoclonal antibody #41 (mAb41) in our pool cross-reacted with KpnFepAs qualitatively but not quantitatively (Figure 3.7B). We cloned these KpnfepA genes under the control of both EcofepA promoters and their respective native promoters. We looked for the expression of proteins in outer membrane fractions in both *E. coli* and *K. pneumoniae* backgrounds. Both KpnFepA_1658 and KpnFepA_4984 were expressed in *E. coli* and *K. pneumoniae* background, although KpnFepA_4984 expressed poorly compared to KpnFepA_1658. We cloned *KpnfepA_2380* also under the control of *EcofepA* promoter and *EcofepA* signal sequence upstream. Instead of using the same approach, KpnFepA_2380 expression was lesser than any other KpnFepA we expressed in *E. coli* and *K. pneumoniae* backgrounds. Our FM labeling experiments also revealed minimal labeling of Cys derivatives of KpnFepA_2380. Also, the siderophore nutrition test and fluorescence transport

assays did not provide any concrete evidence of FeEnt transport in given conditions. It could be possible that codon optimization could help the better expression of these proteins, or some other native factors are necessary for proper expression of these proteins in vitro or in vivo (host), about which we don't have enough knowledge.

In conclusion, after expressing both KpnFepA_1658, KpnFepA_4984, and KpnFepA_2380 in *E. coli* and *K. pneumoniae* background, we observed both KpnFepA_1658 and KpnFepA_4984 transport FeEnt in siderophore nutrition test and fluorescence transport assay. Also, siderophore nutrition and transport assay data concluded that KpnFepA_1658 transport FeEnt faster than KpnFepA_4984. On the other side, KpnFepA_2380 binds to FeEnt but does not transport FeEnt in the given time in fluorescence transport assay. Siderophore nutrition tests also supported this observation as we did not see bacterial growth around the disk in the case of KpnFepA_2380.

There are 18 TBDTs so far that have been structurally resolved. Their solved structures reiterate the point that, in general, the 22-stranded β- sheets (C-terminal) surround a ∼150 amino acid globule (N-terminal) which regulates the transport of high-affinity ligand through the pore. We initially developed and optimized fluorescence spectroscopic assays for monitoring FeEnt binding and consequently transport of ligand inside the cell for crystallographic resolved EcoFepA (Smallwood, Jordan et al. 2014) and later adapted this methodology on AbaFepA (Nairn, Eliasson et al. 2017) and in this study, various putative KpnFepAs. We concluded that this method applies to different bacterial originated FepAs for observation of FeEnt transport process, which tends to resume basic TBDT structure based on our structural modeling program CHIMERA. In the later part, we showed that this fluorescence spectroscopic approach was applied to other iron complexes, i.e., ferric aerobactin transport through EcoIutA. None of the IutA orthologs from any

Gram-negative bacterial species have been structurally solved so far, making it harder for us to predict its proper tertiary structure. So, we used all available structurally determined ferric siderophores receptors' primary sequence and found out sequence identity with EcoIutA primary structure sequence using CLUSTALW and found out EcoIutA shared around 22% sequence identity with EcoBtuB. Based on the predicted EcoIutA tertiary structure using the Modeler function of CHIMERA, we selected six residues (S172, A174, A245, T251, A389, and T548) in the loop region and substituted them to Cys and labeled them with FM. Surprisingly out of 6 selected Cys mutants, only three, A245C, T251C, and T548C, got labeled, and the other three, S17C, A174C, and A389C, did not. It is possible that the last three residues were not at all substituted to Cys, but we eliminated this possibility in two ways; first, DNA sequencing results showed proper substitution of these individual residues to Cys encoding codon. Second, we isolated the outer membrane fractions of all six individual Cys mutants grown under iron-deficient conditions and treated these fractions with SDS, boiled, and then labeled them with FM. In this case, those three mutants also showed labeling with FM, which did not label previously without any SDS treatment. From the second observation, we inferred that it is possible that the predicted EcoIutA tertiary structure does not portray exact loop positions and the selected mutated residues are somewhere in the B-barrel or to other locations where FM could not access Cys.

Nevertheless, Cys substitutions did not affect FeAbn transport as we could see in the siderophore nutrition test. All the Cys mutants of EcoIutA were well expressed in the outer membrane fraction, visualized upon subjecting them to the SDS PAGE followed by Coomassie blue staining. Upon monitoring the FeAbn binding and transport to these IutA mutants using fluorescence spectrophotometer, we observed that using 5 nM FeAbn caused fluorescence quenching in the range of 5% (A245C) to 20% (T548C), and within 10 min., fluorescence

rebounded. To summarize, this is another example where we adapted this spectroscopic fluorescence method to functionally characterize IutA and showed binding of FeAbn and transport through IutA. A series of bacterial siderophore transporters exist in the Gram-negative bacterial outer membrane for ferric siderophore binding and transport. Few TBDTs exist that bind metal complexes with high affinity transport them inside cells, e.g., BtuB; Vit B_{12} transport. So, we used the crystal structure of BtuB and selected few residues, T186, S286, T450, and T491, in the loop region for substitution to Cys and looked for expression of these constructs in the outer membrane. All the constructs were expressed as expected and labeled with FM. For the observation of vit. B_{12} binding and transport, we used 2.5 nM of ligand. We observed that only FM labeled S286C got quenched up to 30%, and within 10-15 minutes, fluorescence was recovered to the original level.

In summary, these spectroscopic assays can be applied to observe binding and transport of any high-affinity TonB dependent ligand, followed by developing a standard high throughput screening format for finding drugs or therapeutics against TonB action. These novel therapeutics may be used for inhibiting bacterial pathogenesis and, ultimately, bacterial infections.

Chapter 4 - Universal fluorescent sensors of high affinity iron transport applied to ESKAPE pathogens

Chakravorty, S., Y. Shipelskiy, A. Kumar, A. Majumdar, T. Yang, B. L. Nairn, S. M. Newton and P. E. Klebba (2019). *J Biol Chem* **294**(12): 4682-4692.

My contribution to this work includes the creation of addition fluorescence sensor of FeEnt (KpnFepA_1658), FeAbn (EcoIutA) and Vitamin B_{12} (EcoBtuB). Most of the work on these sensors include cloning of respective receptor in *E. coli* background, creation of Cys mutants, analyzing the best mutant to be used as universal fluorescent sensor for their respective ligand.

4.1. Introduction:

Biological applications such as the discovery of new therapeutic compounds, biochemical measurements of living cells require cell and/or protein-based sensitive assays with high specificity, affinity, and capacity. According to scientific reports, two-thirds of the mortality in US hospitals is caused by Gram-negative bacterial strains. More importantly, up to 20% of these strains are resistant to all known antibiotics (Elemam, Rahimian et al. 2009). The World Health Organization identified Gram-negative carbapenem-resistant (CRE) strains of *E. coli* and *K. pneumoniae*, and additional ESKAPE pathogens *P. aeruginosa*, *A. baumannii*, and *Enterobacter spp.* as urgent targets for drug discovery (Tacconelli, Sifakis et al. 2018). Chemical compounds that interfere with cell envelope processes were formerly some of the most effective antibiotics, but most of them lost efficacy due to bacterial adaptation (Fisher and Mobashery 2016). The increased antibiotic resistance of Gram-negative bacteria primarily originates from their cell envelope biochemistry: the outer membrane (OM) excludes large or hydrophobic antibiotics (Nikaido 2003); periplasmic enzymes degrade or inactivate antibiotics that breach the OM barrier;

inner membrane (IM) pumps expel hydrophobic compounds, including antibiotics (Yu, McDermott et al. 2003). Similar but distinct processes occur in Gram-positive bacteria, creating a clinical crisis in the treatment of bacterial infections, necessitating the need for novel therapeutics to treat bacterial infections.

Nevertheless, in eukaryotic hosts, e.g., humans and animals, bacteria face nutritional obstacles. For example, iron is a nearly universally essential element in intermediate and energy metabolism (Rouault and Maio 2017). Eukaryotic hosts sequester iron to reduce or eliminate bacterial virulence. Still, successful microbial pathogens secrete siderophores that capture the metal from host proteins (Konopka, Bindereif et al. 1982), and ferric-siderophore complexes enter bacterial cells through high-affinity uptake systems (Nagy, Moreland et al. 2013). Iron deprivation retards bacterial growth; iron acquisition promotes it (Klebba, McIntosh et al. 1982). The balance of these host-pathogen competing mechanisms influences the outcome of infection, so bacterial iron uptake systems are potential targets for novel antibiotics.

The Gram-negative CRE/ESKAPE organisms obtain iron with TonB-dependent OM systems (Noinaj, Guillier et al. 2010). These organisms synthesize aposiderophores that chelate and remove iron from host proteins and use TonB-dependent OM transporters (TBDT) to internalize the resulting ferric siderophores. Their ability to scavenge iron makes them a target of innate immune systems: mammals elaborate an entire family of proteins, the lipocalins, to antagonize catecholate iron complexes like ferric enterobactin (FeEnt). Conversely, the bacteria produce OM TBDTs that specifically bind and transport iron complexes (Schauer, Rodionov et al. 2008, Jordan, Zhou et al. 2013, Klebba 2016). Each Gram-negative bacterium produces many TBDTs for iron acquisition: *E. coli* K12 encodes 7, and wild isolates produce more, that either

internalize a ferric siderophore, or strip iron from eukaryotic binding proteins, or extract and transport heme from myoglobin or hemoglobin (Klebba, Newton et al. 2021). Their sub-nanomolar binding affinities impart specificity for a particular iron complex to each individual TBDT, but they all require interactions with TonB to achieve iron uptake. TonB action transmits IM proton motive force (PMF) potential energy to TBDT in the OM, facilitating their internalization of bound iron complexes. TonB protein is ubiquitously conserved among Gram-negative bacterial pathogens, including the ESKAPE bacteria, which makes it a determinant of bacterial pathogenesis (Williams 1979). We have previously designed a spectroscopic fluorescence method to monitor high-affinity ligand binding and transport reactions (Smallwood, Jordan et al. 2014, Hanson, Jordan et al. 2016). We created sensors to detect FeEnt concentration in the environment by genetically engineering EcoFepA and labeled it with fluorescein maleimide (FM). When FeEnt is bound to labeled FepA, fluorescence is quenched, and as FeEnt is depleted in the environment due to cellular uptake, fluorescence rebounded to its normal level. Consequently, FepA-FM tracked the binding and transport of FeEnt by live bacteria in real-time.

We created universal fluorescence spectroscopic assays that measure ligand uptake by any pathogenic bacteria. Despite the sensitivity and accuracy of species-specific fluorescent spectroscopic methods, experimental manipulations of ESKAPE pathogens are always concerning due to potential hazardousness and technical difficulties. Hence, we modified the assay in a manner that allowed the observation of FeEnt transport by any organisms, including clinical isolates, without genetically engineering them. A TonB-deficient bacterium, with fluorescently labeled FepA, acts as a sensor strain that binds FeEnt but cannot transport it. When cohabiting an environment with other wild isolates of *A. baumannii*, *P. aeruginosa*, or *E. cloacae*, the sensor strain monitored FeEnt uptake and thereby TonB action in the wild isolates. Apart from these

binding competent and transport defectives universally fluorescently labeled sensors for FeEnt and Fc detection, we also generated fluorescent-labeled purified protein for hemin binding. These sensors report ligand concentration in the solution and monitor the transport of these ligands by other bacteria, e.g., ESKAPE bacteria.

4.2. Methodology:

Generation of Cys mutants for cell-based sensors are a continuation from the previous chapter and have been discussed in detail there. To create sensors, we chose each individual mutant for different receptors which gave better quenching and sensitivity in our experiments and transformed them in OKN1 (*tonB*$^{-}$) background: FhuA_D396C and OKN13 (*tonB*$^{-}$, *fepA*$^{-}$) background: KpnIroN_T210C.

To generate Cys mutants in LmoHbp2, we cloned *the hbp2* structural gene in pAT28 (Trieu-Cuot, Carlier et al. 1990). We introduced Cys substitutions at the position of interest, verified the construct by DNA sequencing, and transformed the pAT28 derivative pLmoHbp2_S154C into *L. monocytogenes* EGDe*Δhbp2* (Xiao, Jiang et al. 2011). The strain was grown to late exponential phase in iron-deficient media (MOPS-L) and then we purified secreted mutant protein from iron-deficient bacterial cultures (Newton, Klebba et al. 2005). To get secreted Hbp2_S154C from the culture, we removed cells by centrifugation, precipitated the supernatant with 0.6 M neutralized trichloroacetic acid, and collected the precipitate at 10,000 x g for 45 minutes, washed the pellet twice with 70% ethanol, and resuspended the pellet in 50mM $NaHPO_4$, at pH 6.7. We labeled LmoHbp2_S154C with 5 uM 7-diethylamino-3-(4'-maleimidylphenyl)-4-methyl coμMarin (CPM), in 50 nM $NaHPO_4$, pH 6.7 for 30 minutes at 37°C. After this process, we immediately quenched the reaction with 130 mM BME and incubated the reaction mixture

with ice-cold acetone (7 volumes) at -20°C for 4 hours and precipitated protein by centrifugation at 10,000 x g for 20 min. Next, we chromatographically removed the impurities and collected pure protein fractions for spectroscopic studies.

For fluorescence decoy assays, we incubated 2 x 10^7 sensor cells and 2 x 10^7 cells of test organisms (*E. coli* MG1655, *K. pneumoniae* Kp52.145, *A. baumannii* I7878/19606, *P. aeruginosa* PA01, *E. cloacae*) together in 2 ml of PBS + 0.4% glucose, at 37°C, in a quartz cuvette and incubated until fluorescence stabilized. After adding relevant ferric siderophore in the cuvette at 100s, we monitored the time-course of fluorescence emissions at 520 nm for about 20-40 min, with constant stirring. FD assays in microtiter plates (Hanson, Jordan et al. 2016) had 4 x 10^6 FD sensor cells with 3 x 10^6 test organisms in 200 ul of PBS + 0.4% glucose at 37°C. We used 5 nM of ferric siderophore's final concentration to observe the quenching and recovery of fluorescence in the presence and absence of CCCP. For protein-based assay; Hn transport, we used labeled protein as a sensor with test organism and observed Hn transport in the spectroscopic assay for about 2 h. We performed each experiment in triplicate and calculated the mean value and standard deviation, plotting the resulting data using Grafit 6.0.12.

4.3. Results:

4.3.1. Universal fluorescence sensors of FeEnt acquisition:

We originally devised a transporter- or species-specific spectroscopic fluorescence assay of FeEnt uptake of *E. coli* (Hanson, Jordan et al. 2016) and *A. baumannii* (Nairn, Eliasson et al. 2017). The same approach was effective against *K. pneumoniae* for FeEnt uptake. From the strain Kp52.145, we cloned and genetically engineered (Cys-substitutions) KpnfepA structural gene to enable site-directed fluoresceination in its native cellular (i.e., *K. pneumoniae*) and in *E.*

coli environment. FM exclusively labeled KpnFepA in living cells likewise FepA orthologs of *E. coli* and *A. baumannii* and the fluoresceinated OM protein detected and quantified its ligand, FeEnt in the solution. When FeEnt bound to KpnFepA-FM, fluorescence gets quenched, and as the transporter's activity depleted FeEnt from the solution, fluorescence rebounded. Thus, by the species-specific approach, EcoFepA-FM (Smallwood, Jordan et al. 2014, Hanson, Jordan et al. 2016), AbaFepA-FM (Nairn, Eliasson et al. 2017), and KpnFepA-FM detected its native ligand and reflected its transport in the spectroscopic assay (Figure 4.1A and 4.2A). These transporters require inner membrane protein TonB action for the active transport of these ligands (i.e., FeEnt and FeAbn). In the absence of TonB, ligand is not transported across OM (i.e., fluorescence recovery). So ultimately engineering in the transporter of specific bacteria, we observed, monitored, and characterized their TonB-dependent iron uptake processes.

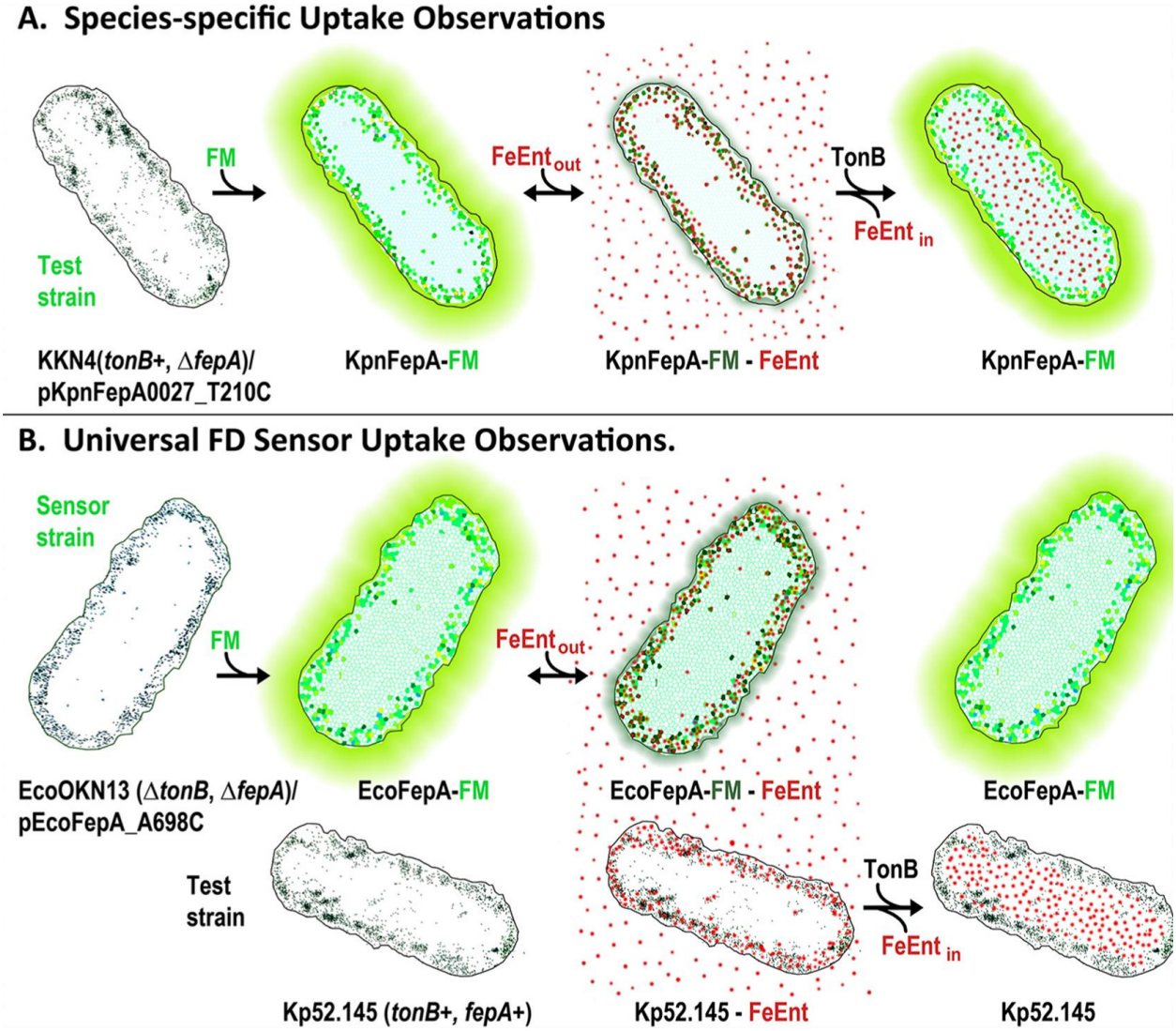

Figure 4.1. Fluorescence spectroscopic assay design:

(A) Shows the species-specific design of fluorescence spectroscopic assay in which OM siderophore receptor from target organism contains Cys substitution in the loop region labeled with FM. Fluorescence quenching depicts FeEnt binding followed by fluorescence recovery, which represents TonB dependent transport in *K. pneumoniae*. **(B)** Shows the universal FD sensor assay design. The sensor strain OKN13 (binding competent but transport deficient) reflects TonB dependent transport in the target organism in the same solution. Figure adapted from (Chakravorty, Shipelskiy et al. 2019).

This species-specific method for observation of high-affinity ligand transport was sensitive and accurate. Still, genetic and biochemical manipulations of ESKAPE organisms and other

pathogens are technically challenging and potentially hazardous. By modifying this method, we extended the scope of this assay to allow observation of FeEnt uptake by other organisms, including clinical isolates, without genetically engineering them. TonB-deficient *E. coli* or other Gram-negative bacterial cells adsorb ferric siderophores and other TonB dependent ligands, i.e., metal complexes but cannot transport them. Thus, FeEnt bound to *E. coli* OKN13(*ΔtonB*, *ΔfepA*)/pEcoFepA-FM, quenching its fluorescence but prevented FeEnt transport or internalization. The placement of EcoFepA-FM in OKN13 transformed the cell into a fluorescence decoy (FD) sensor, whose emissions are inversely related to the concentration of FeEnt. These modified, transport-defective, physiologically inert, and fluorescent *ΔtonB* bacteria detected the presence and concentration of FeEnt in the solution. When this sensor strain cohabited an environment with other bacteria in the cuvette (i.e., ESKAPE), it reflected their uptake of FeEnt because of the presence of TonB. Ultimately, *ΔtonB* FD sensor cells monitored FeEnt transport by wild isolates of *K. pneumoniae*, *A. baumannii*, *P. aeruginosa* or *E. cloacae*. So, this FD sensor observed FeEnt uptake by all the organisms we tested, reflecting TonB action in the pathogens (Figure 4.1B and 4.2B).

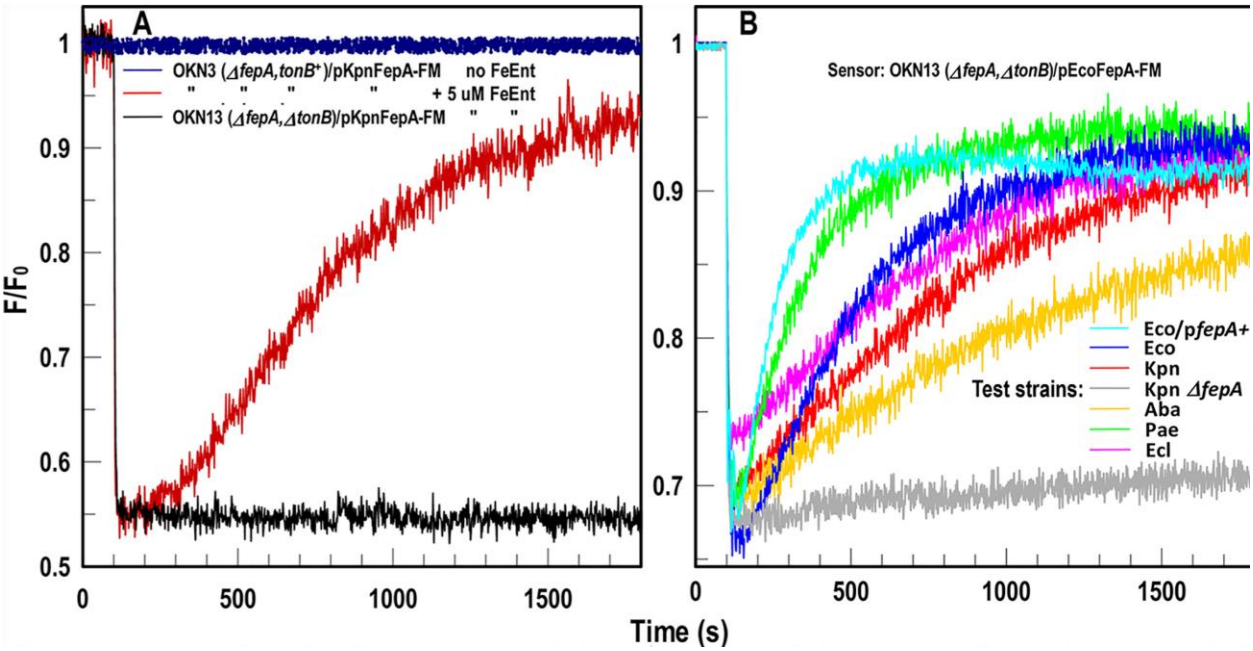

Figure 4.2. FD sensor analysis of FeEnt acquisition by ESKAPE pathogen:

(A) Shows the species-specific fluorescence spectroscopic assay for FeEnt binding and transport. *E. coli* cells which express *K. pneumoniae* OM receptor are labeled with FM and then exposed to FeEnt in PBS + 0.4% glucose solution in cuvette. Tracing shows the emission of living cells in the absence (dark blue) or presence (red or black). In *tonB*$^+$ cells, fluorescence recovers due to transport of FeEnt inside cell but in *tonB*- cells, fluorescence gets quenched all the time due to inability of this cell to transport FeEnt inside cell (OKN13/pEcoFepA-FM behave as FD sensor for FeEnt transport). **(B)** Shows the universal sensor assay of FeEnt transport using OKN13/pEcoFepA-FM as sensor strain). Sensor strain binds to FeEnt so that fluorescence gets quenched but inability of this sensor to transport FeEnt does not allow fluorescence recovery. But in the presence of target bacteria along with sensor strain in the same solution allows transport of FeEnt due to ability of target bacteria to uptake FeEnt. Figure adapted from (Chakravorty, Shipelskiy et al. 2019).

4.3.2. Affinity measurement by spectroscopic assays:

While comparing the recognition of FeEnt and its glucosylated form, FeGEnt (also known as ferric salmochelin; (Williams, Rabsch et al. 2006), by EcoFepA and KpnFepA, analytical capabilities of spectroscopic fluorescence assays were obvious. It is already proven that Gram-negative bacteria, including *K. pneumoniae*, glucosylate enterobactin avoiding its recognition by lipocalin (Smith 2007, Valdebenito, Muller et al. 2007). The ability to transport FeGEnt enhances invasiveness (Bachman, Lenio et al. 2012) whereas *E. coli* K12 contains a single chromosomal

locus fepA that encodes its FeEnt transporter, pathogenic *K. pneumoniae* contains at least four fepA orthologs (chromosomal loci 1658, 2380, 4984; plasmid PII locus 0027). The iroN of *Salmonella typhimurium* has a role in FeGEnt uptake (Williams, Rabsch et al. 2006), and its closest relative in *K. pneumoniae* is plasmid-mediated fepA0027.

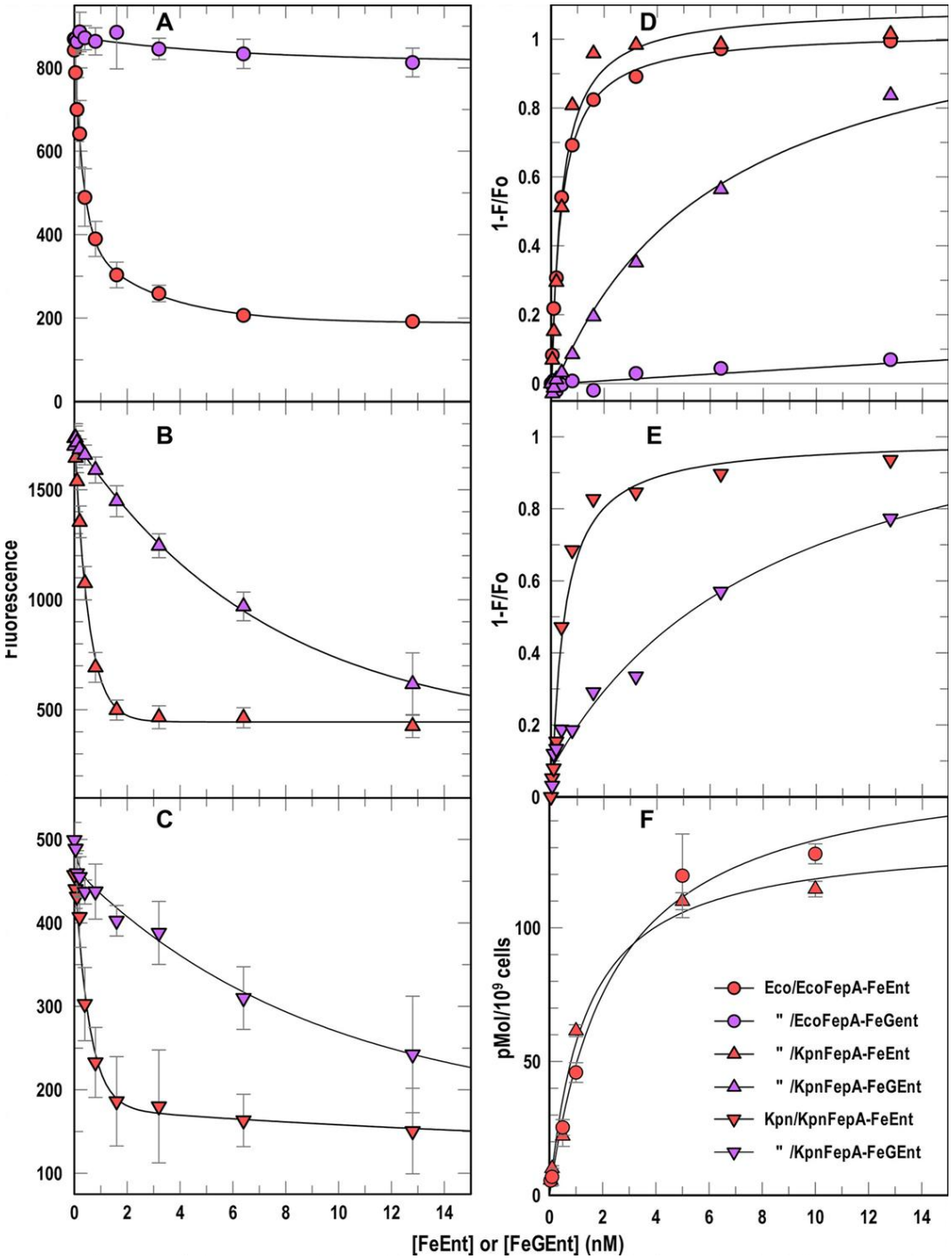

Figure 4.3. Binding affinities measurement from fluorescence spectroscopic assays:

(A-E). Using FD sensor, we increased the concentration of FeEnt gradually in cuvette and observed fluorescence quenching till saturation and converted this quenching pattern to non-linear binding curve using 1-site with background equation and calculated K_D values. **(F). [^{59}Fe]Ent binding measurements.** We added varying concentrations of [^{59}Fe]Ent to OKN3/pEcoFepA or OKN3/pKpnFepA, measured adsorption of the ferric siderophore by filter binding assays, and obtained non-linear fits to the 1-site with background equation of Grafit 6.02, that gave the

affinities (K_D) of the binding reactions (Table 4.1). Figure adapted from (Chakravorty, Shipelskiy et al. 2019).

After bioinformatics analysis and structural analysis of KpnFepA0027, we cloned its structural gene and created Cys substitution T210C, which is nominally equivalent to T216C in EcoFepA (Smallwood, Jordan et al. 2014). We expressed KpnFepA0027_T210C and labeled it with FM (KpnFepA-FM) in *E. coli* OKN13 (*ΔtonB, ΔfepA*), and in *K. pneumoniae* KKN4 (*ΔentB*, *ΔfepA0027*, *ΔfepA1658, ΔfepA4984*), which is relative to EcoFepA-FM in OKN13. We reached a few conclusions after comparing FeEnt and FeGEnt adsorption to KpnFepA-FM and EcoFepA-FM in the different bacterial backgrounds using fluorescence spectroscopic analysis. First, KpnFepA was fluoresceinated to a higher level in *E. coli* background than its native *K. pneumoniae* background. And this better labeling of KpnFepA in *E. coli* sensor strain provided more accurate measurement in terms of quenching because there was less variation in the mean extent of quenching in *E. coli* compared to its native background. Second, both KpnFepA-FM and EcoFepA-FM preferred FeEnt ($K_D \approx 0.38$ nM) over FeGEnt ($K_D = 6$ - 280 nM) in terms of binding. These data using fluorescence assay recapitulate previously published affinities and specificities of EcoFepA to FeEnt. In case of FeGEnt, it binds with KpnFepA with 20-fold less affinity ($K_D \approx$ 6.3 nM) than FeEnt, and FeGEnt barely bound to EcoFepA at all, so weakly that it was difficult to make accurate measurements. Despite the fact, KpnFepA was 3-fold less fluoresceinated in *the K. pneumoniae* background, but it showed the same preferences and affinities for FeEnt and FeGEnt in the spectroscopic assay. Lastly, we compared the spectroscopic fluorescence tests to conventional radioisotopic binding experiments. Using radioisotopic approach with [^{59}Fe]Ent provided comparable affinities of EcoFepA and KpnFepA for FeEnt, but former fluorescence

assays were more sensitive, accurate, and provided better reproducibility and accurate statistical fits. Overall, this species-specific approach using individual fluorescent-labeled transporters accurately depicted the concentration dependence of ligand-binding, with far better sensitivity in the *E. coli* cell envelop rather than in the more complex cell envelops of infectious bacteria, i.e., ESKAPE bacteria.

Table 4.1. Binding affinities of EcoFepA and KpnFepA0027 for ferric catecholates:

	K_D (Standard deviation)			
Strain/Species	FeEnt	FeGEnt	Strain/Species	[^{59}Fe]Ent
OKN13/pEcoFepA-FM	0.39 0.03)	279 (278)	OKN3/pEcoFepA	2.35 (0.68)
OKN13/pKpnFepA-FM	0.38 (0.07)	6.26 (0.54)	OKN3/pKpnFepA	1.34 (0.03)
KKN4/pKpnFepA-FM	0.45 (0.12)	8.57 (2.15)		

This table illustrate the binding affinities of the decoy sensors towards ferric siderophores using fluorescence spectroscopic assay and radioisotopic binding experiments (Chakravorty, Shipelskiy et al. 2019).

4.3.3. Universal fluorescence assay of Fc acquisition:

We also tested the FD sensor approach for the transport of other siderophores and iron complexes by *E. coli* and other bacteria. We engineered the OM ferrichrome (Fc) transporter, created mutation D396C in EcoFhuA, and labeled it with FM. In *tonB+ E. coli*, EcoFhuA-FM measured Fc uptake. In contrast, in the TonB- deficient strain OKN1, EcoFhuA-FM worked as an Fc sensor that detected Fc uptake by any of the ESKAPE/CRE bacteria (Figure 4.4). The binding of Fc to EcoFhuA-FM quenched its emission, and depletion of Fc in the solution gradually by

microbial transport restored fluorescence intensity. Transport of TonB dependent FeEnt and Fc transport by microbial pathogens by FD assay without modifying them showed the power of FD sensor assay: properly labeled TBDT in a TonB-deficient host became transport-deficient FD sensor which reflects the siderophore concentration in the solution. This FD sensor approach potentially applies to variety of microbial ferric siderophores and their membrane protein receptors. It is also adaptable to other metal complexes that microbes utilize and non-metal, high-affinity ligand-receptor pairs.

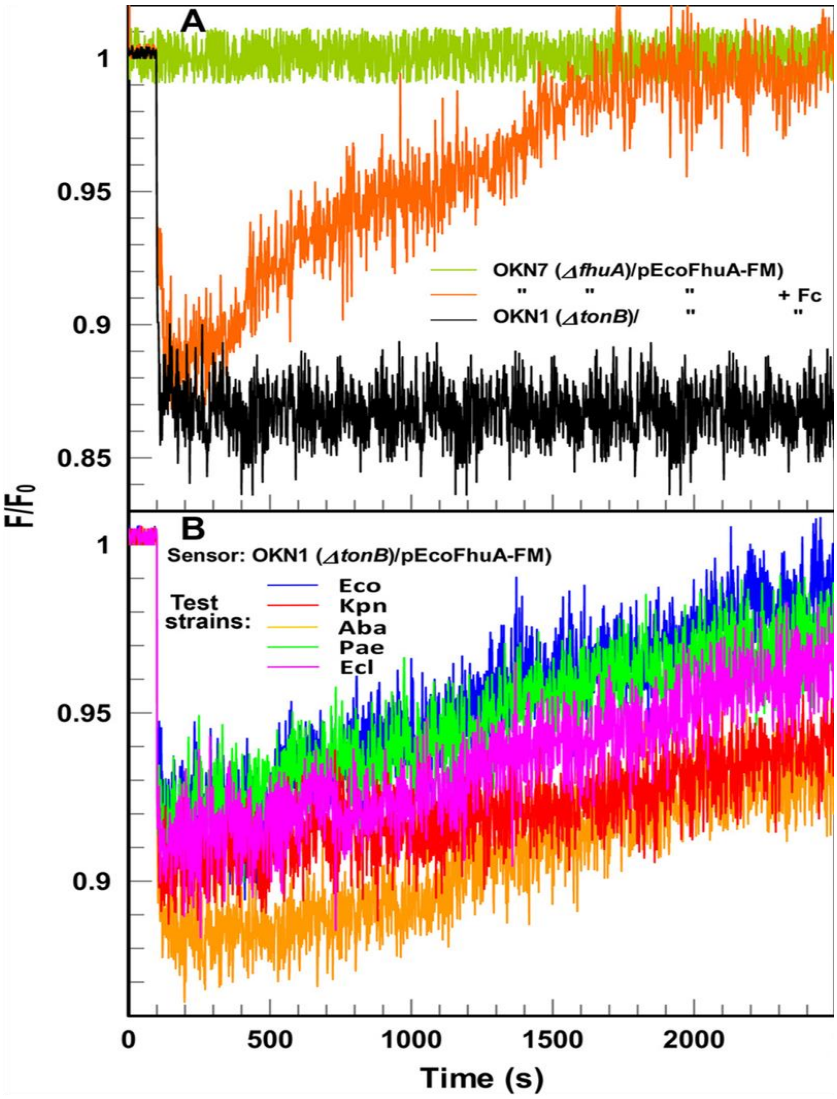

Figure 4.4. FD sensor analysis of Fc acquisition by ESKAPE pathogens:

(A) Fluorescence assay of Fc uptake. OKN7 (*ΔfhuA*)/pEcoFhuA-FM capable of Fc binding and transport, but in OKN1 (*ΔtonB*), the same construct became an inert sensor of [Fc]: binding of Fc quenched fluorescence, but the absence of transport prevented recovery to original level. **(B) Universal assay of Fc uptake.** We incubated the sensor strain with 2 x 10^7 cells of Gram-negative ESKAPE pathogens. In each case, the pathogens acquired Fc, causing fluorescence recovery to initial level. Figure adapted from (Chakravorty, Shipelskiy et al. 2019).

4.3.4. Universal fluorescence assay of heme uptake:

We described a third relevant microbial transport system using slightly modified FD sensor technology: hemin (Hn) uptake by Gram-positive bacteria. *Listeria monocytogenes, Staphylococcus aureus, Streptococcus pyogenes, Bacillus anthracis,* and other Gram-positive bacteria produce Hn-binding proteins which contain NEAT domain. These proteins are either anchored to PG by the action of sortases A (Mazmanian, Liu et al. 1999) and B (Bierne, Garandeau et al. 2004), or are secreted to the external environment where they act as hemophores (Xiao, Jiang et al. 2011). We engineered *Listerial* NEAT-domain protein Hbp2 to create an FD sensor of Hn binding and uptake.

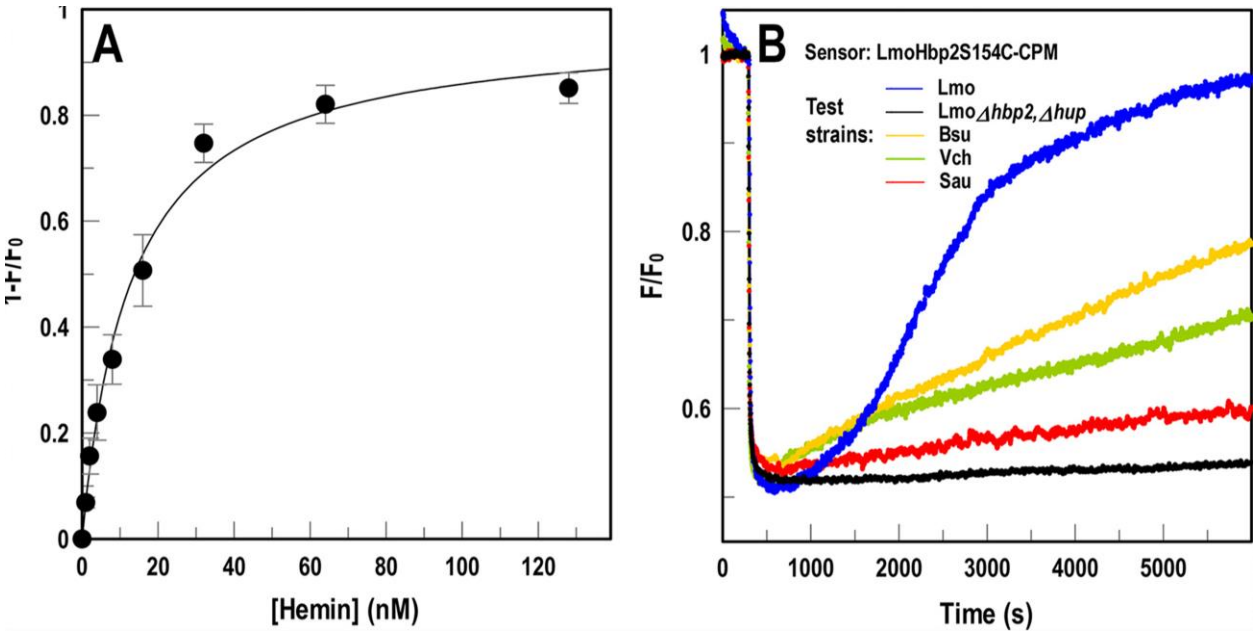

Figure 4.5. Universal fluorescence assay of hemin uptake:

We substituted residue S154 to Cys in NEAT1 of LmoHbp2, expressed and purified the binding protein, and labeled coumarin maleimide (CPM). (**A) Concentration-dependence of hemin binding to LmoHbp2-CPM.** Using purified LmoHbp2-CPM, we gradually increased hemin concentration in the cuvette until saturation and plotted $1\text{-}F/F_0$ vs [hemin], which produced a saturation curve with K_D = 12 nM. **(B) Hbp2-CPM detects and quantifies bacterial hemin transport.** When we mixed hemin sensor (Hbp2-CPM) with target bacteria in solution, it reflected

their hemin uptake. Conversely, hemin transport-deficient cells (EGDe *Δhbp2, Δhup*) did not show fluorescence recovery. Figure adapted from (Chakravorty, Shipelskiy et al. 2019).

We introduced Cys in the NEAT-1 of LmoHbp2 and labeled it by fluorophores, transforming purified labeled protein into Hn's sensitive sensor whose emissions were inversely proportional to [Hn]. LmoHbp2_S154C- CPM (LmoHbp2- CPM) detected the presence of Hn in the solution, with an affinity (K_D = 12 nM) that was consistent with other data produced before; isocalorimetric (K_D = 25-48 nM; (Malmirchegini, Sjodt et al. 2014) and radioisotopic (K_D =12 nm; (Xiao, Jiang et al. 2011) data. This Hn sensor also revealed the transport of Hn by other Gram-positive bacteria at different rates. Overall, the bacterial cells OKN13/pEcoFepA-FM and OKN1/pEcoFhuA-FM and the purified protein LmoHbp2-CPM functioned as universal sensors of extracellular iron in different forms: FeEnt, Fc, and hemin, respectively (Figure 4.5).

4.3.5. Adaptation of FD sensors to fluorescence high-throughput screening (FLHTS):

Chemical compounds that block iron uptake by inhibition of TonB action of ligand transport in Gram-negative bacteria or by reducing Hn uptake in Gram-positive bacterial cells may combat bacterial growth and proliferation in human or other eukaryotic hosts. Previously, we used species-specific fluorescence spectroscopic tests in microtiter to screen chemical libraries to find out inhibitors of TonB action in *E. coli*. Consequently, we adapted all FD sensor assays in microtiter format for FLHTS. Although all the Gram-negative bacteria utilize FeEnt, adapting this method to screen against them faced a few obstacles. First, bacterial pathogens; ESKAPE show reduced cell envelops permeability that lowers susceptibility to chemical compounds. It is possible

that compounds that penetrate *E. coli* may not enter ESKAPE pathogens. Second, TonB orthologs in different species usually shares divergent amino acid sequence than EcoTonB.

For this reason, it is possible that compounds which inhibit EcoTonB may not be as effective against TonB from ESKAPE bacterial species. For these reasons, it is preferable to screen chemical libraries against the target ESKAPE pathogens. The *E. coli* FD sensor cells in microtiter wells followed the TonB-dependent uptake of both FeEnt and Fc by *K. pneumoniae.* The sensors minimized the experimental manipulations of the pathogen while allowing spectroscopic observations of its physiology that were sensitive to varying concentrations of both the ligands and the bacterial cells.

4.4. Discussion:

While giving the designation "Universal", we considered many aspects of FD constructs. (i) We showed sensors of FeEnt, Fc, and heme had the ability to detect and quantify the uptake of their respective target ligand by any Gram-positive or Gram-negative bacteria we tested. This individual pattern of FD sensors supports the term "universal," but FD sensors have other universalities. (ii) FD sensor technical concept applied to any high-affinity binding ligand, whether it is ferric complexes (FeEnt, FeAbn) or other metal complexes (Vit. B_{12}). (iii) From any cloned, high-affinity binding protein, it was easy to create an FD sensor straightforwardly, as we showed for KpnFepA (KpnFepA_IroN, KpnFepA_1658), EcoFepA, EcoFhuA, EcoIutA, EcoBtuB, and LmoHbp2. These fluorescently labeled, Cys-mutant proteins detected and discriminated FeEnt, FeAbn, FeGEnt, Fc, Vit. B_{12} and Hemin ultimately guiding to create sensors for any iron complex or metal complex of interest or any other high-affinity ligand. (iv) For this study, we mainly used fluorescein maleimide (FM) and CPM to labeled Cys mutant. Still, this fluorophore attachment

applies to other fluorophores that differ in structure, mass, and spectrum properties: Alexa Fluors 546M, 555M, 647M, and 680M. (v) These sensor strains can be stored and distributed to any interested researcher because these are expressed from plasmids, and host strains are non-hazardous. (vi) These FD sensors have the potential to achieve many biochemical and microbiological purposes: determination of presence and concentration of siderophores in natural and host environment; transport of siderophore by any bacterial species; survey of microbiological families, genera or species to determine which member uses certain metal complexes. All these applications have the capabilities to discriminate ligands in the nanomolar concentration range.

Another application of these FD sensors is to screen for novel antibiotic discovery. For that purpose, HTS setup needs to be followed by secondary screening assays and controls to eliminate false positives. Previously designed FLHTS assay against TonB already exists that involved secondary screening to eliminate non-specific quenchers and other irrelevant compounds. However, apart from FeEnt sensors, other sensors, e.g., Fc, FeAbn, Vit. B_{12} also exists that can validate or refute the candidate compound in the primary screening itself. These FD sensors in FLHTS formats allow rapid screening, allowing expansion of screening of more extensive chemical libraries. Another advantage of these FD sensors is that respective FD sensors were labeled more in *E. coli* background compared to *K. pneumoniae*, which is a technical advantage, e.g., KpnFepA-FM. This high intensity of fluoresceination is likely derived from un-capsulated laboratory *E. coli* strain, which led to better sensitivity to quenching during ligand binding, which ultimately makes an accurate measurement in *E. coli* background than *K. pneumoniae* background.

Performing binding experiments using fluorescence methods is faster, simpler, more sensitive, reproducible, and less hazardous than previously performed binding experiments

involving radioisotopes (Scott, Cao et al. 2001, Newton, Trinh et al. 2010, Smallwood, Jordan et al. 2014). These fluorescence assays, for optimum binding measurements, do not require the use of large assay volumes as in the case of radioisotopic experiments (~25ml).

It is possible that adventitious iron (Fe^{++} or Fe^{+++}) could interfere with FD sensor observations, but that was not the case here because extraneous iron does not have an affinity for any of the sensors we tested in our experiments. Plus, our sensor strains carry mutations that block siderophore production. Test bacteria, which could also secrete aposiderophores and bind to extraneous iron interfering with our assay, were washed before analysis, circumventing this potential problem. Generally, it requires extended bacterial growth in iron-deficient media for secretion substantial amount of aposiderophores, but our FD sensor assays are relatively short (<30 min), so ultimately, siderophores secreted by bacteria do not provide any false data in our assays.

Overall, these FD sensors provide advantage for observation of ligand transport with high sensitivity. In the absence of excessive turbidity, appropriate selection of fluorophores, FD sensors have the potential to quantify ligands in numerous environments, e.g., blood, serum, and eukaryotic cells. Appropriate adaptations may enable observations of bacterial IM or mammalian plasma membrane uptake reaction. If applied to eukaryotic phenomena like cancer, neurobiology, or metabolism, FD sensors will measure molecular concentrations, facilitate *in vivo* thermodynamic or kinetic characterizations of biochemical reactions, and empower identification of clinically relevant therapeutic agents.

Chapter 5 - Fluorescent sensors for detection, discrimination and quantification of bacterial siderophores and metal complexes

5.1. Introduction:

Iron is a vital component for many biochemical and metabolic pathways in aerobic organisms. For the growth and proliferation in the host system, bacteria utilize strategies to acquire iron from the host system. In response, the host finds ways to keep iron away from these microorganisms. This battle for acquiring iron between host and pathogen influences the outcome of bacterial infection (Klebba, Newton et al. 2021). In aerobic conditions, iron is not readily available in soluble form for bacteria, because it gets oxidized (Neilands 1981), making it difficult for bacteria to utilize it. Nevertheless, to fulfill the need for iron, bacteria secrete low molecular weight organic compounds, which are called siderophores (*Gr., "iron carrier"*). Siderophores chelate Fe^{+3} with such high affinity ($K_D = 10^{-20}$-10^{-50} M) (Neilands 1981) that they release it from its precipitated state as hexadentate, octahedral coordination complexes that are available for microbial acquisition (Noinaj, Guillier et al. 2010). On the other hand, in response to microbial siderophore production to acquire iron, human and animal hosts produce proteins that solubilize, sequester, and store iron, e.g., transferrin, lactoferrin, and ferritin (Anderson and Frazer 2017). This form of avoiding the microbial need for iron by sequestering it is considered part of their innate immune response called "nutritional immunity" (Coffey and Ganz 2017). Nevertheless, bacterial aposiderophores may capture iron with high affinity than host protein, and this resulting ferric siderophore complex is transported inside bacterial cells through TonB dependent outer membrane receptors (TBDTs). For successful infection, bacteria produce multiple active uptake systems for ferric siderophores (Newton, Igo et al. 1999) and heme (Hashimoto-Gotoh, Franklin

et al. 1981, Chakravorty, Shipelskiy et al. 2019). These siderophores can steal iron directly from transport/storage proteins from host cells (Sprencel, Cao et al. 2000, Klebba, Newton et al. 2021). In Gram-negative bacterial cells, iron acquisition starts with the recognition and binding of ferric siderophore complexes to the TonB-dependent OM receptors. We also call these TBDTs ligand-gated porins; LGPs (Sprencel, Cao et al. 2000, Klebba, Newton et al. 2021), because upon binding of ligand to TBDT, conformational changes in the N-domain of TBDT take place, and open the normally closed 22- stranded β-barrels porins. On the other hand, TBDTs do not allow the passage of ligands by diffusion as porins like OmpF or LamB do, as they contain open transmembrane pores. In contrast, TBDTs contains a C- terminal, usually ~675 residues long channel that surrounds N-terminal, ~150-residue globular domain that regulates ligand transport through its association with energy-dependent inner membrane (IM) protein TonB. All TBDT mediated iron uptake receptors require the action of TonB for the transport of ligand through OM to periplasm (Sprencel, Cao et al. 2000, Klebba 2016, Klebba, Newton et al. 2021). For example, the Gram-negative bacterial outer membrane protein FepA actively transports the iron complex ferric enterobactin (FeEnt) in the periplasm. The inner membrane protein TonB provides the energy for this uptake reaction. Once inside periplasm, FepB binds with this iron-siderophore complex FeEnt and carries it to FepCDG, an ATP transporter. FeEnt is then transported inside cytosol by ATP hydrolysis, and then iron is utilized in metabolic and biochemical reactions (Sprencel, Cao et al. 2000, Klebba 2016, Klebba, Newton et al. 2021). Siderophore production at the time of iron deficiency (Holden and Bachman 2015, Coffey and Ganz 2017) and TonB dependent ferric siderophore transport are required for successful colonization of the animal gut (Pi, Jones et al. 2012, Holden and Bachman 2015, Holden, Breen et al. 2016, Klebba, Newton et al. 2021). Although microbial siderophore possesses high affinity and efficiency for stealing iron from the

host, these are highly vulnerable in a manner where disruption of these systems can inhibit bacterial growth, reduce virulence and may thwart pathogenesis as well (Neilands 1981, Noinaj, Guillier et al. 2010, Pi, Jones et al. 2012, Holden and Bachman 2015, Holden, Breen et al. 2016, Coffey and Ganz 2017, Klebba, Newton et al. 2021).

Many reports correlate the acquisition of certain ferric siderophores with infectious diseases and pathogenesis. For example, after infection by *Yersinia pestis*, for the development of plague (bubonic or pneumonic), production of the mixed chelation compound yersiniabactin is necessary (Bachman, Oyler et al. 2011). Second, bacterial pathogens which produce or utilize hydroxamate siderophore compound ferric aerobactin (FeAbn) tend to promote tissue invasion (Williams 1979, Russo, Olson et al. 2015, Russo and Marr 2019). Third, the host innate immune system produces siderocalin (Scn) which usually adsorb ferric enterobactin (FeEnt) secreted by bacterial pathogens and reduce bacterial growth. In response, many bacterial pathogens have evolved with a different mechanism that allows them to glycosylate FeEnt. This glycosylated form of FeEnt (FeGEnt) reduces adsorption/recognition by Scn, leading to enhanced infection to specific tissue by *K. pneumoniae* (Holden, Lenio et al. 2014). Ultimately these kinds of relationship of siderophore secretion and infections, and pattern of different siderophore production leading to pathogenesis, underscore the need of biochemical tools which can offer insight into this phenomenon. We need strategic advancement in the field, which can provide knowledge about the presence and concentration of specific ferric-siderophore complex in the host system quickly so that immediate steps can be taken to undermine lethal consequences presented due to the presence of pathogens.

We created fluorescent sensors of apo- and ferric siderophores, which may provide diagnostic information about the presence of the specific pathogen in clinical settings, e.g., blood

and serum, offer kinetic and thermodynamic data on prokaryotic pathways of iron acquisition during infection and assessment of the relative virulence threats of different microbial pathogens. For example, *A. baumannii* produce siderophore Acinetobactin and its iron conjugated form; FeAcn in biological samples indicates the presence of a particular pathogen. So far there are more than 500 siderophores described in nature, and OM receptors must discriminate among them for recognition internalization. Sensors we created in this report effectively detect specific siderophores in the microenvironment, their concentration and inform about the utilization of siderophores in pathogens. Furthermore, over-expression and fluoresceination of an OM siderophore receptor in a TonB-deficient host system allowed us to create a transport defective "decoy" sensor cell that can detect and quantitate ligand in biological tissues, cell suspensions, and food samples, e.g., meat. Using this strategy, we created a panel of sensors that can detect the production of different kinds of bacterial siderophore, metal complexes and provide data about their concentration in a medically relevant environment. These FD sensors also provide essential information about the uptake of ferric siderophores by any bacterial pathogens.

5.2. Methodology:

To select a suitable Cys mutant for each receptor used in the study, we relied on the crystal structure of the TBDTs if available. For each of the TBDTs, we selected multiple residues in the loop region, mostly near to putative ligand-binding site (s). We substituted these residues to Cys using site-directed mutagenesis and modified them using FM. It was easy to choose multiple residues in the loop region in most cases because of the available crystal structure; EcoFepA, EcoFhuA, EcoBtuB, AbaPiuA AbaBauA, EcoFepB. But it is not the case for each receptor because of unavailability of crystal structure e.g., KpnFepA_1658, KpnFepA_4984, KpnFepA_2380,

EcoIutA, CcrHutA, AbaFepA and PaeFepA. In these cases, we used the CLUSTALW program to identify the closest structurally resolved ortholog/paralog of the unsolved TBDT based on the protein's sequence identity and used the Modeler function of the CHIMERA (UCSF) program to predict its putative tertiary structure. We then selected multiple residues in the loop region and created Cys substitutions. After substitutions, we evaluated their accessibility to FM modification and sensitivity to fluorescence quenching to determine the best sensor for each of the siderophores studied in the study.

We used polymerase chain reaction (PCR) method for the amplification of gene of interest. We confirmed expression of every construct in *the E. coli* background. In short, we copied the nucleotide sequence of the mature protein and inserted it next to *the E. coli* FepA promoter and signal sequence, in pITS23, the low-copy derivative of pHSG575. We used QuikChange (Stratagene) for single Cys substitutions in the TBDT of interest followed by the digestion by Dpn1. We confirmed the presence of Cys in all constructs by DNA sequencing of the recombinant purified plasmid.

For each construct's fluoresceination, we used overnight grown culture in LB and sub-cultured in iron-deficient media; MOPS for 14-16 hours for the proper expression of the respective OM transporter. Then we followed the procedure described earlier to label these constructs with FM (Chapter 2). In brief, we labeled the cells with 5 uM fluorescein maleimide (FM) and incubated cells for 15 min at 37°C (shaking condition). Then we quenched the labeling reaction with 130 mM BME, pelleted cells, washed the pellet with phosphate-buffered saline (PBS) twice, and resuspended the pellet again in phosphate-buffered saline (PBS). We used these cells for spectroscopic fluorescence binding reactions.

To generate EcoFepB mutants, we cloned the *E. coli fepB* structural gene in pET28a, introduced Cys-substitutions at the site of interest, and verified the constructs by DNA sequencing and transformed mutant plasmids in BL-21 *E. coli* cells. We sub-cultured overnight grown culture in the proportion of 1:100 in LB media with appropriate antibiotics and incubated at 37°C in incubating conditions. To get the overexpression of the EcoFepB Cys mutant, we added 0.1 mM IPTG in the culture when the O.D. of the culture was 0.5 to 0.6 and allowed it to grow for another 5 hours. Then we precipitated the cells by centrifugation, resuspended them in lysis buffer, and broke the cells using the French press and eluted protein using Ni-NTA his-tag column chromatography. For labeling, we combined the eluted fractions containing protein of interest and then dialyzed it against labeling buffer ($NaHPO_4$, pH 6.7) and then concentrated the protein using protein concentrators (Millipore: MWCO; 10000 kDa). Then we labeled this protein with 5 µM FM, in 50 mM $NaHPO_4$, pH 6.7 for 30 minutes at 37°C. After this process, we immediately quenched the labeling reaction with 130 mM BME and dialyzed it against the labeling buffer. We concentrated the resulting labeled protein and used it for fluorescence spectroscopic assay to bind various catecholate siderophores.

We also separated OM fractions of these fluorescently labeled cells after growing them in iron-deficient media and checking the extent of expression of the desired proteins. For that, we pelleted down the cells and resuspended them in lysis buffer (DNAse and RNAse included) and broke the cells using French press. We removed intact cells by pelleting them at low speed (3000 x g for 10 minutes) and transferred the supernatant in a microfuge tube. Then we pelleted down the supernatant at high speed (14000 x g for one hour) and dissolved the resulting pellet in lysis buffer with 1% sarkosyl. We incubated this mixture at room temperature for half an hour and pelleted down the outer membrane fractions and resuspended it in PBS. We subjected these

fractions to SDS- PAGE and checked for the protein expression by UVP imager after Coomassie blue staining.

We used 2 x 10^7 cells per ml diluted in PBS in a 3 ml quartz cuvette for the fluorescent spectroscopic binding assays. The temperature of the cuvette chamber was 25°C. After the fluorescence stabilized, we added the same concentration of siderophore for each Cys derivative of the OM receptor we investigated. For example, we used 20 nM FeEnt with all Cys derivatives of KpnFepA_1658 and looked for the most sensitive mutant that showed the greatest extent of quenching in this experiment and used that Cys derivative as FD sensor of FeEnt. We started adding an increasing concentration of respective siderophores at a 100-second interval until the fluorescence got quenched to the maximum level and stabilized for the binding assay. We converted this fluorescence quenching pattern into a binding curve (concentrations on the x-axis and (1- normalized fluorescence quenching (F1/F0) on the y-axis) and calculated the K_D values for each sensor with siderophore of the same chemical groups, e.g., for KpnFepA_1658, we used all catecholate siderophores to check binding.

To check the specificity of these sensors to siderophores, we used a high concentration of siderophores for checking the binding. For example, with EcoIutA_T548C, we used 5-10 µM of ferric aerobactin (FeAbn), ferrichrome (Fc), ferrioxamine (FxB), ferric acinetobactin (FeAcn), ferric yersiniabactin (FeYbt) in separate experiments to check the quenching which reflects binding.

For quantitative analysis of the siderophore produced by clinical strains, we grew these strains in iron-deficient media and collected the supernatant and saturated them with Fe^{+3} in the form of $FeCl_3$ and used a diluted form of this supernatant with the sensor of our choice. We gradually increased the amount (ul) of diluted supernatant in the cuvette and looked for half-

saturation of fluorescence, e.g., quenching (compared with the standard graph plotted for the sensor with purified siderophore) and calculated the total amount of siderophore produced by bacterial strains.

5.3. Results:

5.3.1. Creation of fluorescent decoy (FD) sensor-siderophore pairs:

In this study, we created fluorescent sensors using various bacterial species for different categories of siderophores. That category includes ferric catecholate siderophores (enterobactin, glycosylate enterobactin, monocatecholates), ferric hydroxamates (aerobactin, ferrichromes), mixed chelators (acinetobactin), and porphyrins (hemin, vitamin B_{12}). The sensor proteins for these siderophores and metal complexes were derived from different Gram-negative bacteria including ESKAPE pathogens which includes *E. coli* (EcoFepA, EcoFhuA, EcoIutA, EcoBtuB), *K. pneumoniae* (KpnIroN, KpnFepA_1658, KpnFepA_4984, KpnFepA_2380), *A. baumannii* (AbaBauA, AbaPiuA, AbaFepA), *P.aeruginosa* (PaeFepA) and *Caulobacter crescentus* (CcrHutA).

Fluorescent sensors, which we mentioned above, are mainly cell-based sensors. Receptors were expressed in *the E. coli* outer membrane and labeled with fluorophores, e.g., FM, and used to detect siderophores. We cloned the structural genes of OM TBDT from respective organisms using PCR in low copy plasmid pITS23, the derivative of pHSG575. In most cases, structural genes with their own signal sequenced were cloned under the control of the EcoFepA promoter (KpnIroN, KpnFepA_1658, EcoIutA, AbaFepA). However, in some cases we switched structural gene's signal sequence with EcoFepA signal sequence for better expression in *E. coli* background

(AbaBauA, AbaPiuA, CcrHutA, EcoBtuB, KpnFepA_4984, KpnFepA_2380) (Figure 5.1, 5.3 and 5.5).

Table 5.1. Binding affinities (K_D values in nM) of TonB dependent sensors for apo and ferric siderophores:

Catecholates siderophores (K_D values in nM)						
Sensors	**Residue**	**FeEnt (Ent)**	**FeEnt***	**FeGEnt**	**FeDHBA**	**FeCrn**
EcoFepA	A698C	0.41 (43)	8.4	3.8×10^2	NB	NB
KpnFepA_1658	A382C	0.62 (74)	23	95	NB	NB
KpnFepA_IroN	T210C	0.43 (39)	7.3	6.3	NB	NB
KpnFepA_4984	A390C	14.3 (3.1×10^3)	1.8×10^2	8.8×10^2	NB	NB
KpnFepA_2380	T255C	13×10^3	NB	NB	22×10^3	13×10^3
AbaFepA	S278C	17 (1195)	13	15	22×10^2	NB
AbaPiuA	S696C	53×10^2	2.4×10^3	NB	1.5×10^4	NB
PaeFepA	S271C	8.1 (1.5×10^3)	15	1.7×10^2	2.1×10^3	NB
EcoFepB	T297C	43 (4.6×10^3)	1.9×10^2	1.1×10^4	7.1×10^3	9.4×10^3
Hydroxamates/Mixed siderophores (K_D values in nM)						
		Fc (apo-Fc)	**FcA**	**FeAbn (Abn)**	**FxB**	**FeAgn**
EcoFhuA	D396C	3.2 (2.1×10^2)	61	NB	10×10^4	NB
EcoIutA	T548C	NB	NB	5.4 (1.2×10^3)	NB	NB
AbaBauA	S385C	NB	NB	NB	NB	1.1×10^3
Porphyrins (K_D values in nM)						
		Hemin	**B_{12}**			
EcoBtuB	S286C	NB	1.9			
CcrHutA	A635C	1.31×10^2	NB			

This table illustrates the K_D values for different sensors for different siderophores (catecholates (ferric enterobactin (FeEnt), degraded ferric enterobactin (FeEnt*), glycosylated ferric enterobactin (FeGEnt), ferric dihydroxybenzoic acid (FeDHBA), and ferric cornybactin (FeCrn)), hydroxamates (ferrichrome (Fc), ferrichrome A (FcA), ferric aerobactin (FeAbn) and ferrioxamine B (FxB)), mixed chelation (ferric anguibactin (FeAgn), and porphyrins (hemin (Hn) and Vitamin B_{12} (B_{12})). To create a particular sensor, we first predicted putative tertiary structure for that

receptor if that has not resolved yet and then selected multiple residues in the loop region. We mutagenized these residues to Cys and labeled them with FM. We checked the extent of quenching of these Cys mutants upon addition of equal concentration of cognate siderophore and selected the Cys mutant, which quenched the most. We transformed this Cys mutant in OKN1 (*tonB*$^-$) or OKN13 (*tonB*$^-$ and *fepA*$^-$) cells and used them as FD sensor of siderophore (s). To calculate binding affinity, we put 2 x 10^7 FD sensor in the cuvette with PBS and waited for stable fluorescence. Then we gradually increased siderophore concentration in the cuvette and observed quenching till saturation. We plotted non-linear curve; concentration (x-axis) vs 1-(F1/F0) (y-axis) and calculated the K_D value, using 1-site binding with no background equation. (**NB** = no binding)

Apart from these cell-based sensors, we also created protein-based sensor which detect and bind to FeEnt. This sensor was derived from EcoFepB protein, which is periplasmic protein, binds with FeEnt with nanomolar affinity. We cloned the structural gene in pET28a (+), (Novagen) that contained 6-His tag on its C-terminal. After the construction of each recombinant product, we verified the presence of clone with the help of PCR using universal M13 primers followed by agarose gel electrophoresis and sequencing of purified plasmids. In general, we mutated around 5-7 residues to Cys in the loop region in each of the protein.

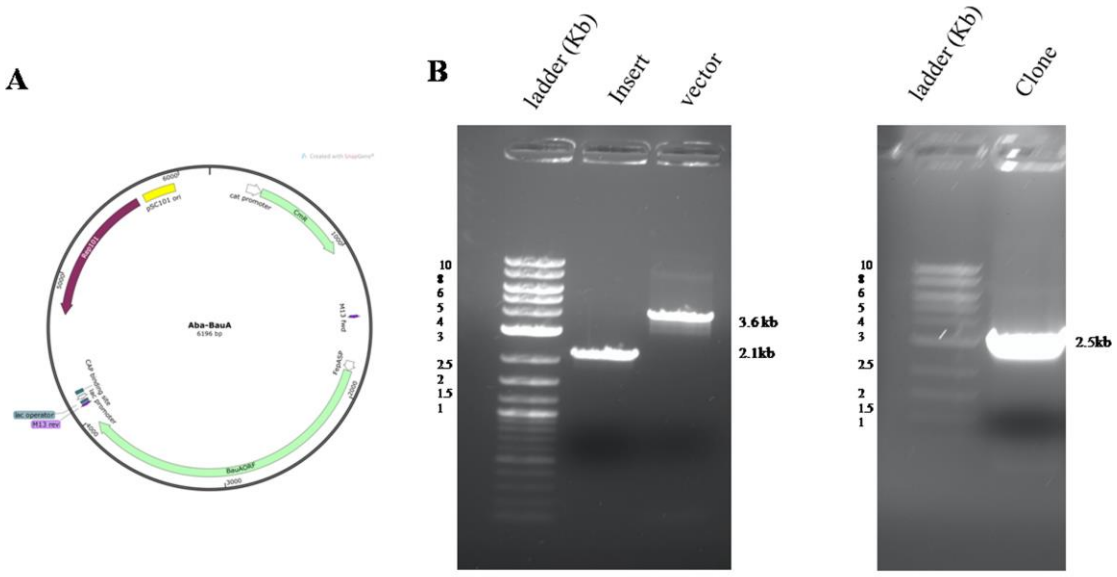

Figure 5.1. Recombinant plasmid and cloning strategy of *AbabauA*:

Panel A shows the vector map of recombinant plasmid *pAbabauA*, and panel B shows the amplification of *AbabauA*, pITS23 (left), and confirmation of recombinant plasmid (right) using agarose gel electrophoresis. We used M13 universal primers for the amplification of the desired insert gene.

To create Cys mutants, we chose residues based on the crystal structure of relevant protein (EcoFepA, EcoFhuA, EcoFepB (Figure 5.7A), EcoBtuB, AbaBauA (Figure 5.2A), AbaPiuA (5.4A)), or by hypothetical tertiary structure calculated by Modeler algorithm of the CHIMERA program (EcoIutA, KpnIroN, KpnFepA_1658, KpnFepA_4984, KpnFepA_2380, AbaFepA, PaeFepA). After construction of each Cys mutant, we grew these constructs in iron-deficient condition, labeled them with FM (5 µM for 15 min. at 37°C) (Smallwood, Jordan et al. 2014), and analyzed the expression extent of expression, fluoresceination, and fluorescence quenching that occurred while binding of cognate metal complex to mutated receptors. Based on these data, we selected the most sensitive Cys mutant for each receptor. We used it to spectroscopically characterize their affinities and specificities for various apo- and ferric siderophore within the

relevant class of siderophore (Table 5.1). For example, AbaBauA and Cys mutants; S258C, S318C, S358C, and S448C were poorly labeled (Figure 5.2B and C) and expressed in *E. coli* outer membrane (Figure 5.2D. In the spectroscopic fluorescence assay, we used 2 µM ferric anguibactin (FeAgn) to see the extent of quenching of Cys mutants of AbaBauA. Among all Cys mutants, S385C showed maximum quenching, and we used OKN1/pAbaBauA_S385C-FM as FD sensor of FeAgn (Figure5.2E). Likewise, Cys mutants of different OM receptors that are FD sensors of relevant siderophores are mentioned in table 5.1.

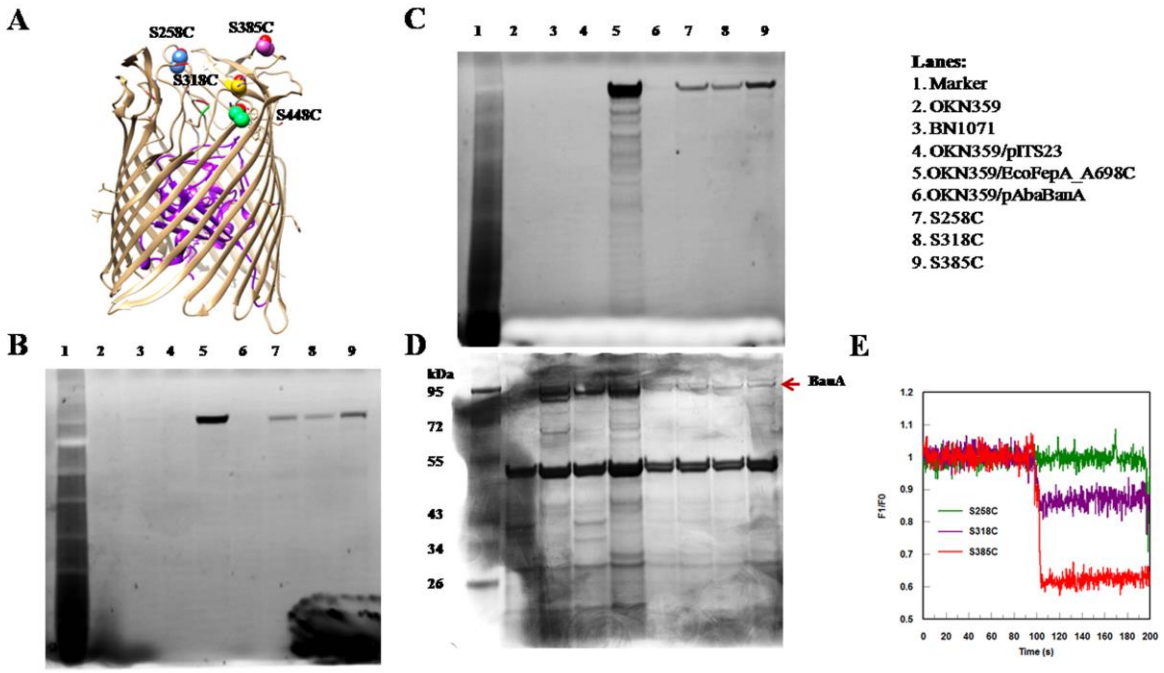

Figure 5.2. The tertiary structure of AbaBauA, fluoresceination of Cys derivatives, OM separation, and fluorescence quenching using ferric anguibactin (FeAgn):

Panel A depicts the protein structure of AbaBauA with selected residues in the loop regions, which were mutagenized to Cys using site-directed mutagenesis; S258C, S318C, S385C, and S448C. Panel B shows the fluorescent image of the SDS PAGE of the whole cell lysate of AbaBauA and its Cys derivatives with proper controls. Cells were grown under iron-deficient conditions and

labeled with FM. We used SDS-PAGE to analyze the labeling of AbaBauA Cys derivatives. Panel C shows the fluorescent image of the OM fractions of AbaBauA and its Cys derivatives using SDS-PAGE. Panel D shows the separation of OM proteins followed by Coomassie blue staining. Panel E shows the extent of fluorescence quenching (binding) of FeAgn (2µM) to different Cys derivatives of AbaBauA using fluorescence spectroscopic assay. S385C showed maximum quenching among all Cys mutants of AbaBauA.

5.3.2. Protein expression of Cys mutants and fluorescent labeling:

We made changes in plasmid pITS23 (Scott, Cao et al. 2001) to express all Gram-negative TBDTs used in the study. pITS23 plasmid carries *EcofepA* under the control of its native, Fur-regulated promoter. For most of the TBDT (KpnIroN, KpnFepA_1658, EcoIutA, AbaFepA), we precisely replaced the nucleotide sequence encoding complete EcoFepA polypeptide on pITS23 with the sequence of other TBDT of interest, such that the iron-regulated *EcofepA* promoter-controlled synthesis of the desired TBDT, immediately downstream from its native signal sequence. For TBDT, mostly from other bacterial species (AbaBauA, AbaPiuA, CcrHutA, KpnFepA_4984, KpnFepA_2380), we precisely replaced mature protein-coding nucleotide sequence with that of EcoFepA mature protein-coding nucleotide sequence, leaving expression of TBDT under the control of EcoFepA promoter and signal sequence for proper secretion and expression of TBDT in *E. coli* OM. We transformed all recombinant plasmids containing the gene of interest in OKN13 (*tonB*$^{-}$ and *fepA*$^{-}$) or OKN1 (*tonB*$^{-}$*) E. coli* host so that growth of these constructs in iron-deficient media resulted in the overexpression of recombinant protein of interest.

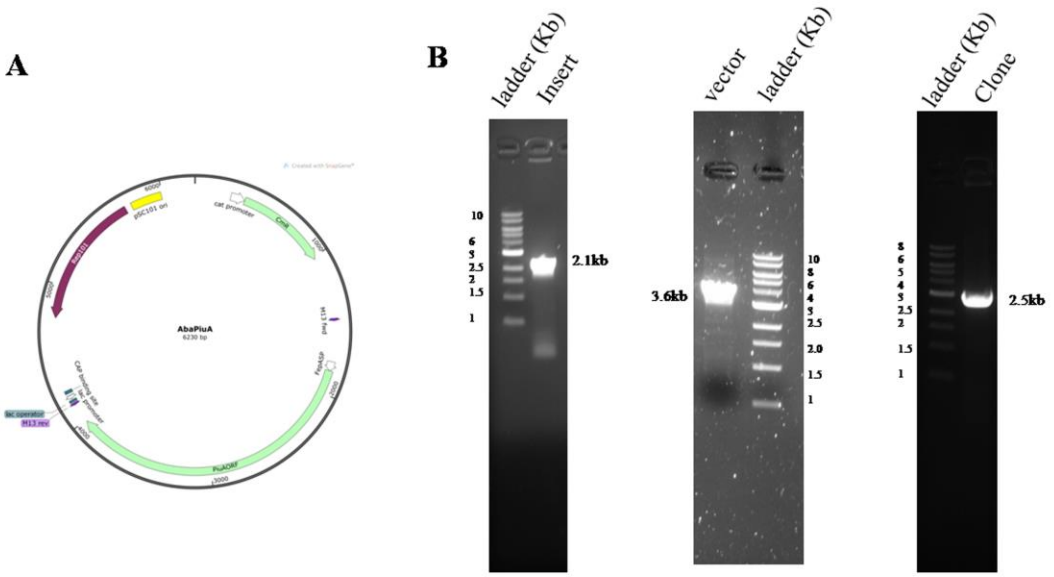

Figure 5.3. Recombinant plasmid and cloning strategy of *AbapiuA*:

Panel A shows the vector map of recombinant plasmid *pAbapiuA*, and panel B depicts the amplification of *AbapiuA* (left), pITS23 (middle), and confirmation of recombinant plasmid (right) using agarose gel electrophoresis. We used M13 universal primers for the amplification of the desired insert gene.

For soluble binding protein, EcoFepB, we cloned structural *EcofepB* in pET28a (+), containing a 6-his tag on C- terminal. We over-expressed this protein using IPTG and purified 6-his tagged Cys mutant proteins from cell lysate using Ni-NTA affinity chromatography, labeled them with 5 µM FM at pH 6.75 for 30 min, removed excess fluorophore by dialysis against PBS, and used this fluorescent-labeled protein for spectroscopic fluorescence analysis.

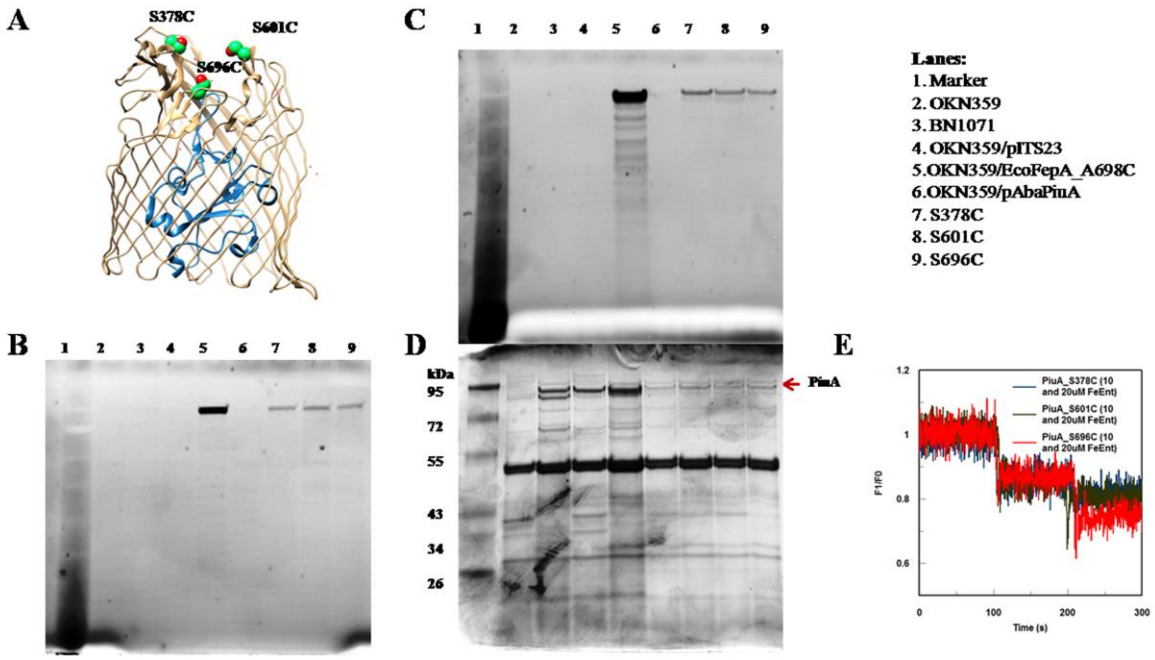

Figure 5.4. The tertiary structure of AbaPiuA, fluoresceination of Cys derivatives, OM separation, and fluorescence quenching using FeEnt:

Panel A depicts the protein structure of AbaPiuA with selected residues in the loop regions, which were mutagenized to Cys using site-directed mutagenesis; S378C, S601C, and S696C. Panel B shows the fluorescent image of the SDS PAGE of the whole cell lysate of AbaBauA and its Cys derivatives with proper controls. Cells were grown under the iron-deficient condition and labeled with FM. We used SDS-PAGE to analyze the labeling of AbaPiuA Cys derivatives. Panel C shows the fluorescent image of the labeled OM fractions of AbaPiuA and its Cys derivatives using SDS-PAGE. Panel D shows the separation of OM proteins followed by Coomassie blue staining. Panel E shows the extent of fluorescence quenching (binding) of FeEnt (10 µM at 100 seconds and total 20 µM at 200 seconds) to different Cys derivatives of AbaPiuA using fluorescence spectroscopic assay. S696C showed maximum quenching among all Cys mutants of AbaPiuA.

We evaluated the expression and fluorescence labeling of each of the cloned TBDT by growing the appropriate recombinant construct in OKN359 background in iron-deficient media (MOPS) to late log phase (A_{600} nm = 2 - 2.5). Then we labeled them with fluorophore; FM and analyzed the sample by resolving them on SDS-PAGE and observed the fluorescence emissions at 520 nm before staining with Coomassie blue or the quantitative analysis. We separated OM fractions of these labeled cells, ran the SDS-PAGE sample, and then analyzed each sensor protein

expression level compared to EcoFepA. Most of the cases we got comparable, albeit in some cases less, iron-regulated expression of the heterologous TBDT under the control of *EcofepA* promoter. One of the advantages we had by expressing and labeling these heterologous proteins in *E. coli* background compared to pathogenic bacterial background was that we did not have to deal with either LPS O-antigen or capsule, which created a problem in labeling.

In conclusion, we obtained consistent labeling in each of the receptors, which we could use as a sensor of the ferric siderophore complex. For each of the receptors we used in this study, we selected 3-6 positions in the surface loop for Cys substitution for each one. We got mixed responses for different positions in terms of labeling. So, after analyzing expression, fluorescence labeling, and sensitive binding in terms of fluorescence quenching, we selected the best site as a suitable sensor for their respective cognate ferric siderophore binding.

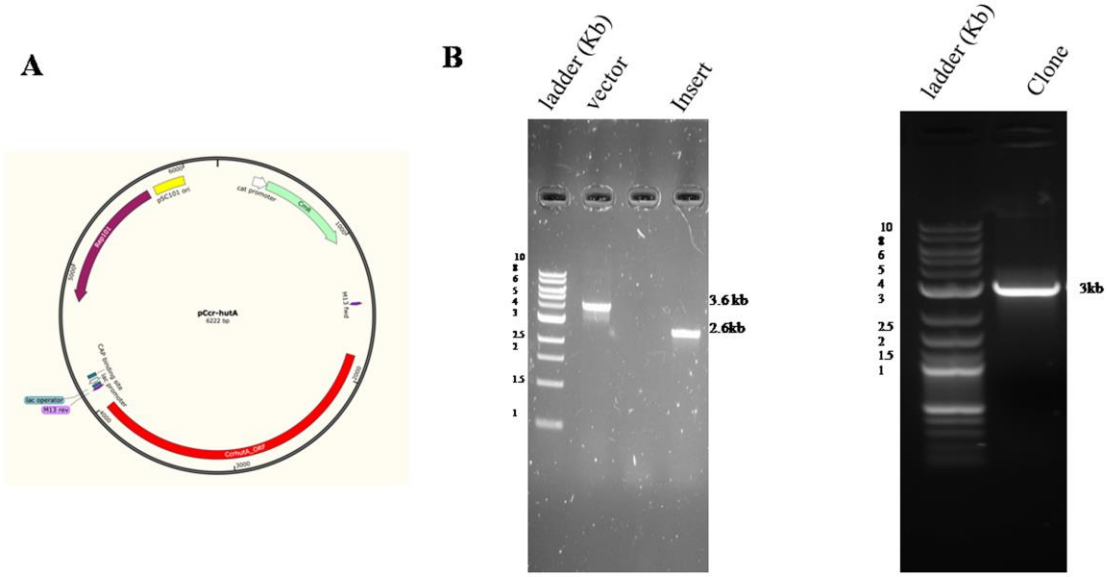

Figure 5.5. Recombinant plasmid and cloning strategy of *CcrhutA*:

Panel A shows the vector map of recombinant plasmid *pCcrhutA*, and panel B shows the amplification of *AbapiuA*, pITS23 (left), and confirmation of recombinant plasmid (right) using agarose gel electrophoresis. We used M13 universal primers to amplify the desired insert gene and confirmed the presence of the insert gene using sanger sequencing.

5.3.3. Differences in the binding affinity of ferric siderophores for same TBDT.

There are differences in the binding of ferric siderophores to TBDT so that certain siderophores bind to the TBDT with high affinity. In contrast, few siderophores show less binding to the same TBDT, showing the discriminating specificities of metal complexes to their TBDT in the binding reactions. For example, EcoFepA binds with its cognate ligand FeEnt with high affinity (K_D = 0.1 - 0.4 nM (Newton, Igo et al. 1999, Cao, Qi et al. 2000, Cao, Warfel et al. 2003, Chakravorty, Shipelskiy et al. 2019) and that helps it to steal FeEnt at even nanomolar range of concentrations.

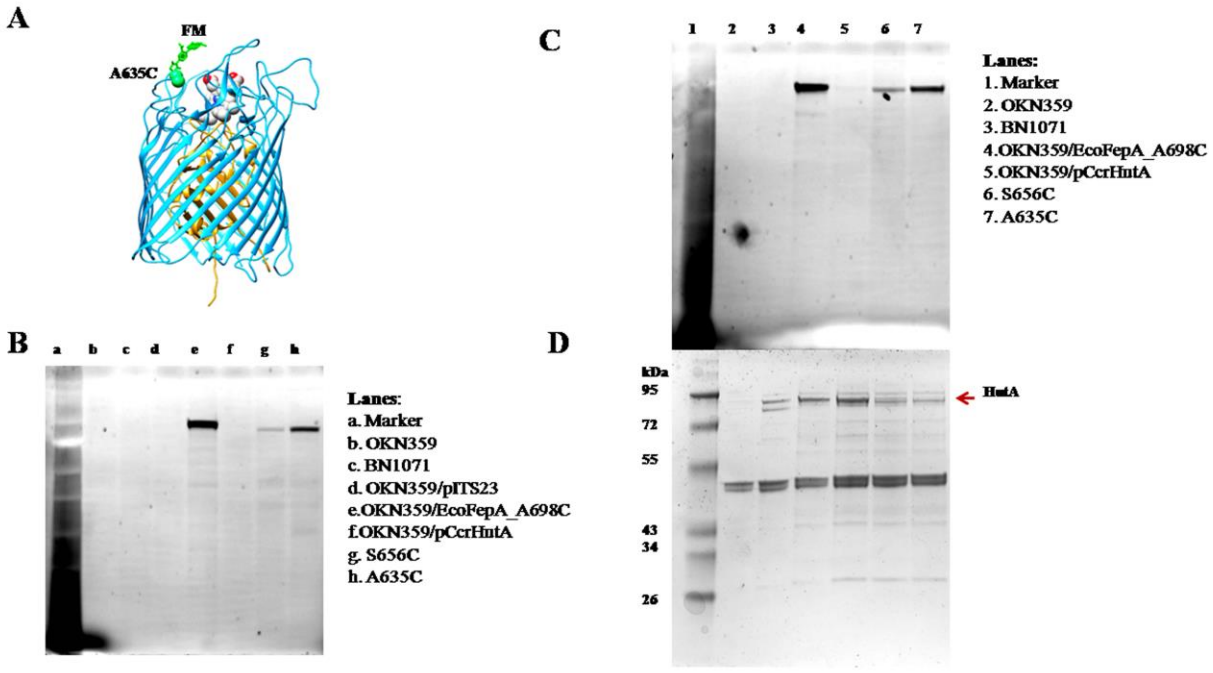

Figure 5.6. The predicted tertiary structure of CcrHutA, fluoresceination of Cys derivatives, and OM fractions:

Panel A depicts the predicted protein structure of CcrHutA using the modeler function of CHIMERA. We selected residues in the loop region and replaced them with Cys using site-directed mutagenesis. Panel B shows the fluorescent image of the SDS PAGE of the whole cell lysate of CcrHutA and its Cys derivatives with positive and negative controls. Cells were grown under iron-deficient conditions and labeled with FM. We used SDS-PAGE to analyze the labeling of CcrHutA Cys derivatives. Panel C shows the fluorescent image of the OM fractions of CcrHutA and its Cys derivatives using SDS-PAGE. Panel D shows the separation of OM proteins followed by Coomassie blue staining.

Apart from this, EcoFepA also binds with other ligands but with much lower affinity than it has for FeEnt, but still high affinity, Ent (K_D = 43 nM), FeEnt* (K_D = 8 nM), and weak affinity for FeGEnt (K_D = 3.4 x 10^2 nM). We found this trend general in our study where TBDT showed primary high affinity for a particular metal complex (EcoFepA; FeEnt, EcoFhuA= Fc) and comparatively lower affinity for secondary structural related metal complexes (Table 5.1).

We also looked for the specificities and binding of these metal complexes in the orthologs TBDTs in related Gram-negative bacteria, e.g., ESKAPE pathogens and results were

unpredictable. For example, first, EcoFepA ortholog KpnFepA (82% identity) and PaeFepA (61% identity) showed overall same preferences for ligand as EcoFepA; FeEnt > FeEnt* >FeGEnt. However, AbaFepA (46% identity) showed differed preferences for ligand; it showed high affinity for FeEnt* (K_D = 13 nM) and FeGEnt (K_D = 15 nM) and almost equal affinity for FeEnt (K_D = 17 nM) (Figure 5.10 and table 5.1). Secondly, orthologs of other ferric siderophore complexes showed somewhat unpredictable binding preferences. For example, AbaPiuA showed highest affinity for FeEnt* (K_D = 2.4 x 10^3 nM) than FeEnt (K_D = 53 x 10^2 nM) and FeDHBA (K_D = 1.5 x 10^4 nM) (Figure 5.12 and table 5.1).

Another ortholog TBDT was KpnIroN (KpnFepA_0027) which falls in the category EcoFepA and AbaFepA in terms of protein sequence identity. These all three proteins recognize FeEnt, FeEnt*, and FeGEnt but with different affinities.

EcoFepA: FeEnt>FeEnt*>FeGEnt

KpnIroN: FeEnt>FeGEnt>FeEnt*

AbaFepA: FeEnt* ≈ FeGEnt ≈ FeEnt >> FeDHBA

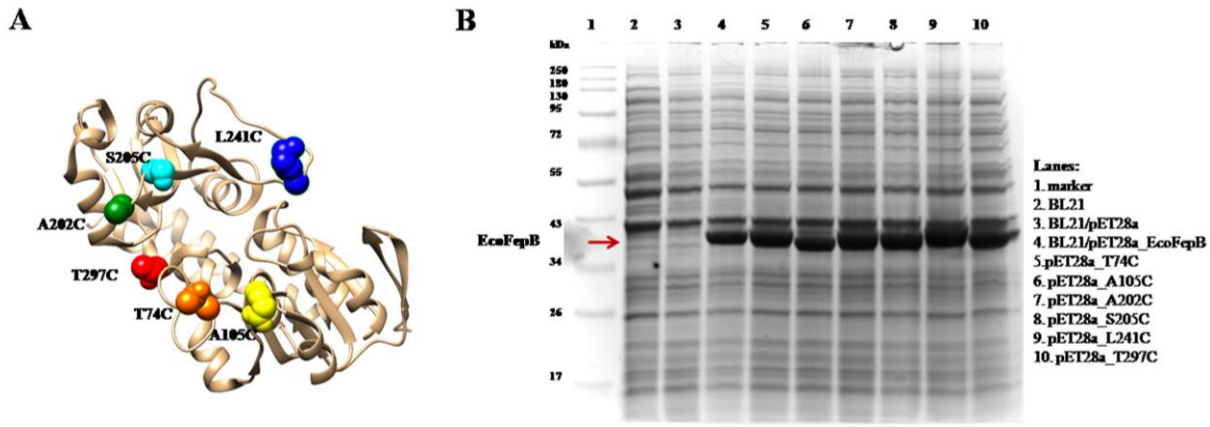

Figure 5.7. The tertiary structure of EcoFepB and overexpression of its Cys derivatives: Panel A depicts the crystal structure of EcoFepB. We selected residues in the region near to ligand (FeEnt) binding site and replaced these residues with Cys using site-directed mutagenesis. Panel B shows the overexpression of EcoFepB and its Cys derivatives. We grew the cells in LB broth and added IPTG (0.1 mM) when the O.D. of the culture was 0.5-0.6 and allowed them to grow for another 4-5 hours and then lysed the cells. We ran these samples using SDS-PAGE followed by Coomassie blue staining.

We looked for differences in the binding affinities in the EcoFepA orthologs in *K. pneumoniae*, which we characterized in this study (See chapter 3). All the putative FeEnt transporter showed differences in the preferences for ferric catecholates and varied in binding affinity. Both KpnFepA_1658 and KpnFepA_4984 showed the same preferences for FeEnt, FeEnt*, and FeGEnt, with different binding affinities in the nanomolar range. Whereas KpnFepA_2380 does not bind with FeEnt* and FeGEnt. Additionally, KpnFepA_2380 also shows affinity for FeDHBA and FeCrn, but both KpnFepA_1658 and KpnFepA_4984 did not bind to it at all (Figure 5.9).

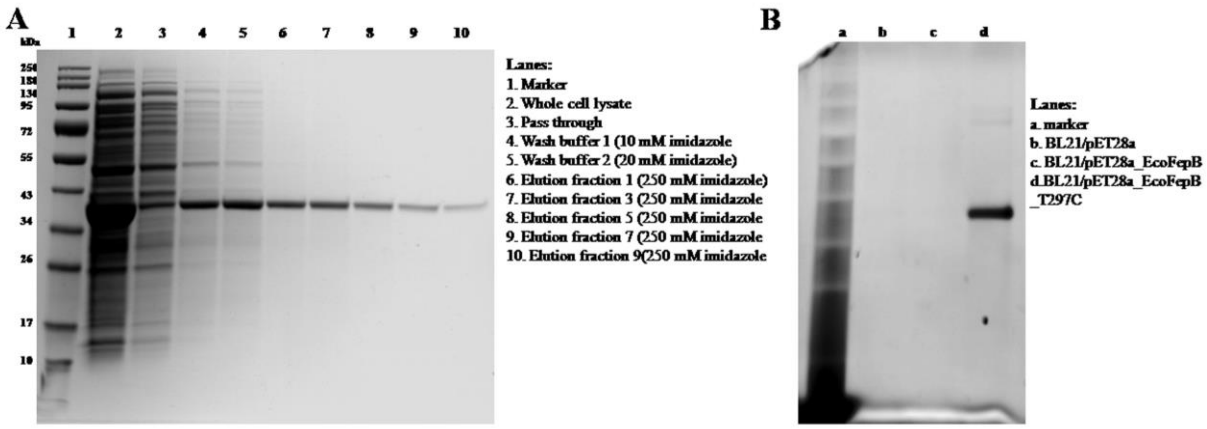

Figure 5.8. EcoFepB_T297C purification and fluorescent labeling:

Panel A shows the Coomassie blue gel staining which shows purification of EcoFepB_T297C using metal affinity chromatography, and panel B show the fluorescent image of SDS-PAGE of the EcoFepB_T297C using proper controls.

These FD sensor data suggest that TBDTs of OM of different Gram-negative bacteria possess specificities and binding to a variety of ligands, and preferences may vary based on the adaption of these bacterial pathogens in the environment they encounter to obtain iron complexes, e.g., animal and human host. Our results indicate that some receptors bind ligands with very weak affinity, in µM range. So ultimately, these receptors span a range of nM to µM binding affinity towards its ligand. Binding data collected on AbaPiuA or AbaBauA suggested that to obtain iron in the host through these receptors, there should be the presence of iron in a much higher concentration or quantity compared to what it is available for EcoFepA.

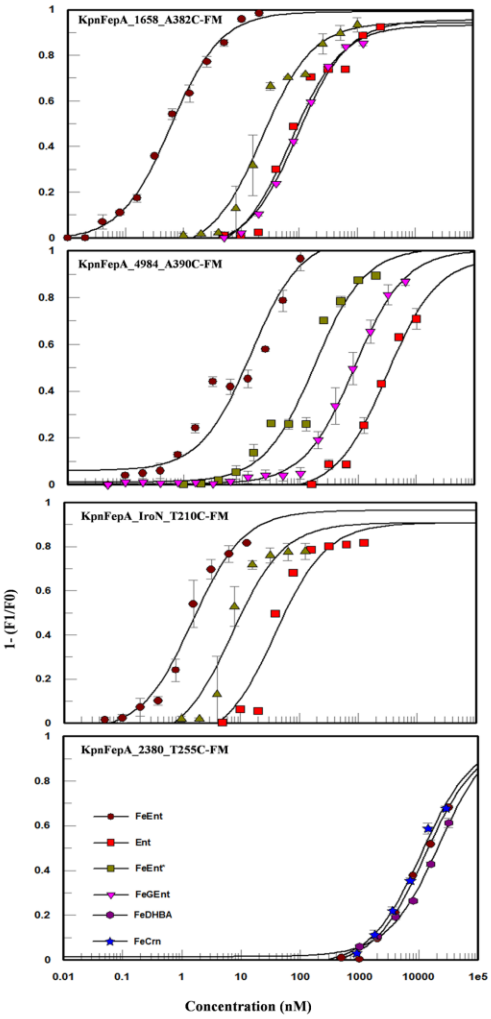

Figure 5.9. Broad recognition of ferric catecholates by different KpnFepAs:

This figure illustrates the recognition of different ferric siderophores; FeEnt, Ent, FeEnt*, FeGEnt, FeDHBA and FeCrn by different KpnFepAs sensor strains; KpnFepA_1658_A382-FM, KpnFepA_IroN_T210C-FM, KpnFepA_4984_A390C-FM and KpnFepA_2380_T255C-FM. (Please see table 5.1 for K_D values).

5.3.4. Specificity of TBDTs for metal complexes:

Some of the catecholate receptors discussed above, we observed that each receptor recognized several metal complexes in addition to their primary one with less binding affinity. However, most of the other siderophore receptors showed singular specificity. For example, EcoIutA, EcoBtuB, CcrHutA, and AbaBauA bind exclusively to FeAbn, Vitamin B_{12}, hemin, and

FeAgn, respectively. None of the receptors bind with any other siderophore other than its primary ligand. For example, EcoIutA bound with FeAbn in nanomolar range but did not show any affinity to other siderophores of the same class, e.g., Fc, FcA, FxB, FeYbt, and FeAgn (Table 5.1). Another example is AbaBauA which exclusively binds to FeAgn (Figure 5.11). Each of the receptors in this class was suited to its biochemical role. For example, Abn biosynthesis and FeAbn uptake receptor are encoded on the same plasmid. The presence of this plasmid on bacterial strains confers virulence and able to invade the host.

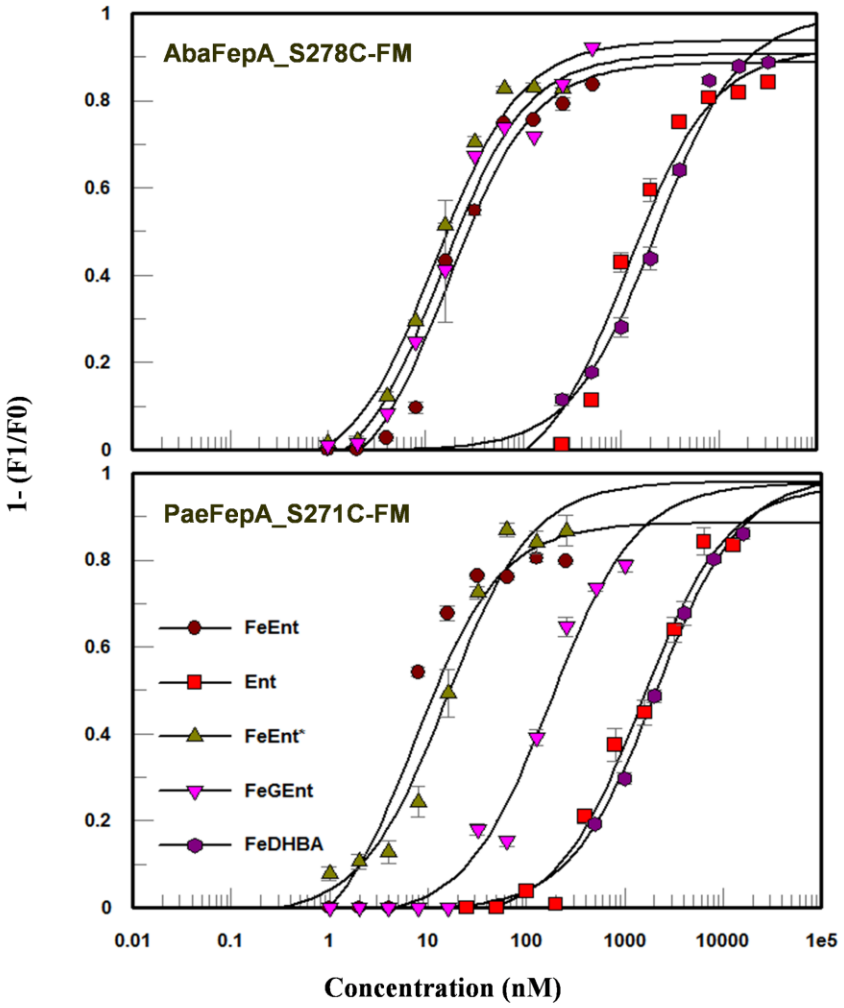

Figure 5.10. Broad recognition of ferric catecholates by FepA orthologs from different bacteria:

This figure illustrates the recognition of different ferric siderophores; FeEnt, Ent, FeEnt*, FeGEnt, and FeDHBA by FepA from different organisms; AbaFepA_S278C-FM and PaeFepA_S271C-FM. (See table 5.1 for K_D values).

Hence binding and selectivity of EcoIutA to FeAbn and avoiding to every other ferric siderophore complex complemented Abn production by the plasmid-containing strains. Similarly, AbaBauA specifically recognizes FeAcn, and this receptor is also associated with pathogenesis. EcoBtuB and CcrHutA were also typical examples of the binding specificity of these receptors in

a manner where they recognize their cognate siderophores despite slight differences in their structures.

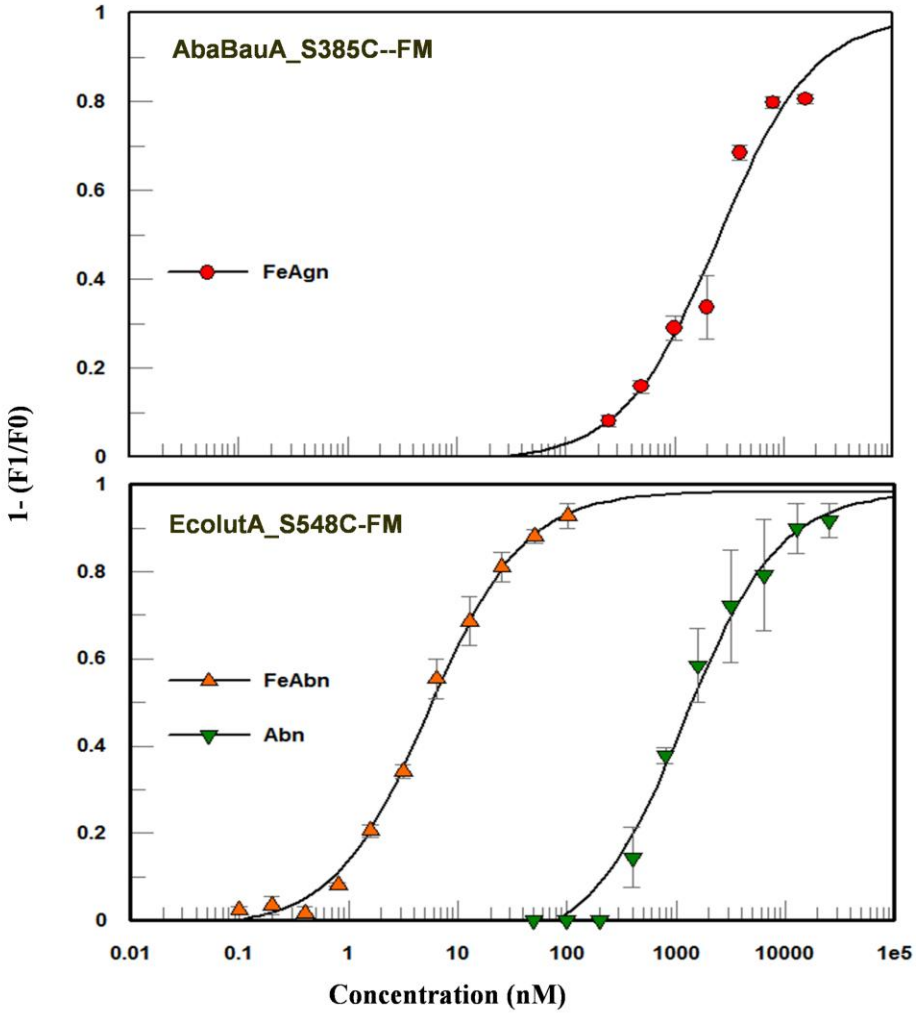

Figure 5.11. Specific recognition of siderophores:

This figure illustrates the recognition of different FeAgn by AbaBauA sensor and recognition of FeAbn and Abn by EcoIutA sensor. These TBDT sensors were exclusively bound to their defined ferric/apo siderophore and did not recognize any other siderophore used in the study. (Please see table 5.1 for K_D values).

5.3.5. Recognition of apo- and ferric siderophores:

In our investigation, several ferric siderophores tightly bind (K_D in the range of nanomolar) to their cognate outer membrane receptor: FeEnt-EcoFepA, Fc-EcoFhuA, B_{12}-EcoBtuB, and FeAbn-EcoIutA. FepA binds to apo FeEnt with around 100-fold less affinity than its ferric form. Experiments with other receptors in our panel showed the same pattern where they bind to apo-form of siderophores with about 60-100-fold less affinity than it binds with ferric form (Table 5.1). For example, apart from EcoFepA, FeEnt was primary ligand for KpnFepA_1658, KpnFepA_4984, KpnIroN, EcoFepB, AbaFepA, PaeFepA. All these receptors bind with FeEnt in the nanomolar range and absorbed Ent with about 60-100-fold lesser affinity than seen for ferric complexes (Figure 5.9, 5.10, and table 5.1).

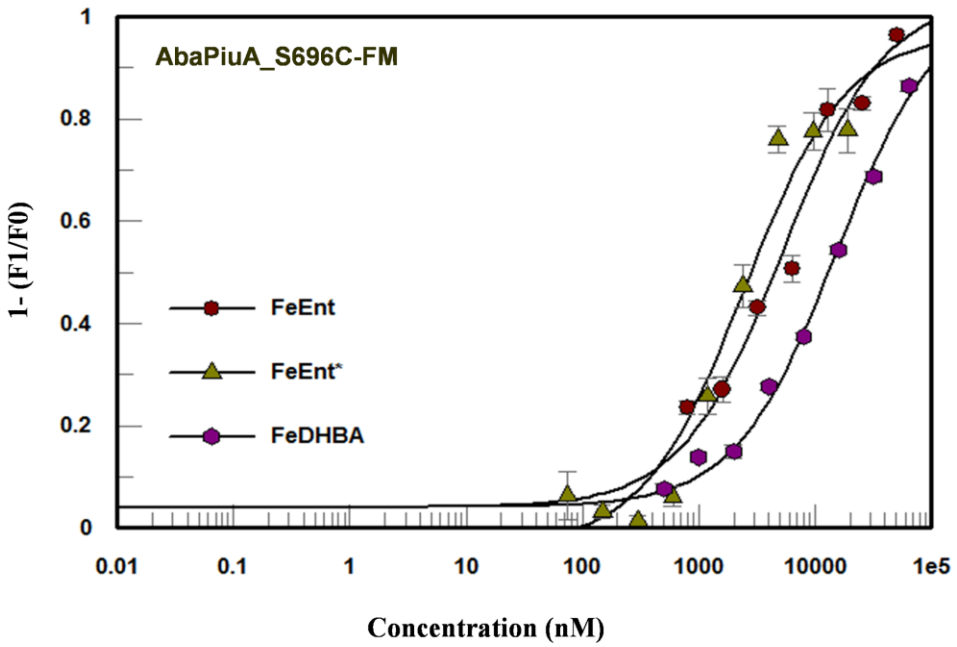

Figure 5.12. Recognition pattern of catecholates siderophores by AbaPiuA:

This figure illustrates the recognition of different ferric catecholates siderophores by AbaPiuA. (See table 5.1 for K_D values).

5.3.6. Ferric siderophore binding by EcoFepB:

In the prototypic bacterial iron transport system, once FeEnt is transported across OM and enters the periplasm, periplasmic protein FepB binds it with high affinity and transfers this ferric siderophore complex to its inner membrane (IM) ABC transporter FepCDG. We cloned the structural gene fepB from *E. coli* MG1655 chromosome, genetically engineered the substitution T297C, purified the over-expressed binding protein on Talon Superflow Co2+ agarose, and labeled it with FM (Figure 5.7 and 5.8).

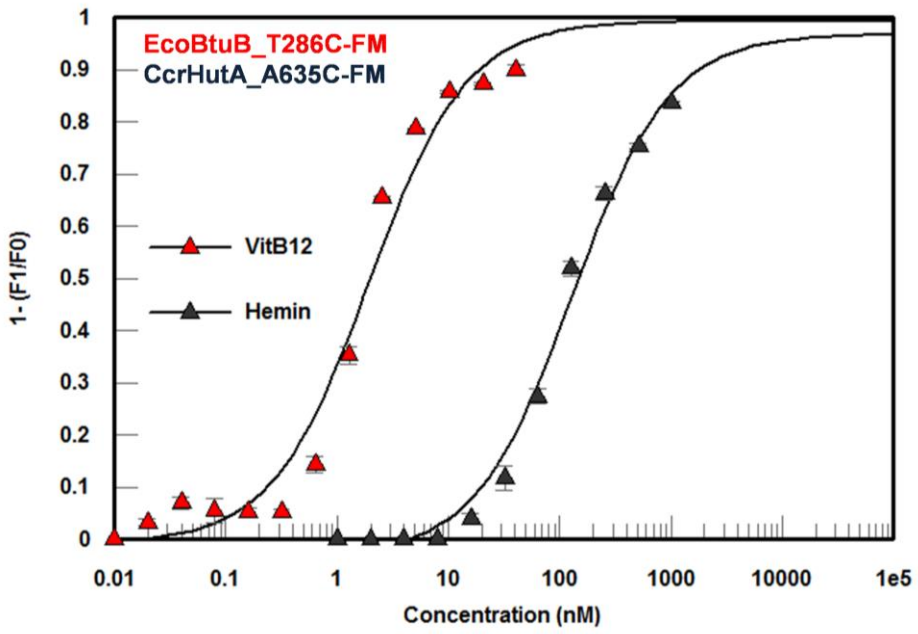

Figure 5.13. Recognition pattern of Hn and B_{12} by CcrHutA and EcoBtuB:
This figure illustrates the recognition of Hn by CcrHutA, and Vit. B_{12} by EcoBtuB. (See table 5.1 for K_D values).

Like other TBDT sensors we tested for catecholate categories, EcoFepB-FM also showed binding preference for over a range ferric complex but FeEnt as the primary one. According to our investigation, EcoFepB-FM binds with FeEnt (K_D = 43 nM), about the same as reported before

(Sprencel, Cao et al. 2000), which is about 100-fold less binding affinity than EcoFepA. Likewise, other sensors we tested in our study, EcoFepB, also binds with apo enterobactin with about 100-fold less affinity (K_D = 4.6 x 10^3 nM) than FeEnt. EcoFepB also binds with other ferric catecholate siderophores with different binding affinities: FeEnt* (K_D = 1.9 x 10^2 nM), FeGEnt (K_D = 1.1 x 10^4 nM), FeCrn (K_D = 9.5 x 10^3 nM), FeDHBA (K_D = 7.1 x 10^3 nM). Overall, EcoFepB showed broad recognition of multiple iron complexes, with the affinities ranged from nM to µM (Table 5.1).

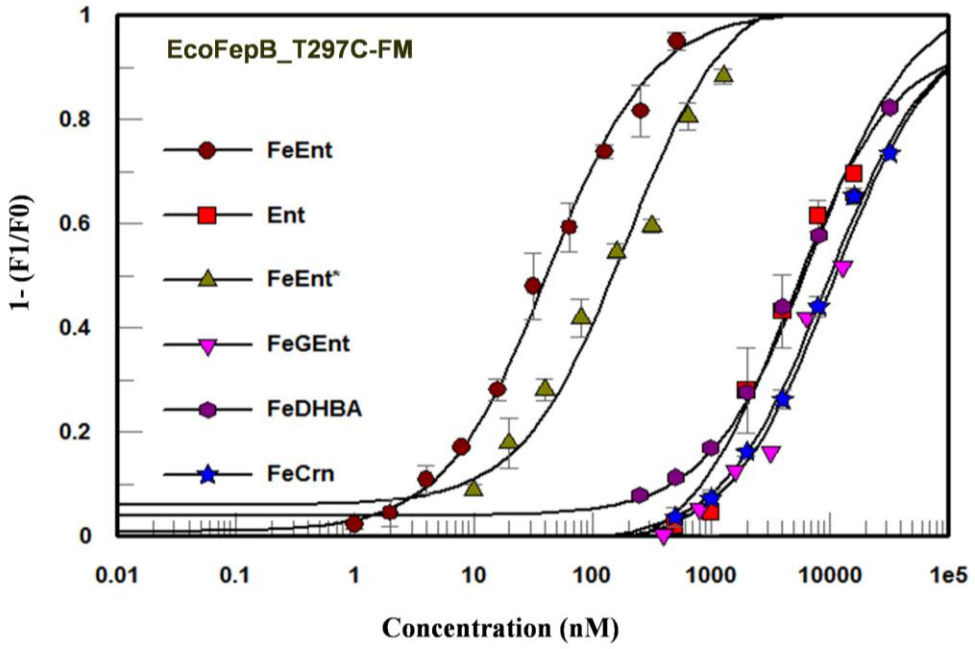

Figure 5.14. Binding of various ferric catecholates by EcoFepB:

We used metal affinity chromatography to purify EcoFepB_T297C. We labeled it with FM followed by gel filtration chromatography to purify labeled protein. EcoFepB recognize various catecholates siderophores which includes FeEnt, Ent, FeEnt*, FeGEnt, FeDHBA and FeCrn. (See table 5.1 for K_D values.

5.3.7. Quantification of ferric siderophores in complex samples:

We tested binding affinities of the sensors, which we created in our study using purified ferric complexes and further illustrated the capabilities of our FD sensors in detecting and quantifying siderophores in biological fluid and extracts (Figure 5.15 and table 5.2).

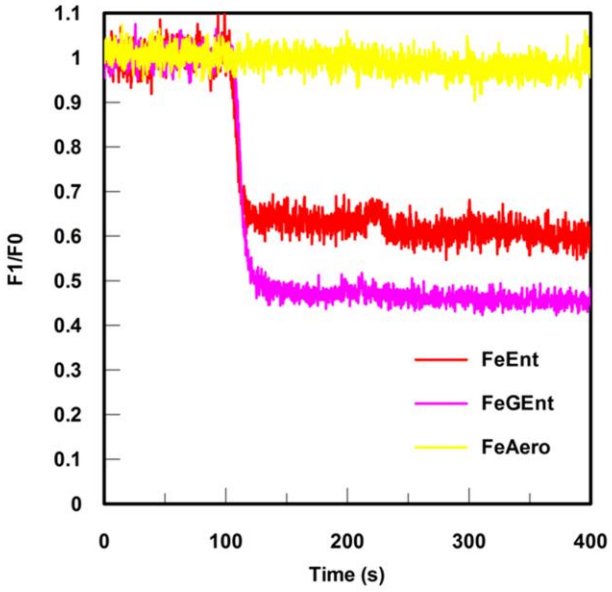

Figure 5.15. FD sensor assay of siderophores in the culture supernatant:
E. coli CP9 strain was grown under iron-deficient conditions, and the supernatant was collected. This supernatant was tested against different sensors; EcoIutA, EcoFepA, and KpnIroN. At 100 seconds, fluorescence quenching indicates the presence of siderophore in the supernatant. In this case, the CP9 strain produced Ent, GEnt, and Ybt (data not shown), but it did not produce Abn.

We used pathogenic strain *E. coli* (CP9) and *K. pneumoniae* (HvKpn1 and HvKpn2), grew them in iron-deficient media, removed the cells by centrifugation, and collected them supernatant and an excess amount of FeCl3. These three pathogenic bacterial strains secrete four siderophores: Ent, GEnt, Abn, and Ybt (Cao, Qi et al. 2000, Cao, Warfel et al. 2003, Chakravorty, Shipelskiy et al. 2019). To determine the amount of siderophore secreted by these strains as a test of these

sensor's efficiency, we used ferrated supernatant with 4 of our sensors: EcoFepA, KpnIroN and EcoIutA.

Table 5.2. Quantification of ferric siderophores in culture supernatant using FD sensor:

		(Ferric siderophores) in samples (µM)		
Sensor	**Complex**	***E. coli* CP9 (PBS)**	**HvKpn1 (Beef extract/PBS)**	**HvKpn2 (PBS)**
EcoFepA-FM	FeEnt	10	5.7/3.8	1.3
EcoIutA-FM	FeAbn	0	105/108	36
KpnIroN-FM	FeGEnt	40	103/85	20

This table illustrates the concentration of various siderophores produced by pathogenic bacterial strains of *E. coli* (CP9) and *K. pneumoniae* (HvKpn1 and HvKpn2) under iron-deficient conditions.

These assays precisely revealed the presence and concentration of these siderophores in the respective supernatants. Our sensors showed that CP9 does not produce aerobactin and GEnt, is the siderophore produced in the highest amount compared to Ybt and Ent. In HvKpn1 and HvKpn2, the former did not produce Ybt, which decreased the invasive potential of this strain compared to HvKpn2, which produced all four siderophores (Table 5.2).

5.3.8. Ferric siderophore uptake by ESKAPE pathogens using FD sensors:

Apart from recognizing and binding FD sensors to various siderophores, these sensors have the ability to show cellular uptake of siderophores by other bacteria. For example, the FD sensor of FeAbn, EcoIutA_T548C-FM binds specifically to FeAbn with nanomolar affinity but does not transport it. However, when this FD sensor cohabits with other bacterial cells, fluorescence

recovery reflects the latter's ability to transport this ferric complex (Figure 5.15). Using the FD sensor of FeAbn, we showed that *E. coli* (Eco), *P. pneumoniae* (Pae), *K. pneumoniae* (Kpn), and *Enterobacter cloacae* (Ecl) transported FeAbn but *A. baumannii* (Aba) did not (Figure 5.15). We showed the transport of other siderophores using the FD sensor of FeEnt as well (Figure 5.16 and chapter 4).

5.4. Discussion:

In most cases, the production of a particular siderophore or group of siderophore production correlates with the presence, tropism, invasiveness, or lethality of a particular bacterial. For example, in the case of *A. baumannii*, which exclusively produce three virulence enhancing siderophores: acinetobactin, baumoferrins and fimsbactins. These siderophores are only produced by this organism, and the production of these siderophores is related to the pathogenesis exclusively by *A. baumannii*. However, there are siderophores or groups of siderophores whose production is directly associated with the virulence of many bacterial species. For example, hypervirulent *K. pneumoniae* produces four siderophores: Ent, GEnt, Abn, and Ybt, but the production of Abn is directly related to pathogenesis. Deleting the Abn synthetic locus *iucA* reduced the virulence of hypervirulent *K. pneumoniae*, whereas loss of other siderophore synthesis did not affect the virulence.

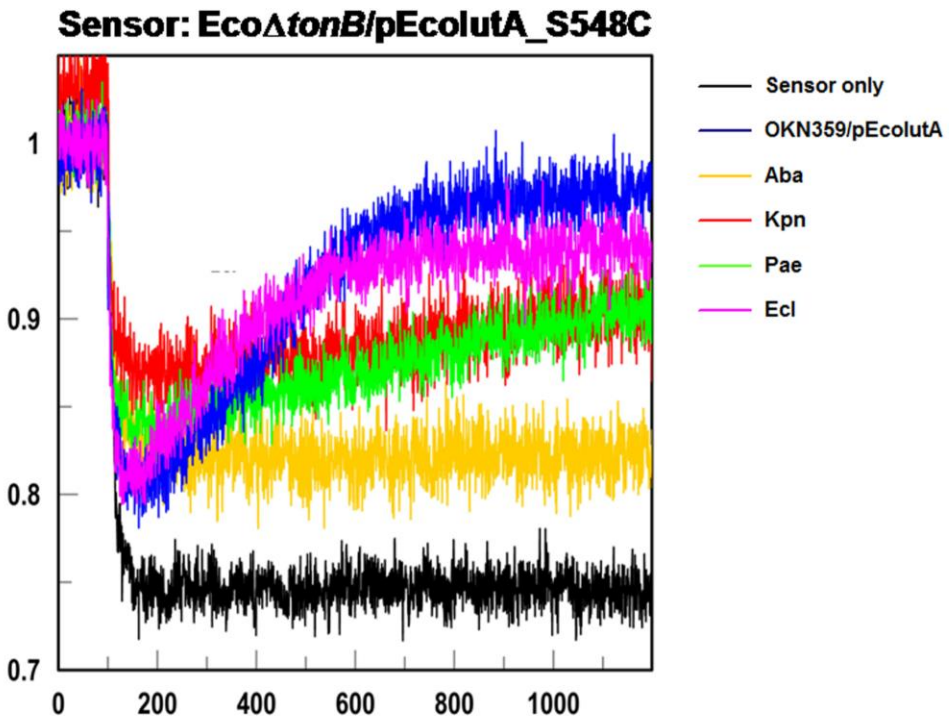

Figure 5.16. Fluorescence decoy sensor of FeAbn transport:

We used EcoIutA sensor along with noted bacteria in the panel which were grown under iron deficient condition. Decoy sensor observed the uptake of FeAbn by all the bacteria except *Acinetobacter baumannii*. (Sensor = OKN13/pEcoIutA_T548C, Aba = *A. baumannii*, Kpn = *K. pneumoniae*, Pae = *P. aeruginosa* and Ecl = *Enterobacter cloacae*). **(x-axis = Time (second) and y-axis = 1-(F1/F0))**

This citrate-based siderophore; Abn, is well known to confer bacterial pathogenesis (Williams 1979), and in the case of hypervirulent *K. pneumoniae*, production of Abn is considered as a virulence factor, but that is not the case with classical *K. pneumoniae*, which does not harbor the plasmid which encodes Abn biosynthetic and OM receptor genes. Broadly simultaneous elaboration of aerobactin, yersiniabactin, and glycosylated enterobactin by strains of *E. coli*, *K. pneumoniae* (Bachman, Oyler et al. 2011, Holden, Breen et al. 2016), *S. typhimurium* (Bister, Bischoff et al. 2004) and other bacteria are related to pathogenesis as behaving these siderophores as virulence factors. Each of these specific siderophores in this mixture promotes the infection of

specific target organs, increasing the organism's virulence. We developed fluorescent sensors that can provide sensitive, accurate information about the presence of siderophores even at very low concentrations and characterizing apo- or ferric siderophores in research, clinical and pharmaceutical settings.

Even small changes in the structure of related siderophores can be meaningful in terms of pathogenesis. For example, Ent and GEnt are catecholate siderophores. However, they differ with the presence of glycosylated groups in the latter, which influences the outcome of the encounters between host and pathogen, demarcating the fine line between colonization and pathogenesis. For example, Ent production and FeEnt utilization are associated with the colonization in the human gut (Pi, Jones et al. 2012). In contrast, glycosylation of its catecholate group to form GEnt and utilization of FeGEnt is associated with invasiveness and pathogenesis (Williams, Rabsch et al. 2006, Lee and Helmann 2007, Bachman, Lenio et al. 2012)(Williams, Rabsch et al. 2006, Lee and Helmann 2007, Bachman, Lenio et al. 2012).

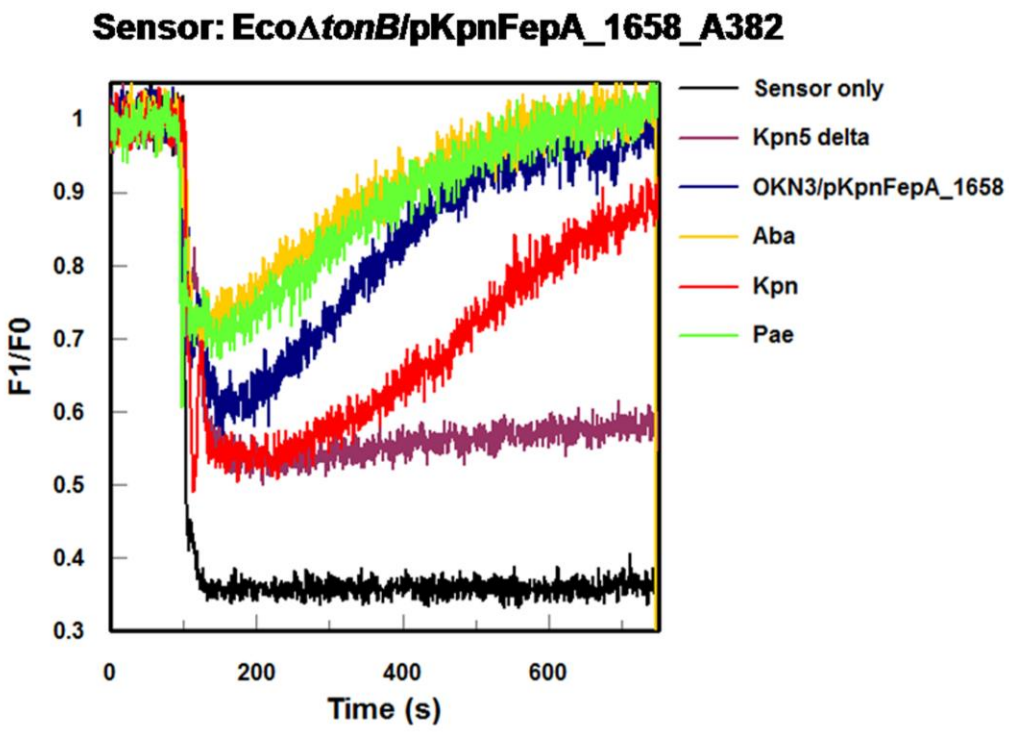

Figure 5.17. Fluorescence decoy sensor of FeEnt transport:

We used KpnFepA_1658 sensor along with noted bacteria which were grown under iron deficient condition. Decoy sensor observed the uptake of FeEnt by all the bacteria except sensor strain which is *tonB* deficient. (Sensor = OKN13/pKpnFepA_1658_A382C, Kpn5 delta = entA deficient and all four *fepA* deficient, Aba = *A. baumannii*, Kpn = *K. pneumoniae*, Pae = *P. aeruginosa* and Ecl = *Enterobacter cloacae*).

Both Ent and GEnt steal iron from the host. However, SCN can adsorbs Ent and remove it from circulation and starve bacteria for iron and ultimately weaken them. However, SCN similarly cannot remove the low concentration of GEnt/FeGEnt. Thus, not evading by host cells creates an opportunity for GEnt to be in high concentration in blood, serum, and tissues, which ultimately creates an environment for the proliferation of bacteria throughout the host. Plus, GEnt/FeGEnt is not the only siderophore that SCN cannot recognize, this is the same case for Abn, Ybt, and Acn. Ultimately production of these siderophores correlates with the potential of these siderophores to be behaving as virulence factors of Gram-negative bacteria.

Chapter 6 - Conformational rearrangements in the N-domain of *Escherichia coli* FepA during ferric enterobactin transport

Majumdar, A., V. Trinh, K. J. Moore, C. R. Smallwood, A. Kumar, T. Yang, D. C. Scott, N. J. Long, S. M. Newton and P. E. Klebba. *J. Biol. Chem.* (2020) 295(15) 4974 –4984.

My personal contribution to this paper includes creation of some of single and double Cys substitutions in EcoFepA we used in the study, functional analysis of these Cys constructs using siderophore nutrition test, analyzing the presence of di-sulfide bonds in the double Cys mutants using SDS-PAGE followed by immunoblotting, and looked for fluorescence labeling in these single and double Cys constructs.

6.1. Introduction:

Not all but most of the Gram-negative bacterial outer membrane (OM) protein's functions are logically explained with the help of their crystal structure. For example, the presence of 10Å constriction zone in open trans-OM channels of general porins explained the rationale behind the size-exclusion properties of the pore (Cowan, Schirmer et al. 1992). This property clearly helped understanding why OmpF and related family proteins specifically allow passage of small hydrophilic (< 600 Da) molecules but do not allow passage of relatively large molecules (Nikaido and Vaara 1985). Similarly, one another crystal structure of maltoporin, LamB, suggested the presence of pore, around 6Å in diameter, and a constriction zone in the pore surrounded by aromatic residues explains its selectivity for maltodextrins (Klebba, Hofnung et al. 1994). However, this is not the case for OM siderophore transporters, e.g., FepA and its relatives, as their

crystal structures do not explain the siderophore transport mechanism. Typically, these transporters contain 22 stranded beta-barrels in the C-domain, which possess loops in the exterior portion that makes cell surface vestibules for ligand binding. A globular N-domain (~150 residues) is situated in the transmembrane channel, potentially obstructing transport (Buchanan, Smith et al. 1999, Ferguson, Chakraborty et al. 2002, Chimento, Mohanty et al. 2003). Unlike OM porins, these OM transporters do not contain transmembrane pores. So conformational rearrangements must occur in the N-domain for active transport inside the cell upon binding of ligand to the receptor. The IM protein TonB helps transfer energy to OM, and the binding of C-domain of TonB to TonB box is the basis of this energy transfer (Jordan, Zhou et al. 2013). However, what kind of structural changes facilitate ligand transport are not well understood.

Previously, a model has been proposed that explains N-domain's possible movement happening in the β-barrel of FepA that might create a pathway for internalization of FeEnt into the periplasm. One model is the ball-and-chain method which ultimately would open a large (40-Å diameter) trans-OM channel for ligand transport. According to this model, N-domain dislodges into the periplasm in two possible ways; either as a globule based on its hinge-like connection to the barrel or by unfolding of its structure. This proposed mechanism rationalized ligand transport because if metal complex binds to the N-domain loops, then dislodging the N-domain into the periplasm will transport FeEnt into the periplasm (Ma, Kaserer et al. 2007). Another possible mechanism is explained by the Transient Pore model, which suggests necessary conformational changes must occur in the globular N-domain while residing in the β-barrel, ultimately creating a smaller pore (~20Å in diameter) for the passage of the metal complex. This mechanism suggests that the ligand transits the transporter’s interior by passing between sequential binding sites with different affinities. In the case of FeEnt (-3 charged), it might happen by sequential binding to

basic residues that exist close to the top of the N-domain of FepA and lining its membrane channel (Ma, Kaserer et al. 2007).

In this work, we genetically engineered Cys substitutions in *E. coli fepA*, keeping the fact in mind that sulfhydryl pairs encoded by these substitutions are close enough to form disulfide bonds. We basically divided these substitutions into two classes; one which we created exclusively in N-domain (intra-N) and the other involving residues located in its N- and C- domains (inter -N-C) (Figure 6.2). So, during FeEnt transport, if the N-domain unfolds or undergoes rearrangements, we expected intra-N Cys pairs to impair or abolish FeEnt uptake. On the other hand, if N-domain moves to periplasm as a rigid (folded) body, we expected intra-N would not abrogate FeEnt transport instead. However, inter-N-C domain disulfides, which hold the N-domain within the barrel, would block it. From our experiments, we observed that intra-N disulfides prevented ligand transport, but the majority of inter-N-C disulfides did not. Findings from this work suggest that N-domain must rearrange itself during ligand uptake, staying in the barrel but undergoing changes as transport occurs.

6.2. Methodology:

We used the Quick-Change site-directed mutagenesis kit to create single and double Cys substitution in *E. coli* FepA (PDB sequence 1FEP). The available crystal structure of FepA made it easy for us to predict single and double Cys substitutions sites that can be involved in disulfide bond formation (usually less than 5Å distance between two substitutions). All the Cys substitutions construct were confirmed by DNA sequencing.

We constructed and analyzed six intra-N Cys pairs (G27C- R126C, A33C-E120C, D44C-T111C, N56C-D73C, I84C- V142C, and L125C-V141C) in the N-domain of the structure which

may be involved in the formation of disulfide bonds and nine inter-N-C domain Cys pairs (I14C-G300C, A42C-N162C, T51C-N608C, G54C- T585C, M77C-E511C, P128C-A463C, A137C-A465C, A138C- A445C, and G149C-T180C). In inter-N-C domain Cys pairs, one Cys substitution was on the surface of the N-domain, and another was on the internal wall of the beta-barrel (C-domain of FepA) (Figure 6.2).

We performed a siderophore nutrition test to qualitatively check the ability of mutant FepA strains to transport FeEnt. Results were expressed as diameter around the paper disk, which shows the growth of bacteria and compared nature and diameter compared to wild-type strain OKN3/pITS23 *(fepA+)*. To perform the ability of disulfide bond reduction on ligand transport by WT and mutant FepA strain, we added 1mM β-mercaptoethanol (βME) in the media.

We also analyzed the cell envelope fractions of WT and mutants electrophoretically and immunochemically in the presence/absence of 1mM βME to check for the presence of disulfide bonds in both denatured and non-denatured conditions. To estimate the extent of disulfide bond formation in Cys-pair mutants of FepA, we also modified the fractions by FM and subjected them to SDS-PAGE and western immunoblot after proper processing of the samples as described in detail in chapter 2. Because in most of the experiments, we used βME to check the effect of disulfide bond formation on the FeEnt transport, we also collected the data which shows the effect of disulfide bonds formation on the binding capacity of the mutants and WT, in the presence and absence of βME. We used a slightly different approach where we measured the binding capacity of all the constructs at saturating concentration of radiolabeled substrate instead of collecting data over a range of substrate concentrations. We also assessed the effect of disulfide bond formation on the transport by ferric enterobactin accumulation assay.

Another approach we used to monitor the uptake of TonB dependent FeEnt transport with the help of an FD sensor (Chakravorty, Shipelskiy et al. 2019), which revealed whether the presence of engineered disulfide bond formation affected the FeEnt transport. In the fluorescence spectroscopic assay, we used OKN13/pEcoFepA_A68C-FM (FepA-FM) as decoy sensor (binding competent but transport defective), and the presence of Cys engineered FepA strain (transport competent) at the same time reflected the transport functionality of FepA quantitatively during in a time-dependent manner. For each assay, we used 50 ml of FD sensor at 5 X 10^8 cells/ml in a cuvette containing PBS + 0.4% glucose at 37ºC and recorded the fluorescence intensity for 100s. At 100s, we added FeEnt in the cuvette to a final concentration of 5 nM, which caused quenching of fluorescence (around 60%). We allowed incubation for 100 additional seconds, then added 50 ul of test strain (5 X 10^6 per ml). A decrease in fluorescence quenching (increment of fluorescence) indicates the transport of FeEnt into the cell from the solution. If there was no fluorescence increment (which shows no uptake of ligand), then we added 10 mM βME (final concentration in the cuvette) at 800 sec.; if necessary, another aliquot of βME was added at 1000 sec. to 20 mM total concentration.

6.3. Results:

6.3.1. Formation of disulfide bonds in site directed Cys pair substitutions mutants:

We analyzed 6 pairs of Cys substitution in N-domain (intra-N domain) and 9 pairs of Cys pairs in the region, potentially connecting N-domain and β-barrel (inter-N-C domain). We selected these Cys substitution sites based on the relative distance in the tertiary structure of FepA (Figure 6.2), expecting them to form disulfide bonds. It is possible for both types of mutants, disulfide

bond formation may abrogate FeEnt transport by interfering with N-domain conformational dynamics or motion.

We used non-reducing SDS-PAGE followed by western blot analysis to see the quantification of FepA expression and show the extent of disulfide bond formation by these Cys pair mutants. Few of the Cys pairs (33-120, 42-162, 56-73, and 14-180) did not show evidence of disulfide bond formation in SDS-PAGE/immunoblot analysis but showed the presence of disulfide bond by other methods. However, we saw multiple bands for many of the Cys pairs in SDS-PAGE/Immunoblot analysis, which verified disulfide bond formation in these mutants (Figure 6.3A).

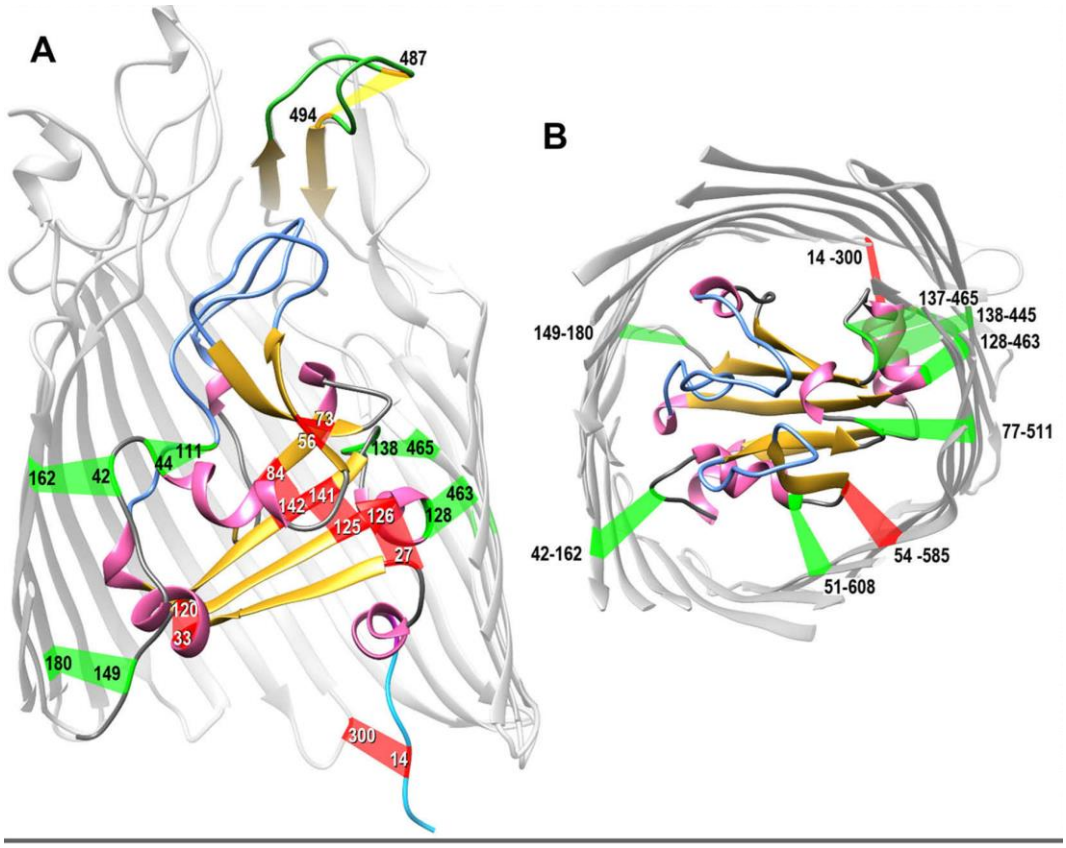

Figure 6.1. Native and engineered Cys pairs in FepA:

A, shows the side view of FepA and B, shows the top view. Putative disulfide bond formation is shown between Cys pair with different color, red if they inhibited FeEnt transport and green, if they allowed transport. Figure adapted from (Majumdar, Trinh et al. 2020).

However, these experiments did not provide a concrete idea about the disulfide bond formation as some of the mutants' electrophoretic mobility exactly matched that of WT FepA. Several mutants showed the incomplete formation of disulfide bonds, and only I14C-G300C showed homogeneous band formation at a different size than WT FepA, indicating complete disulfide bond formation. Some of the mutants that did not wholly form disulfide bonds suggested that a fraction of Cys residue side chains were not oxidized and native. To validate and estimate the extent of unreactive Cys-pairs in mutants, we incubated SDS-denatured cell envelope fractions to FM (5µM; 5 min) before and after exposure of βME.

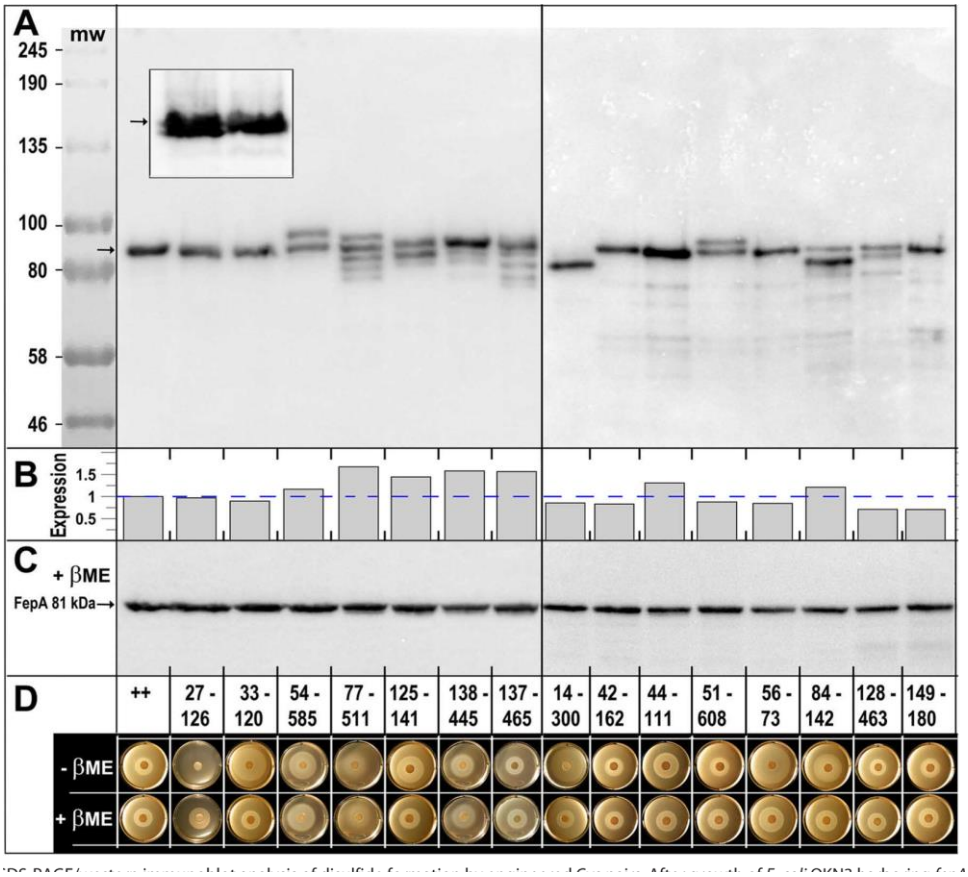

Figure 6.2. SDS/immunoblot and siderophore nutrition assay:

A, immunoblot indicating the presence of disulfide bond in form of differential electrophoretic mobility of different Cys pairs than of WT FepA or sometimes same as well. **B,** quantification of FepA expression. **C,** Immunoblot of WT FepA and Cys pair mutants in the presence of 3 mM βME. **D,** siderophore nutrition test of all FepA mutant in the absence and presence of βME. Figure adapted from (Majumdar, Trinh et al. 2020).

As expected, WT FepA (form stable disulfide bond; C487-C494) (Liu, Rutz et al. 1994) did not react with the fluorophore in the absence of βME. The fluorescent image of the gel provided valuable information about the disulfide bond formation in different mutants (Figure 6.4). We analyzed FM labeling in the six Intra-N Cys pairs before the addition of βME, and results demonstrated the different extent of labeling in these mutants, showing different amounts of disulfide bond formation:

- 27-126 and 125-141were least affected by FM, showing the complete formation of disulfide bonds.
- 14-300, 33-120, 56-73, and 84-142 were more reactive with FM, indicating the incomplete formation of disulfide bonds.
- 44-111 was most reactive to FM, suggesting that this mutant did not form disulfide bond in vivo but fully appeared disulfide-bonded in SDS-PAGE/immunoblot (Figure 6.3A).
- After the addition of βME, as expected, all the intra-N mutants showed better labeling with FM.

Overall, electrophoretic mobility and reactivity to FM of these mutants revealed the presence of disulfide bonds in vivo. Apart from intra-N mutants, we observed that inter-N-C mutants were also reactive to different extents to FM. Among these mutants, 14-300 appeared fully disulfide-bonded (Figure 6.3A) but also reacted to some extent with the fluorophore, indicating the presence of free sulfhydryl.

6.3.2. Effect of engineered Cys pairs on FeEnt utilization in nutrition test:

We performed the siderophore nutrition test (Wayne, Frick et al. 1976) in the absence and presence of βME, and results showed intra-N Cys-pair mutants FepA impaired FeEnt transport. None of the single Cys-substitution mutant FepA strain weakened FeEnt transport (Figure 6.3D).

In the absence of any reducing agent (βME), every time we observed that disulfide form formation in intra-N Cys pairs also inhibited FeEnt transport in the siderophore nutrition test. For pairs 27-126, 33-120, 56-73, 84-142, and 125-141, we observed 2-3 fold larger and fainter halos compared to WT FepA, which reflected lower FeEnt uptake (Cao, Qi et al. 2000, Annamalai, Jin

et al. 2004) and these difference in halos were reverted when we used 1mM βME in the plate (Figure 5.3D). Cys Pair 44-111 (did not show evidence of disulfide bond formation) was designed to bond short helices in the N-domain, did not inhibit FeEnt transport. In summary, each Cys pair substitution that formed disulfide bonds impaired FeEnt uptake through FepA in this test.

Among inter-N-C domain Cys pairs, 14-300 has been previously characterized (Ma, Kaserer et al. 2007) and, Because of the location of residue I14 at the TonB box region of N-domain and, of G300 at the periplasmic rim of β-barrel, disulfide bond formation in this mutant does not allow FeEnt transport and we observed in nutrition test as well in the absence of βME (Figure 6.3D).

Among other some of the Cys pairs (42-162, 51-608, 128-463, 137-465, 138-445, and 149-180) showed typical halos of growth even in the absence of the reducing agent. Among these six mutants, 42-162 and 149-180 did not show any aberrant band with altered mobility in gels/blots, and others did. These results showed that tethering of N-domain to β-barrel did not inhibit FeEnt.

For two mutants (54-585 and 77-511), we could not interpret the results in the nutrition test as these mutants showed slightly aberrant halos in the absence of βME, and even the presence of βME could not revert it to normal.

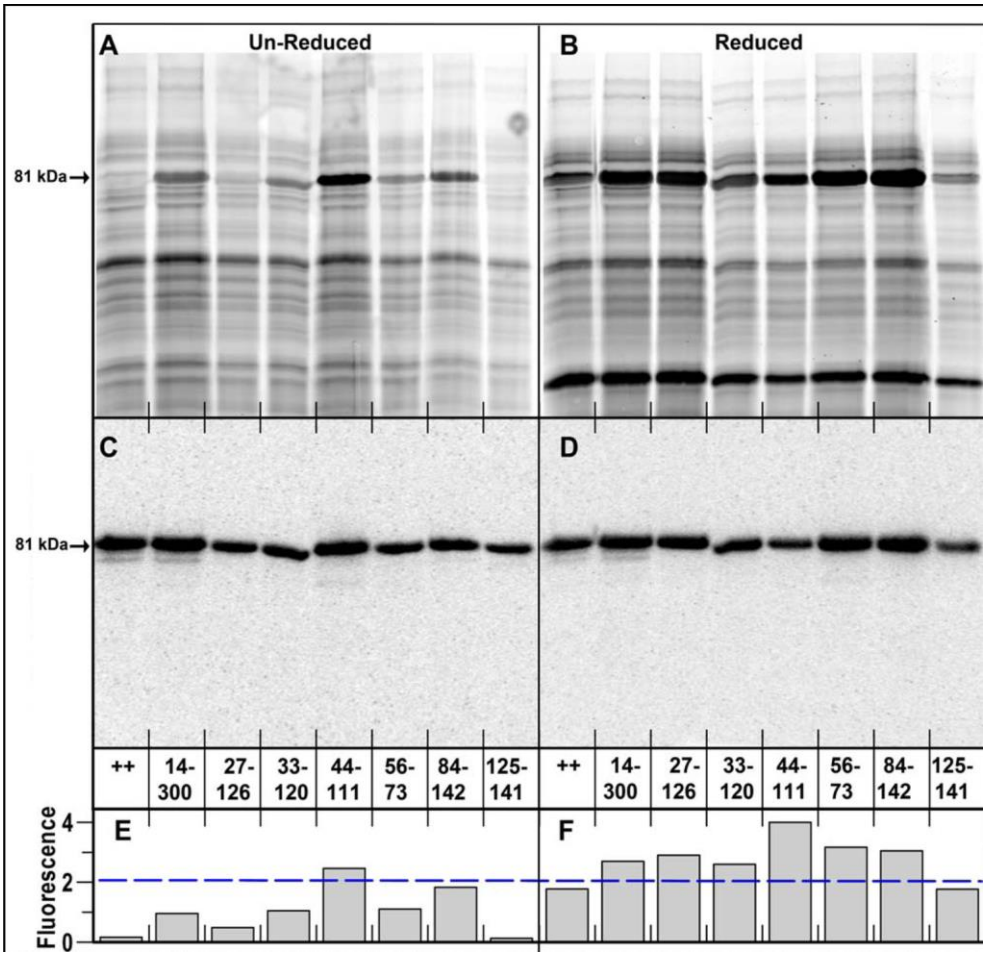

Figure 6.3. FM labeling of Cys mutant:

A and B, FM labeling of Cys mutants cell envelop in the absence and presence of βME. C and D, showing the SDS/Immunoblot of gels shown in panel A and B respectively. E and F, quantification of FM-labeling. Figure adapted from (Majumdar, Trinh et al. 2020).

6.3.3. Effect of βME on the binding of [59Fe]Ent by FepA and effect of engineered disulfide bonds on [59Fe]Ent transport:

Native *E. coli* FepA contains 2 Cys residues at positions C487 and C494, which are involved in disulfide bond formation (separated by six amino acids). This disulfide bond formation is needed for efficient transport of FeEnt through FepA (Liu, Rutz et al. 1994, Cao, Qi et al. 2000, Annamalai, Jin et al. 2004). Most of our experiments involved the use of βME to reduce engineered

disulfide bonds in FepA. We also determined the effect of different concentration βME on the binding of [^{59}Fe]Ent by OKN3/pITS23 (*fepA*+). Our results (Figure 5.5) (Majumdar, Trinh et al. 2020) showed little impact of reducing agent (<1mM) on the binding capacity of [^{59}Fe]Ent, and around 20% reduction in binding capacity when we used 5 mM βME.

In the uptake assay, we saw a decrease in [^{59}Fe]Ent uptake rate by intra-N disulfides as we noticed in the nutrition test except 44-111 (Figure 6.5C). [^{59}Fe]Ent uptake rate was decreased by 20-25% in the absence of βME than of WT FepA but reverted to normal transport when βME was used, reiterating that intra-N domain interferes with FeEnt transport. On the other side, inter-N-C, Cys pairs that we tested showed decrease in the uptake rate in the range of 10-45%, except 54-585 (65%).

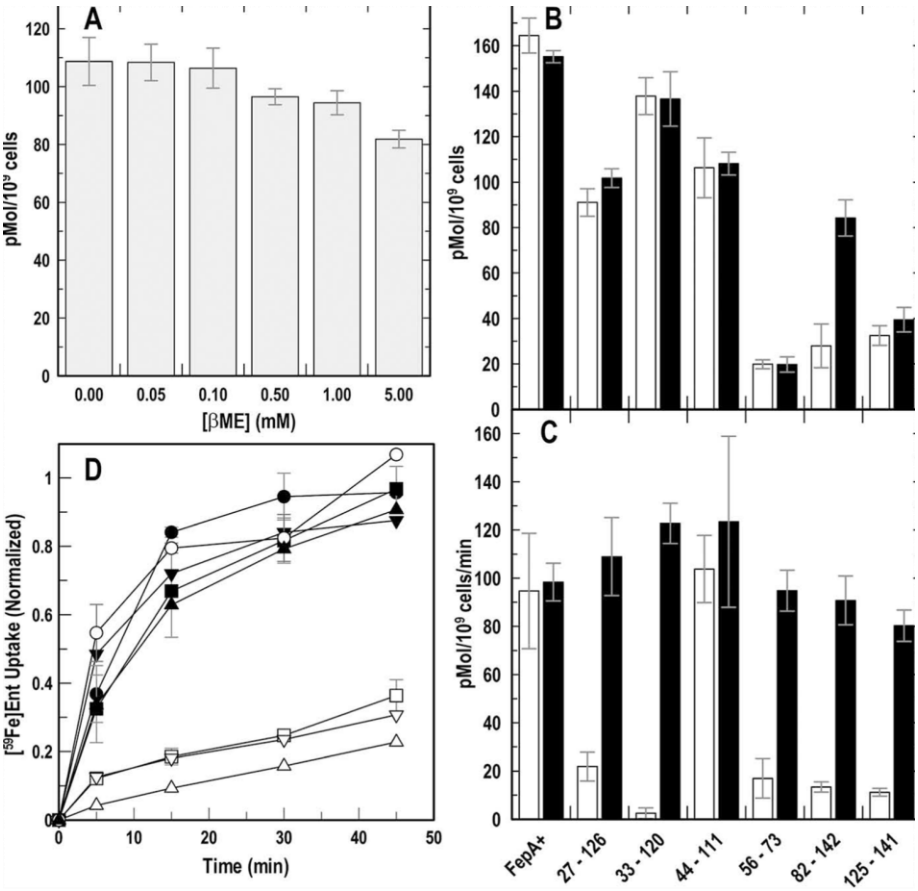

Figure 6.4. Binding and transport of [59Fe]Ent by intra-N Cys mutants:

A, effect of increasing concentration of βME on [^{59}Fe]Ent to WT FepA. B and C, binding capacity and [^{59}Fe]Ent uptake of Cys pair mutants in the presence of saturating [^{59}Fe]Ent, in the absence or presence of βME. D, accumulation of [^{59}Fe]Ent in absence (open symbols) and presence (filled symbols) of βME. Figure adapted from (Majumdar, Trinh et al. 2020).

6.3.4. Fluorescent measurement of FeEnt uptake by Cys-pair mutants:

Previously we utilized three different assays to show FeEnt transport through FepA and engineered Cys pairs of FepA. In electrophoretic mobility assays, we observed partial disulfide bond formations and partial reduction of FeEnt transport in nutrition assay and [59Fe]Ent uptake, which were a little difficult to interpret. We used a fluorescence decoy sensor (Chakravorty, Shipelskiy et al. 2019) to observe TonB dependent uptake of FeEnt by engineered FepA to see whether disulfide bonds in different mutants interfere with ligand transport. FD sensor of FeEnt

(OKN13/pEcoFepA-FM) can bind (quench) but not transport FeEnt, and the extent of quenching reflect [FeEnt] in the solution and presence of binding and transport competent cells at the same time deplete the FeEnt from the solution and fluorescence recovers. Incubation of FD sensor in the presence of Cys pair mutant cells shows the latter's ability to transport FeEnt, resulting in a decrease in quenching. These data provided functionality of FeEnt transport by different mutant FepA in a quantitative manner.

For intra-N mutants, five out of six mutants did not show FeEnt transport when employed with FD sensor in the absence of βME, but the presence of βME in the cuvette reduced the disulfide bond and allowed the transport of FeEnt. One exception was 44-111, which transported FeEnt similarly to WT FepA (i.e., fluorescence recovery but slower transport rate). Data on 44-111 suggested that maybe this pair did not form a disulfide bond, or its presence did not affect FeEnt transport. Overall, these data support that disulfide bonds in N-domain prevent FeEnt transport, and transport begins when a reducing agent is used. All the pairs we tested allowed FeEnt transport for inter-N-C Cys pairs except two of them (14-300 and 54-585). Cys pair 77-511, which showed the inconclusive result in nutrition, showed transport of FeEnt using FD sensor assay. Overall inter-N-C Cys pairs did not inhibit FeEnt transport.

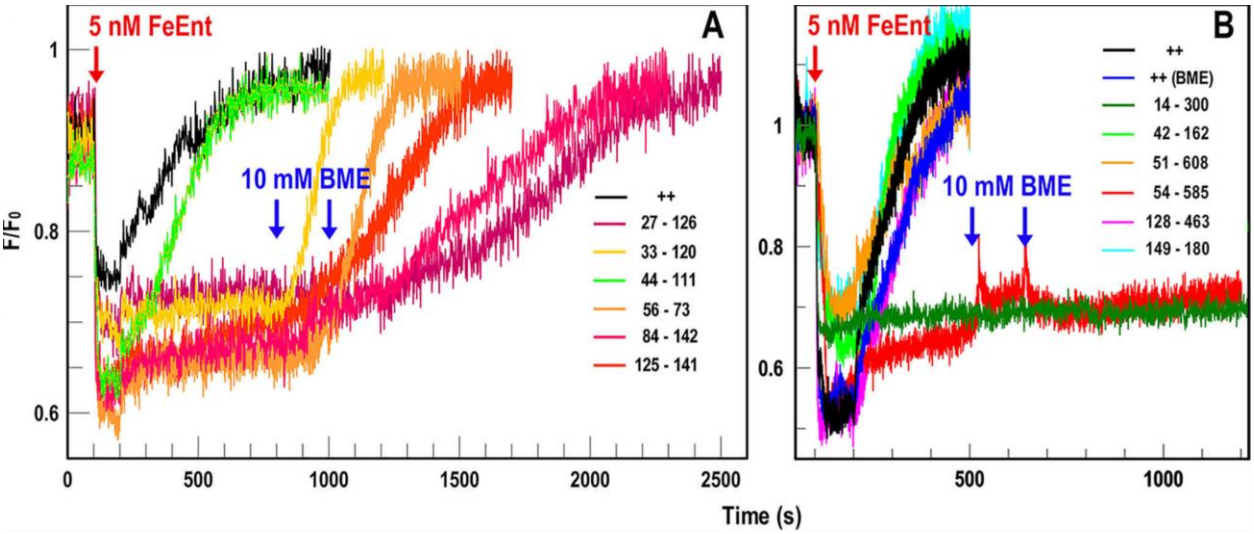

Figure 6.5. FD sensor assay for the measurement of FeEnt transport by Cys pairs:
A, Observation of FeEnt transport by intra-N Cys pairs (βME added at 800s and 1000s). **B**, FeEnt transport by inter-N-C Cys pair mutants. Figure adapted from (Majumdar, Trinh et al. 2020).

6.4. Discussion:

To explain the mechanism of FepA mediated transport, we need to understand the actions of the N-domain during FeEnt internalization. With the help of three different assays, we were able to draw the same conclusion looking at the phenotype of Cys pairs: in general, intra-N disulfide bonds prevented FeEnt transport whereas inter-N-C disulfide bonds did not (Figure 6.2). These data imply several conclusions:

The internal structure of the N-domain should rearrange at the time of FeEnt transport; if not (bonds that blocked these transitions), there is a failure to transport the siderophore.

The disulfide bonds in this region will constrict N-domain motion and will not allow conformational changes necessary for FeEnt uptake.

Bonds that hold N-domain in the channel (inter-N-C) did not interfere in FeEnt transport, imply that N-domain does not exit the transmembrane pore as a rigid body (Ma, Kaserer et al. 2007).

Many of the disulfide bonds that hold the N-domain in the transmembrane did not prevent FeEnt uptake, suggesting that at the time of FeEnt transport without coming out of the channel, N-domain rearranges and create transient pore (Ma, Kaserer et al. 2007) and through which FeEnt passes into the periplasm.

Further, it was difficult to determine the extent of disulfide bond formation *in vivo*, and we observed a variety of outcomes: some Cys pair mutants which formed disulfide bond altered the *Rf*, but some did not; either they did not make disulfide bond or disulfide bond did not change *Rf*, and they migrated same as WT FepA. Sometimes a single amino acid substitution may dramatically change the electrophoretic mobility of a protein on the gel, but the effect of engineered disulfide bonds in FepA, on electrophoretic behavior was difficult to predict. For mutant 33-120 and 56-73, we observed a single band on immunoblot after reacting with anti-FepA antibody, revealing the absence of disulfide bond formation, but the double-mutation inhibited FeEnt transport and phenotype reverted to normal when exposed to βME. Hence, these mutants formed disulfide bonds, but immunoblot did not reveal them. We engineered Cys residues to be close enough to form a disulfide bond (<5 Å between sulfur atoms) (Schauer, Rodionov et al. 2008, Smallwood, Jordan et al. 2014, Chakravorty, Shipelskiy et al. 2019) hypothetically, but in mutants that showed altered *Rf* value, only about 50% of the protein was in an altered state. So, it is plausible that the presence of Cys pairs affected local folding patterns and projection of side chain of residues, which we could not find because of the absence of crystallographic data on each mutant. In many Cys pairs, we observed multiple bands in immunoblots, and besides fully

synthesized, secreted, and folded proteins, these immunoblots may reveal the presence of nascent or incomplete mutant protein, pre-and post-disulfide state. Ultimately electrophoretic studies on Cys-pairs were informative but could not properly explain some of the bands' patterns and extent of disulfide bond formation for different mutants.

In the WT FepA structure, an intrinsic disulfide bond in L7 (C487-C494) was also present, which raised the possibility to interfere with engineered Cys substitutions we created for the study, but we did not observe that scenario. This disulfide bond is stable, does not react with extrinsic fluorophore if not fully reduced (Smallwood, Jordan et al. 2014, Chakravorty, Shipelskiy et al. 2019). Previous studies have shown that this bond is necessary for FeEnt transport. Mutating any of the Cys residue or double Cys sites abrogated FeEnt transport. So even though if any of the engineered Cys substitutions interfere with native disulfide bond formation, FeEnt transport would be halted, we did not observe that phenotype in any single or double mutant we created in our study. These native residues are stable and separated by only six residues, probable bonding immediately as the polypeptide region exits ribosome and folds.

Nutrition tests and [^{59}Fe]Ent assays helped depict the role of each Cys pair in FeEnt transport but were sometimes hard to interpret, whereas FD sensor assays were unique and provided real-time behavior of FepA mutants. The sensor cell OKN13/pFepA-FM depicted the transport behavior of different Cys mutants in real-time *in vivo*. Among intra-N mutants, except (44-111; did not form disulfide bond), all others inhibited FeEnt transport and reverted the phenotype by transporting FeEnt when 10mM βME was added to the solution. On the other hand, among inter-N-C Cys pair, except two (14-300 and 54-585), all other seven Cys pair mutants did not interfere with FeEnt transport through FepA. Cys pair 14-300 is unique because of its involvement in binding to the TonB-box, and maybe disulfide bond formation holds this in the

barrel and interferes with signal transduction to TonB. Double-mutant 54-585 blocked FeEnt even in the presence of βME, suggesting that inhibition of FeEnt transport by this mutant was not related to disulfide bond formation. Apart from these two exceptions, FD sensor assays provided concrete evidence and corroborated and clarified nutrition tests and [^{59}Fe]Ent results.

Many groups have shown the importance of TonB-dependent iron acquisition in Gram-negative bacterial pathogenesis (Furman, Fica et al. 1994, Dhople, Ibanez et al. 1996, Buckling, Harrison et al. 2007, Konings, Martin et al. 2013). Despite the availability of many Gram-negative bacterial TBDT crystal structures - FepA (Buchanan, Smith et al. 1999), Cir (Buchanan, Smith et al. 1999), FhuA, FecA (Ferguson, Hofmann et al. 1998, Locher, Rees et al. 1998), FoxA (Josts, Veith et al. 2019), and BtuB (Chimento, Mohanty et al. 2003) - it is not known how ligand moves through the channel and how TonB helps in uptake. Previously demonstrated data suggested that the N-domain exits to periplasm at the time of transport either as a rigid body or by unfolding. Our data refute both mechanisms because 7 of 9 inter-N-C Cys pairs we tested did not inhibit FeEnt transport, suggesting that N-domain does not exit the transmembrane channel. Tethering Cys residues at 51, 77, 128, 138, or 137 to the barrel did not prevent transport, suggesting the alternative idea that N-domain remains in the pore as FeEnt enters.

Chapter 7 - Conclusions

Genomic analysis revealed that *K. pneumoniae* strain Kp52.145 encodes multiple TonB-dependent FepA homologs. Their function was bioinformatically annotated but not experimentally shown. This includes KpnFepA_1658, KpnFepA_4984, KpnFepA_2380 and KpnIroN, iron-regulated OM receptors. The fluorescence spectroscopic assay that we developed monitored the binding of FeEnt to the outer loops of fluorescently labeled FepA, in *E. coli* and *A. baumannii* (Hanson, Jordan et al. 2016, Nairn, Eliasson et al. 2017). The test depicts ligand binding as a quenching of fluorescence, and ligand transport as fluorescence recovery when bacteria transport and deplete the ferric siderophore from the media. I used this approach to study the putative FeEnt transporters of *K. pneumoniae,* and showed that KpnFepA_1658, KpnFepA_4984 and KpnIroN all efficiently transport FeEnt. KpnFepA_2380 had lower affinity for FeEnt (K_D = 1.3 x 10^4 nM) compared to other receptors we studied but was the only OM receptor that binds FeCrn.

We adapted these assays to monitor FeAbn and vitamin B_{12} transport in *E. coli*, by IutA and BtuB, respectively, in a TonB-dependent manner. Iron is a vital element for bacterial growth and proliferation, and its acquisition is a virulence determinant of many bacterial pathogens. We previously used these assays for high-throughput screening (HTS) to find inhibitors that can inhibit FeEnt transport by blocking TonB action. We also adapted these spectroscopic assays to HTS format for measurement of FeEnt (KpnFepAs), FeAbn, and Vitamin B_{12} transport in CRE/ESKAPE bacteria, in a manner that avoids genetic manipulations or engineering of the

pathogens. The fluorescence assays are broadly applicable because they allow direct, *in vivo* measurement of the high-affinity transport of virtually any ligand, in any organism. Their application to HTS is another advancement in the field, that allowed us to search for potential inhibitors of TonB action. Chemicals that block TonB may prevent iron acquisition in humans and animals host and thereby thwart pathogenesis. Such chemicals may act as novel therapeutics against bacterial infectious diseases.

Using this fluorescence spectroscopic approach, we created a panel of fluorescent sensors of ferric catecholate, ferric hydroxamates, mixed chelators, and porphyrins. We demonstrated that several OM receptors recognize numerous ferric siderophores, whereas few are specific to only one particular metal complex. We also observed a general trend that besides recognizing and primarily binding a ferric siderophore, most sensors additionally bound the corresponding aposiderophore, with around 100-fold lower affinity. Using these sensors, we showed hierarchies of receptors' selectivity for various forms of catecholate siderophores. These sensors provide a sensitive, accurate, and rapid means of analyzing the recognition of metal complexes that are relevant in research, clinical, or commercial settings. Ultimately, the sensors we created may detect, discriminate, and quantify the apo- or ferric siderophores in laboratory samples, clinical samples, and food products. These sensors are useful in characterizing the route of entry (OM receptor) and biochemical parameters of Trojan Horse antibiotics against Gram-negative bacterial pathogens.

References:

Actis, L. A., M. E. Tolmasky, L. M. Crosa and J. H. Crosa (1993). "Effect of iron-limiting conditions on growth of clinical isolates of *Acinetobacter baumannii*." J Clin Microbiol 31(10): 2812-2815.

Adams, T. J., S. Vartivarian and R. E. Cowart (1990). "Iron acquisition systems of *Listeria monocytogenes*." Infect Immun 58(8): 2715-2718.

Agarwal, A. K. and J. Yee (2019). "Hepcidin." Adv Chronic Kidney Dis 26(4): 298-305.

Anderson, G. J. and D. M. Frazer (2017). "Current understanding of iron homeostasis." Am J Clin Nutr 106(Suppl 6): 1559S-1566S.

Annamalai, R., B. Jin, Z. Cao, S. M. Newton and P. E. Klebba (2004). "Recognition of ferric catecholates by FepA." J Bacteriol 186(11): 3578-3589.

Antunes, L. C., F. Imperi, K. J. Towner and P. Visca (2011). "Genome-assisted identification of putative iron-utilization genes in *Acinetobacter baumannii* and their distribution among a genotypically diverse collection of clinical isolates." Res Microbiol 162(3): 279-284.

Ayobami, O., N. Willrich, T. Harder, I. N. Okeke, T. Eckmanns and R. Markwart (2019). "The incidence and prevalence of hospital-acquired (carbapenem-resistant) A*cinetobacter baumannii* in Europe, Eastern Mediterranean and Africa: a systematic review and meta-analysis." Emerg Microbes Infect 8(1): 1747-1759.

Bachman, M. A., S. Lenio, L. Schmidt, J. E. Oyler and J. N. Weiser (2012). "Interaction of lipocalin 2, transferrin, and siderophores determines the replicative niche of *Klebsiella pneumoniae* during pneumonia." mBio 3(6).

Bachman, M. A., V. L. Miller and J. N. Weiser (2009). "Mucosal lipocalin 2 has pro-inflammatory and iron-sequestering effects in response to bacterial enterobactin." PLoS Pathog 5(10): e1000622.

Bachman, M. A., J. E. Oyler, S. H. Burns, M. Caza, F. Lépine, C. M. Dozois and J. N. Weiser (2011). "*Klebsiella pneumoniae* yersiniabactin promotes respiratory tract infection through evasion of lipocalin 2." Infect Immun 79(8): 3309-3316.

Baichoo, N. and J. D. Helmann (2002). "Recognition of DNA by Fur: a reinterpretation of the Fur box consensus sequence." J Bacteriol 184(21): 5826-5832.

Bailey, D. C., E. Alexander, M. R. Rice, E. J. Drake, L. S. Mydy, C. C. Aldrich and A. M. Gulick (2018). "Structural and functional delineation of aerobactin biosynthesis in hypervirulent *Klebsiella pneumoniae*." J Biol Chem 293(20): 7841-7852.

Bailey, D. C., T. J. Bohac, J. A. Shapiro, D. E. Giblin, T. A. Wencewicz and A. M. Gulick (2018). "Crystal Structure of the Siderophore Binding Protein BauB Bound to an Unusual 2:1 Complex Between Acinetobactin and Ferric Iron." Biochemistry 57(48): 6653-6661.

Baker, K. R. and K. Postle (2013). "Mutations in *Escherichia coli* ExbB transmembrane domains identify scaffolding and signal transduction functions and exclude participation in a proton pathway." J Bacteriol 195(12): 2898-2911.

Balhesteros, H., Y. Shipelskiy, N. J. Long, A. Majumdar, B. B. Katz, N. M. Santos, L. Leaden, S. M. Newton, M. V. Marques and P. E. Klebba (2017). "TonB-Dependent Heme/Hemoglobin Utilization by *Caulobacter crescentus* HutA." J Bacteriol 199(6).

Baquero, F. and B. R. Levin (2021). "Proximate and ultimate causes of the bactericidal action of antibiotics." Nat Rev Microbiol 19(2): 123-132.

Bierne, H., C. Garandeau, M. G. Pucciarelli, C. Sabet, S. Newton, F. Garcia-del Portillo, P. Cossart and A. Charbit (2004). "Sortase B, a new class of sortase in *Listeria monocytogenes*." J Bacteriol **186**(7): 1972-1982.

Blattner, F. R., G. Plunkett, 3rd, C. A. Bloch, N. T. Perna, V. Burland, M. Riley, J. Collado-Vides, J. D. Glasner, C. K. Rode, G. F. Mayhew, J. Gregor, N. W. Davis, H. A. Kirkpatrick, M. A. Goeden, D. J. Rose, B. Mau and Y. Shao (1997). "The complete genome sequence of *Escherichia coli* K-12." Science **277**(5331): 1453-1462.

Bohac, T. J., L. Fang, D. E. Giblin and T. A. Wencewicz (2019). "Fimsbactin and Acinetobactin Compete for the Periplasmic Siderophore Binding Protein BauB in Pathogenic *Acinetobacter baumannii*." ACS Chem Biol **14**(4): 674-687.

Boucher, H. W., G. H. Talbot, J. S. Bradley, J. E. Edwards, D. Gilbert, L. B. Rice, M. Scheld, B. Spellberg and J. Bartlett (2009). "Bad bugs, no drugs: no ESKAPE! An update from the Infectious Diseases Society of America." Clin Infect Dis **48**(1): 1-12.

Brandel, J., N. Humbert, M. Elhabiri, I. J. Schalk, G. L. Mislin and A. M. Albrecht-Gary (2012). "Pyochelin, a siderophore of *Pseudomonas aeruginosa*: physicochemical characterization of the iron(III), copper(II) and zinc(II) complexes." Dalton Trans **41**(9): 2820-2834.

Brock, J. H., P. H. Williams, J. Licéaga and K. G. Wooldridge (1991). "Relative availability of transferrin-bound iron and cell-derived iron to aerobactin-producing and enterochelin-producing strains of *Escherichia coli* and to other microorganisms." Infect Immun **59**(9): 3185-3190.

Brown, A. R., R. A. Gordon, S. N. Hyland, M. S. Siegrist and C. L. Grimes (2020). "Chemical Biology Tools for Examining the Bacterial Cell Wall." Cell Chem Biol **27**(8): 1052-1062.

Buchanan, S. K., B. S. Smith, L. Venkatramani, D. Xia, L. Esser, M. Palnitkar, R. Chakraborty, D. van der Helm and J. Deisenhofer (1999). "Crystal structure of the outer membrane active transporter FepA from *Escherichia coli*." Nat Struct Biol **6**(1): 56-63.

Buckling, A., F. Harrison, M. Vos, M. A. Brockhurst, A. Gardner, S. A. West and A. Griffin (2007). "Siderophore-mediated cooperation and virulence in *Pseudomonas aeruginosa*." FEMS Microbiol Ecol **62**(2): 135-141.

Bullen, J., E. Griffiths, H. Rogers and G. Ward (2000). "Sepsis: the critical role of iron." Microbes Infect **2**(4): 409-415.

Bullen, J. J. (1981). "The significance of iron in infection." Rev Infect Dis **3**(6): 1127-1138.

Bullen, J. J., H. J. Rogers, P. B. Spalding and C. G. Ward (2005). "Iron and infection: the heart of the matter." FEMS Immunol Med Microbiol **43**(3): 325-330.

Cao, Z., Z. Qi, C. Sprencel, S. M. Newton and P. E. Klebba (2000). "Aromatic components of two ferric enterobactin binding sites in *Escherichia coli* FepA." Mol Microbiol **37**(6): 1306-1317.

Cao, Z., P. Warfel, S. M. Newton and P. E. Klebba (2003). "Spectroscopic observations of ferric enterobactin transport." J Biol Chem **278**(2): 1022-1028.

Caux-Thang, C., A. Parent, R. Sethu, A. Maiga, G. Blondin, J. M. Latour and V. Duarte (2015). "Single asparagine to arginine mutation allows PerR to switch from PerR box to fur box." ACS Chem Biol **10**(3): 682-686.

Chakravorty, S., Y. Shipelskiy, A. Kumar, A. Majumdar, T. Yang, B. L. Nairn, S. M. Newton and P. E. Klebba (2019). "Universal fluorescent sensors of high-affinity iron transport, applied to ESKAPE pathogens." J Biol Chem **294**(12): 4682-4692.

Chimento, D. P., A. K. Mohanty, R. J. Kadner and M. C. Wiener (2003). "Substrate-induced transmembrane signaling in the cobalamin transporter BtuB." Nat Struct Biol **10**(5): 394-401.

Coffey, R. and T. Ganz (2017). "Iron homeostasis: An anthropocentric perspective." J Biol Chem **292**(31): 12727-12734.

Cohen, M. S., Y. Chai, B. E. Britigan, W. McKenna, J. Adams, T. Svendsen, K. Bean, D. J. Hassett and P. F. Sparling (1987). "Role of extracellular iron in the action of the quinone antibiotic streptonigrin: mechanisms of killing and resistance of *Neisseria gonorrhoeae*." Antimicrob Agents Chemother **31**(10): 1507-1513.

Conte, M. P., C. Longhi, V. Buonfiglio, M. Polidoro, L. Seganti and P. Valenti (1994). "The effect of iron on the invasiveness of *Escherichia coli* carrying the inv gene of Yersinia pseudotuberculosis." J Med Microbiol **40**(4): 236-240.

Coulanges, V., P. Andre and D. J. Vidon (1998). "Effect of siderophores, catecholamines, and catechol compounds on Listeria spp. Growth in iron-complexed medium." Biochem Biophys Res Commun **249**(2): 526-530.

Cowan, S. W., T. Schirmer, G. Rummel, M. Steiert, R. Ghosh, R. A. Pauptit, J. N. Jansonius and J. P. Rosenbusch (1992). "Crystal structures explain functional properties of two *E. coli* porins." Nature **358**(6389): 727-733.

Cowart, R. E. and B. G. Foster (1985). "Differential effects of iron on the growth of *Listeria monocytogenes*: minimum requirements and mechanism of acquisition." J Infect Dis **151**(4): 721-730.

Cox, C. D. and P. Adams (1985). "Siderophore activity of pyoverdin for *Pseudomonas aeruginosa*." Infect Immun **48**(1): 130-138.

da Silva Neto, J. F., V. S. Braz, V. C. Italiani and M. V. Marques (2009). "Fur controls iron homeostasis and oxidative stress defense in the oligotrophic alpha-proteobacterium Caulobacter crescentus." Nucleic Acids Res **37**(14): 4812-4825.

Daniel, C., S. Haentjens, M. C. Bissinger and R. J. Courcol (1999). "Characterization of the *Acinetobacter baumannii* Fur regulator: cloning and sequencing of the fur homolog gene." FEMS Microbiol Lett **170**(1): 199-209.

Datsenko, K. A. and B. L. Wanner (2000). "One-step inactivation of chromosomal genes in *Escherichia coli* K-12 using PCR products." Proc Natl Acad Sci U S A **97**(12): 6640-6645.

Dhople, A. M., M. A. Ibanez and T. C. Poirier (1996). "Role of iron in the pathogenesis of *Mycobacterium avium* infection in mice." Microbios **87**(351): 77-87.

Dorsey, C. W., M. S. Beglin and L. A. Actis (2003). "Detection and analysis of iron uptake components expressed by *Acinetobacter baumannii* clinical isolates." J Clin Microbiol **41**(9): 4188-4193.

Dumas, Z., A. Ross-Gillespie and R. Kummerli (2013). "Switching between apparently redundant iron-uptake mechanisms benefits bacteria in changeable environments." Proc Biol Sci **280**(1764): 20131055.

Dyer, D. W., W. McKenna, J. P. Woods and P. F. Sparling (1987). "Isolation by streptonigrin enrichment and characterization of a transferrin-specific iron uptake mutant of *Neisseria meningitidis*." Microb Pathog **3**(5): 351-363.

Ecker, D. J., J. R. Lancaster, Jr. and T. Emery (1982). "Siderophore iron transport followed by electron paramagnetic resonance spectroscopy." J Biol Chem **257**(15): 8623-8626.

Eijkelkamp, B. A., K. A. Hassan, I. T. Paulsen and M. H. Brown (2011). "Investigation of the human pathogen *Acinetobacter baumannii* under iron limiting conditions." BMC Genomics **12**: 126.

Elemam, A., J. Rahimian and W. Mandell (2009). "Infection with panresistant *Klebsiella pneumoniae*: a report of 2 cases and a brief review of the literature." Clin Infect Dis **49**(2): 271-274.

Escolar, L., J. Perez-Martin and V. de Lorenzo (1998). "Binding of the fur (ferric uptake regulator) repressor of *Escherichia coli* to arrays of the GATAAT sequence." J Mol Biol **283**(3): 537-547.

Faulkner, M. J., Z. Ma, M. Fuangthong and J. D. Helmann (2012). "Derepression of the Bacillus subtilis PerR peroxide stress response leads to iron deficiency." J Bacteriol **194**(5): 1226-1235.

Ferguson, A. D., R. Chakraborty, B. S. Smith, L. Esser, D. van der Helm and J. Deisenhofer (2002). "Structural basis of gating by the outer membrane transporter FecA." Science **295**(5560): 1715-1719.

Ferguson, A. D., E. Hofmann, J. W. Coulton, K. Diederichs and W. Welte (1998). "Siderophore-mediated iron transport: crystal structure of FhuA with bound lipopolysaccharide." Science **282**(5397): 2215-2220.

Fiester, S. E., B. A. Arivett, R. E. Schmidt, A. C. Beckett, T. Ticak, M. V. Carrier, R. Ghosh, E. J. Ohneck, M. L. Metz, M. K. Sellin Jeffries and L. A. Actis (2016). "Iron-Regulated Phospholipase C Activity Contributes to the Cytolytic Activity and Virulence of *Acinetobacter baumannii*." PLoS One **11**(11): e0167068.

Fisher, J. F. and S. Mobashery (2016). "beta-Lactam Resistance Mechanisms: Gram-Positive Bacteria and *Mycobacterium tuberculosis*." Cold Spring Harb Perspect Med **6**(5).

Francis, J., H. M. Macturk, J. Madinaveitia and G. A. Snow (1953). "Mycobactin, a growth factor for Mycobacterium johnei. I. Isolation from *Mycobacterium phlei*." Biochem J **55**(4): 596-607.

Furman, M., A. Fica, M. Saxena, J. L. Di Fabio and F. C. Cabello (1994). "S*almonella typhi* iron uptake mutants are attenuated in mice." Infect Immun **62**(9): 4091-4094.

Gaddy, J. A., B. A. Arivett, M. J. McConnell, R. Lopez-Rojas, J. Pachon and L. A. Actis (2012). "Role of acinetobactin-mediated iron acquisition functions in the interaction of *Acinetobacter baumannii* strain ATCC 19606T with human lung epithelial cells, Galleria mellonella caterpillars, and mice." Infect Immun **80**(3): 1015-1024.

Gao, G., J. Li, Y. Zhang and Y. Z. Chang (2019). "Cellular Iron Metabolism and Regulation." Adv Exp Med Biol **1173**: 21-32.

Gibson, D. G., L. Young, R. Y. Chuang, J. C. Venter, C. A. Hutchison, 3rd and H. O. Smith (2009). "Enzymatic assembly of DNA molecules up to several hundred kilobases." Nat Methods **6**(5): 343-345.

Gibson, F. and D. I. Magrath (1969). "The isolation and characterization of a hydroxamic acid (aerobactin) formed by *Aerobacter aerogenes* 62-I." Biochim Biophys Acta **192**(2): 175-184.

Ginalski, K. (2006). "Comparative modeling for protein structure prediction." Curr Opin Struct Biol **16**(2): 172-177.

Goldenzweig, P., A. J. Schwartz, I. Adachi, H. Aihara, K. Arinstein, V. Aulchenko, T. Aushev, S. Bahinipati, A. M. Bakich, A. Bay, I. Bedny, V. Bhardwaj, U. Bitenc, A. Bondar, A. Bozek,

M. Bracko, T. E. Browder, P. Chang, Y. Chao, A. Chen, K. F. Chen, B. G. Cheon, C. C. Chiang, R. Chistov, I. S. Cho, Y. Choi, J. Dalseno, M. Dash, A. Drutskoy, S. Eidelman, B. Golob, H. Ha, K. Hayasaka, H. Hayashii, M. Hazumi, D. Heffernan, Y. Hoshi, W. S. Hou, Y. B. Hsiung, H. J. Hyun, T. Iijima, K. Inami, A. Ishikawa, H. Ishino, M. Iwasaki, D. H. Kah, J. H. Kang, T. Kawasaki, H. Kichimi, H. J. Kim, S. K. Kim, Y. I. Kim, Y. J. Kim, K. Kinoshita, S. Korpar, P. Krizan, P. Krokovny, R. Kumar, A. Kuzmin, Y. J. Kwon, S. H. Kyeong, J. S. Lange, J. S. Lee, M. J. Lee, S. E. Lee, T. Lesiak, J. Li, A. Limosani, S. W. Lin, C. Liu, Y. Liu, J. MacNaughton, F. Mandl, S. McOnie, K. Miyabayashi, H. Miyata, Y. Miyazaki, R. Mizuk, T. Nagamine, E. Nakano, M. Nakao, H. Nakazawa, S. Nishida, O. Nitoh, S. Ogawa, T. Ohshima, S. Okuno, S. L. Olsen, W. Ostrowicz, H. Ozaki, P. Pakhlov, G. Pakhlova, H. Palka, C. W. Park, H. Park, H. K. Park, L. S. Peak, R. Pestotnik, L. E. Piilonen, H. Sahoo, Y. Sakai, O. Schneider, J. Schumann, C. Schwanda, R. Seidl, A. Sekiya, K. Senyo, M. E. Sevior, M. Shapkin, V. Shebalin, C. P. Shen, J. G. Shiu, J. B. Singh, A. Somov, S. Stanic, M. Staric, K. Sumisawa, T. Sumiyoshi, S. Suzuki, N. Tamura, M. Tanaka, Y. Teramoto, I. Tikhomirov, K. Trabelsi, S. Uehara, T. Uglov, Y. Unno, S. Uno, P. Urquijo, Y. Usov, G. Varner, K. E. Varvell, K. Vervink, C. C. Wang, C. H. Wang, M. Z. Wang, P. Wang, X. L. Wang, Y. Watanabe, R. Wedd, J. Wicht, E. Won, B. D. Yabsley, Y. Yamashita, M. Yamauchi, C. C. Zhang, Z. P. Zhang, V. Zhulanov, T. Zivko, A. Zupanc, O. Zyukova and C. Belle (2008). "Evidence for neutral B meson decays to omegaK*0." Phys Rev Lett **101**(23): 231801.

Guterman, S. K. and L. Dann (1973). "Excretion of enterochelin by exbA and exbB mutants of *Escherichia coli*." J Bacteriol **114**(3): 1225-1230.

Hanson, M., L. D. Jordan, Y. Shipelskiy, S. M. Newton and P. E. Klebba (2016). "High-Throughput Screening Assay for Inhibitors of TonB-Dependent Iron Transport." J Biomol Screen **21**(3): 316-322.

Harding, C. M., S. W. Hennon and M. F. Feldman (2018). "Uncovering the mechanisms of *Acinetobacter baumannii* virulence." Nat Rev Microbiol **16**(2): 91-102.

Hashimoto-Gotoh, T., F. C. Franklin, A. Nordheim and K. N. Timmis (1981). "Specific-purpose plasmid cloning vectors. I. Low copy number, temperature-sensitive, mobilization-defective pSC101-derived containment vectors." Gene **16**(1-3): 227-235.

Higgs, P. I., R. A. Larsen and K. Postle (2002). "Quantification of known components of the *Escherichia coli* TonB energy transduction system: TonB, ExbB, ExbD and FepA." Mol Microbiol **44**(1): 271-281.

Holden, V. I. and M. A. Bachman (2015). "Diverging roles of bacterial siderophores during infection." Metallomics **7**(6): 986-995.

Holden, V. I., P. Breen, S. Houle, C. M. Dozois and M. A. Bachman (2016). "*Klebsiella pneumoniae* Siderophores Induce Inflammation, Bacterial Dissemination, and HIF-1α Stabilization during Pneumonia." mBio **7**(5).

Holden, V. I., S. Lenio, R. Kuick, S. K. Ramakrishnan, Y. M. Shah and M. A. Bachman (2014). "Bacterial siderophores that evade or overwhelm lipocalin 2 induce hypoxia inducible

factor 1α and proinflammatory cytokine secretion in cultured respiratory epithelial cells." Infect Immun **82**(9): 3826-3836.

Holland, J., K. J. Towner and P. Williams (1991). "Isolation and characterisation of *Haemophilus influenzae* type b mutants defective in transferrin-binding and iron assimilation." FEMS Microbiol Lett **61**(2-3): 283-287.

Hsieh, P. F., T. L. Lin, C. Z. Lee, S. F. Tsai and J. T. Wang (2008). "Serum-induced iron-acquisition systems and TonB contribute to virulence in *Klebsiella pneumoniae* causing primary pyogenic liver abscess." J Infect Dis **197**(12): 1717-1727.

Jacobs, A. C., I. Hood, K. L. Boyd, P. D. Olson, J. M. Morrison, S. Carson, K. Sayood, P. C. Iwen, E. P. Skaar and P. M. Dunman (2010). "Inactivation of phospholipase D diminishes *Acinetobacter baumannii* pathogenesis." Infect Immun **78**(5): 1952-1962.

Jeong, B. C., C. Hawes, K. M. Bonthrone and L. E. Macaskie (1997). "Localization of enzymically enhanced heavy metal accumulation by Citrobacter sp. and metal accumulation in vitro by liposomes containing entrapped enzyme." Microbiology (Reading) **143 (Pt 7)**: 2497-2507.

Jordan, L. D., Y. Zhou, C. R. Smallwood, Y. Lill, K. Ritchie, W. T. Yip, S. M. Newton and P. E. Klebba (2013). "Energy-dependent motion of TonB in the Gram-negative bacterial inner membrane." Proc Natl Acad Sci U S A **110**(28): 11553-11558.

Josts, I., K. Veith and H. Tidow (2019). "Ternary structure of the outer membrane transporter FoxA with resolved signalling domain provides insights into TonB-mediated siderophore uptake." Elife **8**.

Klebba, P. E. (2003). "Three paradoxes of ferric enterobactin uptake." Front Biosci **8**: s1422-1436.

Klebba, P. E. (2016). "ROSET Model of TonB Action in Gram-Negative Bacterial Iron Acquisition." J Bacteriol **198**(7): 1013-1021.

Klebba, P. E., M. Hofnung and A. Charbit (1994). "A model of maltodextrin transport through the sugar-specific porin, LamB, based on deletion analysis." EMBO J **13**(19): 4670-4675.

Klebba, P. E., M. A. McIntosh and J. B. Neilands (1982). "Kinetics of biosynthesis of iron-regulated membrane proteins in *Escherichia coli*." J Bacteriol **149**(3): 880-888.

Klebba, P. E., S. M. C. Newton, D. A. Six, A. Kumar, T. Yang, B. L. Nairn, C. Munger and S. Chakravorty (2021). "Iron Acquisition Systems of Gram-negative Bacterial Pathogens Define TonB-Dependent Pathways to Novel Antibiotics." Chem Rev **121**(9): 5193-5239.

Klebba, P. E., S. M. C. Newton, D. A. Six, A. Kumar, T. Yang, B. L. Nairn, C. Munger and S. Chakravorty (2021). "Iron Acquisition Systems of Gram-negative Bacterial Pathogens Define TonB-Dependent Pathways to Novel Antibiotics." Chem Rev.

Kokesova, A., L. Frolova, M. Kverka, D. Sokol, P. Rossmann, J. Bartova and H. Tlaskalova-Hogenova (2006). "Oral administration of probiotic bacteria (*E. coli* Nissle, *E. coli* O83,

Lactobacillus casei) influences the severity of dextran sodium sulfate-induced colitis in BALB/c mice." Folia Microbiol (Praha) **51**(5): 478-484.

Konings, A. F., L. W. Martin, K. J. Sharples, L. F. Roddam, R. Latham, D. W. Reid and I. L. Lamont (2013). "*Pseudomonas aeruginosa* uses multiple pathways to acquire iron during chronic infection in cystic fibrosis lungs." Infect Immun **81**(8): 2697-2704.

Konopka, K., A. Bindereif and J. B. Neilands (1982). "Aerobactin-mediated utilization of transferrin iron." Biochemistry **21**(25): 6503-6508.

Kuhn, A. (2019). "The Bacterial Cell Wall and Membrane-A Treasure Chest for Antibiotic Targets." Subcell Biochem **92**: 1-5.

Lai, Y. C., H. L. Peng and H. Y. Chang (2001). "Identification of genes induced in vivo during *Klebsiella pneumoniae* CG43 infection." Infect Immun **69**(11): 7140-7145.

Lamont, I. L., A. F. Konings and D. W. Reid (2009). "Iron acquisition by *Pseudomonas aeruginosa* in the lungs of patients with cystic fibrosis." Biometals **22**(1): 53-60.

Lee, J. W. and J. D. Helmann (2007). "Functional specialization within the Fur family of metalloregulators." Biometals **20**(3-4): 485-499.

Leong, J. and J. B. Neilands (1976). "Mechanisms of siderophore iron transport in enteric bacteria." J Bacteriol **126**(2): 823-830.

Lery, L. M., L. Frangeul, A. Tomas, V. Passet, A. S. Almeida, S. Bialek-Davenet, V. Barbe, J. A. Bengoechea, P. Sansonetti, S. Brisse and R. Tournebize (2014). "Comparative analysis of *Klebsiella pneumoniae* genomes identifies a phospholipase D family protein as a novel virulence factor." BMC Biol **12**: 41.

Li, B., N. Li, Y. Yue, X. Liu, Y. Huang, L. Gu and S. Xu (2016). "An unusual crystal structure of ferric-enterobactin bound FepB suggests novel functions of FepB in microbial iron uptake." Biochem Biophys Res Commun **478**(3): 1049-1053.

Liu, J., J. M. Rutz, P. E. Klebba and J. B. Feix (1994). "A site-directed spin-labeling study of ligand-induced conformational change in the ferric enterobactin receptor, FepA." Biochemistry **33**(45): 13274-13283.

Liu, P. V. and F. Shokrani (1978). "Biological activities of pyochelins: iron-chelating agents of *Pseudomonas aeruginosa*." Infect Immun **22**(3): 878-890.

Locher, K. P., B. Rees, R. Koebnik, A. Mitschler, L. Moulinier, J. P. Rosenbusch and D. Moras (1998). "Transmembrane signaling across the ligand-gated FhuA receptor: crystal structures of free and ferrichrome-bound states reveal allosteric changes." Cell **95**(6): 771-778.

Ma, L., W. Kaserer, R. Annamalai, D. C. Scott, B. Jin, X. Jiang, Q. Xiao, H. Maymani, L. M. Massis, L. C. Ferreira, S. M. Newton and P. E. Klebba (2007). "Evidence of ball-and-chain transport of ferric enterobactin through FepA." J Biol Chem **282**(1): 397-406.

Majumdar, A., V. Trinh, K. J. Moore, C. R. Smallwood, A. Kumar, T. Yang, D. C. Scott, N. J. Long, S. M. Newton and P. E. Klebba (2020). "Conformational rearrangements in the N-domain of *Escherichia coli* FepA during ferric enterobactin transport." J Biol Chem **295**(15): 4974-4984.

Malmirchegini, G. R., M. Sjodt, S. Shnitkind, M. R. Sawaya, J. Rosinski, S. M. Newton, P. E. Klebba and R. T. Clubb (2014). "Novel mechanism of hemin capture by Hbp2, the hemoglobin-binding hemophore from *Listeria monocytogenes*." J Biol Chem **289**(50): 34886-34899.

Mazmanian, S. K., G. Liu, H. Ton-That and O. Schneewind (1999). "*Staphylococcus aureus* sortase, an enzyme that anchors surface proteins to the cell wall." Science **285**(5428): 760-763.

McIntosh, M. A. and C. F. Earhart (1976). "Effect of iron of the relative abundance of two large polypeptides of the *Escherichia coli* outer membrane." Biochem Biophys Res Commun **70**(1): 315-322.

Miethke, M. and M. A. Marahiel (2007). "Siderophore-based iron acquisition and pathogen control." Microbiol Mol Biol Rev **71**(3): 413-451.

Mihara, K., T. Tanabe, Y. Yamakawa, T. Funahashi, H. Nakao, S. Narimatsu and S. Yamamoto (2004). "Identification and transcriptional organization of a gene cluster involved in biosynthesis and transport of acinetobactin, a siderophore produced by *Acinetobacter baumannii* ATCC 19606T." Microbiology (Reading) **150**(Pt 8): 2587-2597.

Morton, D. J. and P. Williams (1989). "Characterization of the outer-membrane proteins of *Haemophilus parainfluenzae* expressed under iron-sufficient and iron-restricted conditions." J Gen Microbiol **135**(Pt 2): 445-451.

Muller, S. I., M. Valdebenito and K. Hantke (2009). "Salmochelin, the long-overlooked catecholate siderophore of *Salmonella*." Biometals **22**(4): 691-695.

Murphy, C. K., V. I. Kalve and P. E. Klebba (1990). "Surface topology of the *Escherichia coli* K-12 ferric enterobactin receptor." J Bacteriol **172**(5): 2736-2746.

Nagy, T. A., S. M. Moreland, H. Andrews-Polymenis and C. S. Detweiler (2013). "The ferric enterobactin transporter Fep is required for persistent *Salmonella enterica* serovar typhimurium infection." Infect Immun **81**(11): 4063-4070.

Nairn, B. L., O. S. Eliasson, D. R. Hyder, N. J. Long, A. Majumdar, S. Chakravorty, P. McDonald, A. Roy, S. M. Newton and P. E. Klebba (2017). "Fluorescence High-Throughput Screening for Inhibitors of TonB Action." J Bacteriol **199**(10).

Navon-Venezia, S., K. Kondratyeva and A. Carattoli (2017). "*Klebsiella pneumoniae*: a major worldwide source and shuttle for antibiotic resistance." FEMS Microbiol Rev **41**(3): 252-275.

Neidhardt, F. C., P. L. Bloch and D. F. Smith (1974). "Culture medium for enterobacteria." J Bacteriol **119**(3): 736-747.

Neilands, J. B. (1953). "Factors affecting the microbial production of ferrichrome." J Biol Chem **205**(2): 647-650.

Neilands, J. B. (1981). "Microbial iron compounds." Annu Rev Biochem **50**: 715-731.

Neilands, J. B. (1995). "Siderophores: structure and function of microbial iron transport compounds." J Biol Chem **270**(45): 26723-26726.

Newton, S. M., J. D. Igo, D. C. Scott and P. E. Klebba (1999). "Effect of loop deletions on the binding and transport of ferric enterobactin by FepA." Mol Microbiol **32**(6): 1153-1165.

Newton, S. M., P. E. Klebba, C. Raynaud, Y. Shao, X. Jiang, I. Dubail, C. Archer, C. Frehel and A. Charbit (2005). "The svpA-srtB locus of *Listeria monocytogenes*: fur-mediated iron regulation and effect on virulence." Mol Microbiol **55**(3): 927-940.

Newton, S. M., V. Trinh, H. Pi and P. E. Klebba (2010). "Direct measurements of the outer membrane stage of ferric enterobactin transport: postuptake binding." J Biol Chem **285**(23): 17488-17497.

Nikaido, H. (2003). "Molecular basis of bacterial outer membrane permeability revisited." Microbiol Mol Biol Rev **67**(4): 593-656.

Nikaido, H. and M. Vaara (1985). "Molecular basis of bacterial outer membrane permeability." Microbiol Rev **49**(1): 1-32.

Noinaj, N., M. Guillier, T. J. Barnard and S. K. Buchanan (2010). "TonB-dependent transporters: regulation, structure, and function." Annu Rev Microbiol **64**: 43-60.

Nwugo, C. C., J. A. Gaddy, D. L. Zimbler and L. A. Actis (2011). "Deciphering the iron response in *Acinetobacter baumannii*: A proteomics approach." J Proteomics **74**(1): 44-58.

Paczosa, M. K. and J. Mecsas (2016). "*Klebsiella pneumoniae*: Going on the Offense with a Strong Defense." Microbiol Mol Biol Rev **80**(3): 629-661.

Palacios, M., C. A. Broberg, K. A. Walker and V. L. Miller (2017). "A Serendipitous Mutation Reveals the Severe Virulence Defect of a *Klebsiella pneumoniae* fepB Mutant." mSphere **2**(4).

Pawelek, P. D., N. Croteau, C. Ng-Thow-Hing, C. M. Khursigara, N. Moiseeva, M. Allaire and J. W. Coulton (2006). "Structure of TonB in complex with FhuA, *E. coli* outer membrane receptor." Science **312**(5778): 1399-1402.

Payne, S. M. (1988). "Iron and virulence in the family *Enterobacteriaceae*." Crit Rev Microbiol **16**(2): 81-111.

Payne, S. M. (1989). "Iron and virulence in Shigella." Mol Microbiol **3**(9): 1301-1306.

Payne, S. M. (1993). "Iron acquisition in microbial pathogenesis." Trends Microbiol **1**(2): 66-69.

Peek, M. E., A. Bhatnagar, N. A. McCarty and S. M. Zughaier (2012). "Pyoverdine, the Major Siderophore in *Pseudomonas aeruginosa*, Evades NGAL Recognition." Interdiscip Perspect Infect Dis **2012**: 843509.

Penwell, W. F., B. A. Arivett and L. A. Actis (2012). "The *Acinetobacter baumannii* entA gene located outside the acinetobactin cluster is critical for siderophore production, iron acquisition and virulence." PLoS One **7**(5): e36493.

Penwell, W. F., N. DeGrace, S. Tentarelli, L. Gauthier, C. M. Gilbert, B. A. Arivett, A. A. Miller, T. F. Durand-Reville, C. Joubran and L. A. Actis (2015). "Discovery and Characterization of New Hydroxamate Siderophores, Baumannoferrin A and B, produced by *Acinetobacter baumannii*." Chembiochem **16**(13): 1896-1904.

Pettersen, E. F., T. D. Goddard, C. C. Huang, G. S. Couch, D. M. Greenblatt, E. C. Meng and T. E. Ferrin (2004). "UCSF Chimera--a visualization system for exploratory research and analysis." J Comput Chem **25**(13): 1605-1612.

Pi, H., S. A. Jones, L. E. Mercer, J. P. Meador, J. E. Caughron, L. Jordan, S. M. Newton, T. Conway and P. E. Klebba (2012). "Role of catecholate siderophores in gram-negative bacterial colonization of the mouse gut." PLoS One **7**(11): e50020.

Proschak, A., P. Lubuta, P. Grun, F. Lohr, G. Wilharm, V. De Berardinis and H. B. Bode (2013). "Structure and biosynthesis of fimsbactins A-F, siderophores from *Acinetobacter baumannii* and *Acinetobacter baylyi*." Chembiochem **14**(5): 633-638.

Pugsley, A. P. and P. Reeves (1977). "The role of colicin receptors in the uptake of ferrienterochelin by *Escherichia coli* K-12." Biochem Biophys Res Commun **74**(3): 903-911.

Raymond, K. N., E. A. Dertz and S. S. Kim (2003). "Enterobactin: an archetype for microbial iron transport." Proc Natl Acad Sci U S A **100**(7): 3584-3588.

Rich, R. L., G. A. Papalia, P. J. Flynn, J. Furneisen, J. Quinn, J. S. Klein, P. S. Katsamba, M. B. Waddell, M. Scott, J. Thompson, J. Berlier, S. Corry, M. Baltzinger, G. Zeder-Lutz, A. Schoenemann, A. Clabbers, S. Wieckowski, M. M. Murphy, P. Page, T. E. Ryan, J. Duffner, T. Ganguly, J. Corbin, S. Gautam, G. Anderluh, A. Bavdek, D. Reichmann, S. P. Yadav, E. Hommema, E. Pol, A. Drake, S. Klakamp, T. Chapman, D. Kernaghan, K. Miller, J. Schuman, K. Lindquist, K. Herlihy, M. B. Murphy, R. Bohnsack, B. Andrien, P. Brandani, D. Terwey, R. Millican, R. J. Darling, L. Wang, Q. Carter, J. Dotzlaf, J. Lopez-Sagaseta, I. Campbell, P. Torreri, S. Hoos, P. England, Y. Liu, Y. Abdiche, D. Malashock, A. Pinkerton, M. Wong, E. Lafer, C. Hinck, K. Thompson, C. D. Primo, A. Joyce, J.

Brooks, F. Torta, A. B. Bagge Hagel, J. Krarup, J. Pass, M. Ferreira, S. Shikov, M. Mikolajczyk, Y. Abe, G. Barbato, A. M. Giannetti, G. Krishnamoorthy, B. Beusink, D. Satpaev, T. Tsang, E. Fang, J. Partridge, S. Brohawn, J. Horn, O. Pritsch, G. Obal, S. Nilapwar, B. Busby, G. Gutierrez-Sanchez, R. D. Gupta, S. Canepa, K. Witte, Z. Nikolovska-Coleska, Y. H. Cho, R. D'Agata, K. Schlick, R. Calvert, E. M. Munoz, M. J. Hernaiz, T. Bravman, M. Dines, M. H. Yang, A. Puskas, E. Boni, J. Li, M. Wear, A. Grinberg, J. Baardsnes, O. Dolezal, M. Gainey, H. Anderson, J. Peng, M. Lewis, P. Spies, Q. Trinh, S. Bibikov, J. Raymond, M. Yousef, V. Chandrasekaran, Y. Feng, A. Emerick, S. Mundodo, R. Guimaraes, K. McGirr, Y. J. Li, H. Hughes, H. Mantz, R. Skrabana, M. Witmer, J. Ballard, L. Martin, P. Skladal, G. Korza, I. Laird-Offringa, C. S. Lee, A. Khadir, F. Podlaski, P. Neuner, J. Rothacker, A. Rafique, N. Dankbar, P. Kainz, E. Gedig, M. Vuyisich, C. Boozer, N. Ly, M. Toews, A. Uren, O. Kalyuzhniy, K. Lewis, E. Chomey, B. J. Pak and D. G. Myszka (2009). "A global benchmark study using affinity-based biosensors." Anal Biochem **386**(2): 194-216.

Rouault, T. A. and N. Maio (2017). "Biogenesis and functions of mammalian iron-sulfur proteins in the regulation of iron homeostasis and pivotal metabolic pathways." J Biol Chem **292**(31): 12744-12753.

Runci, F., V. Gentile, E. Frangipani, G. Rampioni, L. Leoni, M. Lucidi, D. Visaggio, G. Harris, W. Chen, J. Stahl, B. Averhoff and P. Visca (2019). "Contribution of Active Iron Uptake to *Acinetobacter baumannii* Pathogenicity." Infect Immun **87**(4).

Russo, T. A. and A. M. Gulick (2019). "Aerobactin Synthesis Proteins as Antivirulence Targets in Hypervirulent *Klebsiella pneumoniae*." ACS Infect Dis **5**(7): 1052-1054.

Russo, T. A. and U. MacDonald (2020). "The Galleria mellonella Infection Model Does Not Accurately Differentiate between Hypervirulent and Classical *Klebsiella pneumoniae*." mSphere **5**(1).

Russo, T. A. and C. M. Marr (2019). "Hypervirulent *Klebsiella pneumoniae*." Clin Microbiol Rev **32**(3).

Russo, T. A., R. Olson, C. T. Fang, N. Stoesser, M. Miller, U. MacDonald, A. Hutson, J. H. Barker, R. M. La Hoz and J. R. Johnson (2018). "Identification of Biomarkers for Differentiation of Hypervirulent *Klebsiella pneumoniae* from Classical *K. pneumoniae*." J Clin Microbiol **56**(9).

Russo, T. A., R. Olson, U. MacDonald, J. Beanan and B. A. Davidson (2015). "Aerobactin, but not yersiniabactin, salmochelin, or enterobactin, enables the growth/survival of hypervirulent (hypermucoviscous) *Klebsiella pneumoniae* ex vivo and in vivo." Infect Immun **83**(8): 3325-3333.

Russo, T. A., R. Olson, U. Macdonald, D. Metzger, L. M. Maltese, E. J. Drake and A. M. Gulick (2014). "Aerobactin mediates virulence and accounts for increased siderophore production under iron-limiting conditions by hypervirulent (hypermucoviscous) *Klebsiella pneumoniae*." Infect Immun **82**(6): 2356-2367.

Rutz, J. M., T. Abdullah, S. P. Singh, V. I. Kalve and P. E. Klebba (1991). "Evolution of the ferric enterobactin receptor in gram-negative bacteria." J Bacteriol **173**(19): 5964-5974.

Rutz, J. M., J. Liu, J. A. Lyons, J. Goranson, S. K. Armstrong, M. A. McIntosh, J. B. Feix and P. E. Klebba (1992). "Formation of a gated channel by a ligand-specific transport protein in the bacterial outer membrane." Science **258**(5081): 471-475.

Schauer, K., D. A. Rodionov and H. de Reuse (2008). "New substrates for TonB-dependent transport: do we only see the 'tip of the iceberg'?" Trends Biochem Sci **33**(7): 330-338.

Schoolnik, G. K. (2002). "Microarray analysis of bacterial pathogenicity." Adv Microb Physiol **46**: 1-45.

Scott, D. C., Z. Cao, Z. Qi, M. Bauler, J. D. Igo, S. M. Newton and P. E. Klebba (2001). "Exchangeability of N termini in the ligand-gated porins of *Escherichia coli*." J Biol Chem **276**(16): 13025-13033.

Shapiro, J. A. and T. A. Wencewicz (2016). "Acinetobactin Isomerization Enables Adaptive Iron Acquisition in *Acinetobacter baumannii* through pH-Triggered Siderophore Swapping." ACS Infect Dis **2**(2): 157-168.

Skaar, E. P., M. Humayun, T. Bae, K. L. DeBord and O. Schneewind (2004). "Iron-source preference of *Staphylococcus aureus* infections." Science **305**(5690): 1626-1628.

Smallwood, C. R., L. Jordan, V. Trinh, D. W. Schuerch, A. Gala, M. Hanson, Y. Shipelskiy, A. Majumdar, S. M. Newton and P. E. Klebba (2014). "Concerted loop motion triggers induced fit of FepA to ferric enterobactin." J Gen Physiol **144**(1): 71-80.

Smallwood, C. R., A. G. Marco, Q. Xiao, V. Trinh, S. M. Newton and P. E. Klebba (2009). "Fluoresceination of FepA during colicin B killing: effects of temperature, toxin and TonB." Mol Microbiol **72**(5): 1171-1180.

Smith, K. D. (2007). "Iron metabolism at the host pathogen interface: lipocalin 2 and the pathogen-associated iroA gene cluster." Int J Biochem Cell Biol **39**(10): 1776-1780.

Snyder, J. A., B. J. Haugen, E. L. Buckles, C. V. Lockatell, D. E. Johnson, M. S. Donnenberg, R. A. Welch and H. L. Mobley (2004). "Transcriptome of uropathogenic *Escherichia coli* during urinary tract infection." Infect Immun **72**(11): 6373-6381.

Sprencel, C., Z. Cao, Z. Qi, D. C. Scott, M. A. Montague, N. Ivanoff, J. Xu, K. M. Raymond, S. M. Newton and P. E. Klebba (2000). "Binding of ferric enterobactin by the *Escherichia coli* periplasmic protein FepB." J Bacteriol **182**(19): 5359-5364.

Stokes-Rees, I. and P. Sliz (2010). "Protein structure determination by exhaustive search of Protein Data Bank derived databases." Proc Natl Acad Sci U S A **107**(50): 21476-21481.

Tacconelli, E., F. Sifakis, S. Harbarth, R. Schrijver, M. van Mourik, A. Voss, M. Sharland, N. B. Rajendran, J. Rodriguez-Bano and E. P.-N. C.-M. Group (2018). "Surveillance for control of antimicrobial resistance." Lancet Infect Dis **18**(3): e99-e106.

Tang, F. and M. H. Saier, Jr. (2014). "Transport proteins promoting *Escherichia coli* pathogenesis." Microb Pathog **71-72**: 41-55.

Testi, C., A. Boffi and L. C. Montemiglio (2019). "Structural analysis of the transferrin receptor multifaceted ligand(s) interface." Biophys Chem **254**: 106242.

Torres, A. G. and S. M. Payne (1997). "Haem iron-transport system in enterohaemorrhagic *Escherichia coli* O157:H7." Mol Microbiol **23**(4): 825-833.

Trieu-Cuot, P., C. Carlier, C. Poyart-Salmeron and P. Courvalin (1990). "A pair of mobilizable shuttle vectors conferring resistance to spectinomycin for molecular cloning in *Escherichia coli* and in gram-positive bacteria." Nucleic Acids Res **18**(14): 4296.

Tsolis, R. M., A. J. Baumler, F. Heffron and I. Stojiljkovic (1996). "Contribution of TonB- and Feo-mediated iron uptake to growth of *Salmonella typhimurium* in the mouse." Infect Immun **64**(11): 4549-4556.

Valdebenito, M., S. I. Muller and K. Hantke (2007). "Special conditions allow binding of the siderophore salmochelin to siderocalin (NGAL-lipocalin)." FEMS Microbiol Lett **277**(2): 182-187.

Vallenet, D., P. Nordmann, V. Barbe, L. Poirel, S. Mangenot, E. Bataille, C. Dossat, S. Gas, A. Kreimeyer, P. Lenoble, S. Oztas, J. Poulain, B. Segurens, C. Robert, C. Abergel, J. M. Claverie, D. Raoult, C. Medigue, J. Weissenbach and S. Cruveiller (2008). "Comparative analysis of *Acinetobacters*: three genomes for three lifestyles." PLoS One **3**(3): e1805.

Warner, P. J., P. H. Williams, A. Bindereif and J. B. Neilands (1981). "ColV plasmid-specific aerobactin synthesis by invasive strains of *Escherichia coli*." Infect Immun **33**(2): 540-545.

Wasserman, S. I., N. A. Soter, D. M. Center and K. F. Austen (1977). "Cold urticaria. Recognition and characterization of a neutrophil chemotactic factor which appears in serum during experimental cold challenge." J Clin Invest **60**(1): 189-196.

Wayne, R., K. Frick and J. B. Neilands (1976). "Siderophore protection against colicins M, B, V, and Ia in *Escherichia coli*." J Bacteriol **126**(1): 7-12.

Weinberg, E. D. (1975). "Nutritional immunity. Host's attempt to withold iron from microbial invaders." JAMA **231**(1): 39-41.

Wencewicz, T. A. (2016). "New antibiotics from Nature's chemical inventory." Bioorg Med Chem **24**(24): 6227-6252.

Williams, P. H. (1979). "Novel iron uptake system specified by ColV plasmids: an important component in the virulence of invasive strains of *Escherichia coli*." Infect Immun **26**(3): 925-932.

Williams, P. H., W. Rabsch, U. Methner, W. Voigt, H. Tschape and R. Reissbrodt (2006). "Catecholate receptor proteins in *Salmonella enterica*: role in virulence and implications for vaccine development." Vaccine **24**(18): 3840-3844.

Wolf, S. L., J. S. Hogan and K. L. Smith (2004). "Iron uptake by *Escherichia coli* cultured with antibodies from cows immunized with high-affinity ferric receptors." J Dairy Sci **87**(7): 2103-2107.

Wolz, C., K. Hohloch, A. Ocaktan, K. Poole, R. W. Evans, N. Rochel, A. M. Albrecht-Gary, M. A. Abdallah and G. Doring (1994). "Iron release from transferrin by pyoverdin and elastase from *Pseudomonas aeruginosa*." Infect Immun **62**(9): 4021-4027.

Xiao, Q., X. Jiang, K. J. Moore, Y. Shao, H. Pi, I. Dubail, A. Charbit, S. M. Newton and P. E. Klebba (2011). "Sortase independent and dependent systems for acquisition of haem and haemoglobin in *Listeria monocytogen*es." Mol Microbiol **80**(6): 1581-1597.

Yamamoto, S., N. Okujo and Y. Sakakibara (1994). "Isolation and structure elucidation of acinetobactin, a novel siderophore from *Acinetobacter baumannii*." Arch Microbiol **162**(4): 249-254.

Yeowell, H. N. and J. R. White (1982). "Iron requirement in the bactericidal mechanism of streptonigrin." Antimicrob Agents Chemother **22**(6): 961-968.

Yu, E. W., G. McDermott, H. I. Zgurskaya, H. Nikaido and D. E. Koshland, Jr. (2003). "Structural basis of multiple drug-binding capacity of the AcrB multidrug efflux pump." Science **300**(5621): 976-980.